TAMPEREEN TEKNILLINEN YLIOPISTO
TAMPERE UNIVERSITY OF TECHNOLOGY

PETRI MÄKINEN

MODELING AND CONTROL OF A SINGLE-LINK FLEXIBLE HYDRAULIC ROBOT

Master of Science thesis

Examiner: Prof. Jouni Mattila
Examiner and topic approved by the Faculty Council of the Faculty of Engineering Sciences on 6th of April 2016

ABSTRACT

PETRI MÄKINEN: Modeling and control of a single-link flexible hydraulic robot
Tampere University of Technology
Master of Science thesis, 71 pages, 9 Appendix pages
October 2016
Master's Degree Programme in Automation Technology
Major: Machine Automation
Examiner: Prof. Jouni Mattila
Keywords: Virtual decomposition control, flexible link, finite element model, flexible beam

The use of lighter construction materials is desirable in robotic arms and manipulators alike due to their cost advantage and high payload to weight ratio. Lightweight materials also lead to increasing structural flexibility, which induces challenges to the control problem of endpoint positions of flexible arms. This is caused by the complex dynamics of flexible links.

In this thesis a single-link flexible beam was studied, which is a part of a 1-degree-of-freedom assembly, actuated by a hydraulic cylinder. The beam's dimensions are $60 \times 60 \times 3$ mm and its length is 4.5 m, while a load mass of 60 kg is bolted near the tip. Therefore, the system at hand is highly flexible.

The objective of this thesis was to build and implement a VDC (Virtual Decomposition Control) type controller to the system and test its performance. The VDC approach is a model-based, nonlinear control method, developed especially for robots with high numbers of degrees-of-freedom. The VDC approach is subsystem based, enabling individual control of each of the subsystems. The dynamics of each subsystem remain relatively simple, no matter how complex the entire robot is. A finite element model of the boom was also created in order to simulate the system before real-time implementation. The FEM (Finite Element Method) is a popular method in modeling structural flexibility.

The VDC controller was implemented with success. The L_2 and L_∞ stabilities of the subsystems were mathematically shown, leading to the guaranteed stability of the entire system. The results of this thesis show promise in the use of the VDC approach in controlling flexible arms with hydraulic actuation.

TIIVISTELMÄ

PETRI MÄKINEN: Yksivapausasteisen joustavan hydraulirobotin mallinnus ja säätö
Tampereen teknillinen yliopisto
Diplomityö, 71 sivua, 9 liitesivua
Lokakuu 2016
Automaatiotekniikan koulutusohjelma
Pääaine: Koneautomaatio
Tarkastajat: Prof. Jouni Mattila
Avainsanat: Virtual decomposition control, joustava käsivarsi, osaelementtimalli, puomimalli

Entistä kevyempien rakennusmateriaalien käyttö robottikäsivarsissa sekä muissa manipulaattoreissa vähentää kustannuksia sekä kasvattaa manipulaattorin hyötykuorman ja painon suhdetta. Kevyet materiaalit luonnollisesti lisäävät rakenteen joustoa, mikä aiheuttaa haasteita erityisesti manipulaattorin kärjen tarkan asemasäädön näkökulmasta.

Tässä opinnäytetyössä tarkastellaan yksivapausasteista manipulaattoria, joka koostuu joustavasta puomista sekä jäykästä tukirakenteesta. Puomin dimensiot ovat $60 \times 60 \times 3$ mm ja kokonaispituus 4.5 m. Puomin päähän on kiinnitetty 60 kg:n massa ja kääntönivelen liike on toteutettu hydraulisylinterillä.

Työn tarkoituksena on toteuttaa VDC (Virtual Decomposition Control) tyyppinen säädin ja testata sen suorituskykyä joustavan rakenteen säädössä. VDC on mallipohjainen ja epälineaarinen säätötapa, joka on kehitetty erityisesti huomattavan määrän vapausasteita omaavien robottien tarkkaan säätöön. Perusajatus VDC:ssä on monimutkaisen robotin jako alisysteemeihin, jolloin kunkin alisysteemin dynamiikka pysyy suhteellisen yksinkertaisena. Puomille muodostettiin myös osaelementtimalli (finite element model) simulointitarkoituksia varten.

Säädin toteutettiin menestyksekkäästi ja sen suorituskykyä testattiin reaaliaikajärjestelmässä. Alisysteemien L_2 ja L_∞ stabiiliudet osoitettiin matemaattisesti VDC teorian mukaisesti, johtaen koko järjestelmän taattuun stabiiliuteen. Mittaustulosten perusteella VDC:n käyttö hydraulisesti aktuoitujen joustavien manipulaattoreiden säädössä näyttää lupaavalta.

PREFACE

This master's thesis was part of a research project conducted at the department of Intelligent Hydraulics and Automation (IHA) in Tampere University of Technology (TUT).

First, I would like to express my gratitude to my supervisor, prof. Jouni Mattila, for giving me this opportunity, providing an interesting topic and guidance during this work. I also thank Mohammad Thabet for providing the dynamic observer, which was needed for this thesis to be finished. Also a shout-out to Janne Koivumäki for his insight and advice with the VDC approach.

Secondly, thanks to Jarkko and Mikael for all the laughs and making these years go fly by. Finally, thanks to my parents for their endless support.

Tampere, 21.10.2016

Petri Mäkinen

TABLE OF CONTENTS

LIST OF ABBREVIATIONS AND SYMBOLS

AMM	Assumed Modes Method
DOF	Degree of Freedom
DPS	Distributed Parameter System
FE	Finite Element
FEM	Finite Element Method
IMU	Inertial Measurement Unit
VCP	Virtual Cutting Point
VDC	Virtual Decomposition Control
VPF	Virtual Power Flow

α_n	load distribution factor, $n \in \{1,2\}$
α_{ray}	Rayleigh damping coefficient related to mass
$\{\mathbf{A}\}$	a coordinate system (or frame)
β_{ray}	Rayleigh damping coefficient related to stiffness
$\mathbf{C}$	Rayleigh damping matrix
$\mathbf{C_A}(^{\mathbf{A}}\omega)$	centrifugal and Coriolis forces related to frame $\{\mathbf{A}\}$
E	Young's modulus of elasticity
$^{T_{cc}}\eta$	internal force/moment vector related to the closed chain
$^{T_{cc}}\eta_r$	required internal force/moment vector related to the closed chain
$^{\mathbf{A}}f$	force vector related to frame $\{\mathbf{A}\}$
$^{\mathbf{A}}f^*$	net force vector related to frame $\{\mathbf{A}\}$
$^{\mathbf{A}}F$	force/moment vector related to frame $\{\mathbf{A}\}$
$^{\mathbf{A}}F_r$	required force/moment vector related to frame $\{\mathbf{A}\}$
$^{\mathbf{A}}F^*$	net force/moment vector related to frame $\{\mathbf{A}\}$
g	acceleration due to gravity
$\mathbf{G_A}$	gravitation force related to frame $\{\mathbf{A}\}$
G_e	element gravity vector
I	cross-sectional area moment of inertia
$\mathbf{I_A}$	moment of inertia related to frame $\{\mathbf{A}\}$
$\mathbf{I}_0$	moment of inertia around a center mass
$\mathbf{I}_3$	3×3 identity matrix
$\mathbf{K}$	global stiffness matrix
K_e	element potential energy

$\mathbf{K}_{qq}$	flexible terms of the global stiffness matrix
$\mathbf{K}_e$	element stiffness matrix
L	Lagrangian
L_2	Lebesgue space L_2
L_∞	Lebesgue space L_∞
${}^{\mathbf{A}}m$	moment vector related to frame $\{\mathbf{A}\}$
${}^{\mathbf{A}}m^*$	net moment vector related to frame $\{\mathbf{A}\}$
$m_{\mathbf{A}}$	rigid body mass related to frame $\{\mathbf{A}\}$
m_{tip}	load mass at the tip of the boom
$\mathbf{M}$	global mass matrix
$\mathbf{M}_{\mathbf{A}}$	mass matrix related to frame $\{\mathbf{A}\}$
$M_{\theta\theta}$	rigid term of the global mass matrix
$\mathbf{M}_{qq}$	flexible terms of the global mass matrix
$M_{\theta q}$	coupling term of the global mass matrix
$M_{q\theta}$	coupling term of the global mass matrix
$\mathbf{M}_e$	element mass matrix
${}^{\mathbf{A}}\omega$	angular velocity vector related to frame $\{\mathbf{A}\}$
$p_{\mathbf{A}}$	virtual power flow related to frame $\{\mathbf{A}\}$
Φ_n	Hermite polynomial, $n \in \{1,2,3,4\}$
${}^{\mathbf{A}}\mathbf{R}_{\mathbf{B}}$	a rotation matrix
$({}^{\mathbf{A}}r_{\mathbf{AB}}\times)$	a skew-symmetric matrix
ρ	mass per unit length
$\Theta_{\mathbf{A}}$	parameter vector related to frame $\{\mathbf{A}\}$
T_e	element kinetic energy
${}^{\mathbf{A}}\mathbf{U}_{\mathbf{B}}$	a transformation matrix
${}^{\mathbf{A}}v$	velocity vector related to frame $\{\mathbf{A}\}$
${}^{\mathbf{A}}V$	linear/angular velocity vector related to frame $\{\mathbf{A}\}$
${}^{\mathbf{A}}V_r$	required linear/angular velocity vector related to frame $\{\mathbf{A}\}$
x_d	desired piston position
x_r	required piston position
$\dot{x}_d$	desired piston velocity
$\dot{x}_r$	required piston velocity
$\mathbf{Y}_{\mathbf{A}}$	regressor matrix related to frame $\{\mathbf{A}\}$

1. INTRODUCTION

Steel is perhaps the single most important material of the humankind. It has been used avidly ever since its mass production began in the 19th century. Mainly composed of iron and carbon, steel can be combined into numerous alloys with different substances. Adding chromium results in stainless steel, for example. Steel alloys are heavily used in construction and machinery. The most considerable improvement in structural steel over the years has been increasing its strength. Two material-specific variables are used: The yield strength is the limit, after which a structural deformation is permanent, while the tensile strength is the point, where the tension is enough to break the structure. The type of steel used in this work has a yield strength of 700 MPa and a tensile strength of $750-950$ MPa. Young's modulus, also known as elastic modulus, is a measure that describes material's ability to resist elastic deformation applied by a force. An non-permanent deformation is called elastic, while a permanent one is called plastic. Relative deformation can be defined as the quotient of the strain and the total length of a given object. Very strong steel, like the one used in this work, is highly flexible due to the fact that as the strength increases, the elastic modulus hardly changes. Thus, the structure will flex more.

Robotic manipulators with lightweight, flexible links are becoming common in the manufacturing industry. The trend is to build lighter, more efficient robot manipulators that have a high payload to weight ratio. This is achieved by using lighter materials, which understandably increases structural flexibility. However, using lightweight and especially long links causes the tip end to vibrate, along with deflection. Tip deflections and vibration are both very problematic, when it comes to control. With less flexing links it is typical that the vibration is simply waited out, but with truly flexible links the controller needs to be able to effectively dampen the vibration.

Modeling flexible structures is a well developed field of engineering. The finite element method (FEM) used in this work being perhaps the most common one. There are many commercial softwares for generalized formulation of the finite elements. Another popular method for modeling flexible structures is the assumed modes method (AMM), used for

example in [10] to model a flexible crane structure and in [4] along with the Langrange approach to derive an infinite dimensional dynamic model of a single-link flexible manipulator. The FEM and AMM are distributed parameter systems (DPS), which are considered infinite dimensional and are described by partial differentiation equations. Hence, there are variables of interest as a function of time and one or more spatial variables. Lumped parameter systems can also be used to model flexible systems. These are simple spring and mass models, generally based on ordinary differential equations and the variables of interest are as a function of time only. Flexible links can be considered continuous, or infinite dimensional dynamical systems. Building a model or designing a controller for a system with infinite degrees of freedom is not practically possible. The systems are discretized using finite elements, assumed modes or lumped parameter methods, which gives an estimate of the infinite dimensional system. An extensive literature review on dynamic analysis of flexible manipulators was conducted in [2]. In a more recent literature review [12], intelligent control techniques for flexible manipulators were studied in addition to dynamic analysis. The control techniques under review were fuzzy logic, neural network and genetic algorithm.

Control of single-link flexible manipulators has been under research in the recent years. A relatively simple method was explored in [14], where strain feedback and acceleration feedback, separately, were used in combination with a PID controller. Both control designs improved the stability and yielded a faster system response. Backstepping control schemes for tip tracking of a single-link flexible manipulator were developed in [15] and [4], with good results. An approximation of the tip position was utilized in both papers. A flexible beam in a gravitational field was studied in [9] and [11]. In [17], the virtual decomposition control (VDC) approach was applied for the first time to the control problem of flexible link robots, in simulation, with success.

Dynamics based control takes advantage of the mathematical representation of robots, which can be relatively easily formed by using for example Denavit-Hartenberg parameters to derive forward kinematics. Known dynamics of a robot can be utilized to apply feedforward control to the given system. An ideal feedforward loop's transfer function would be the exact inverse of the system to be controlled, which would make the perfect controller. Inverse kinematics of a robot can be derived by using the Lagrangian formulation, for instance. In the real world, however, feedforward is never fully accurate. A feedback loop can be paired with the feedforward to increase the controller's performance. In this kind of dynamics based control, the feedforward loop should be designed as close to the real system as possible for it to be useful. The VDC approach is dynamics

based, utilizing both feedforward and feedback.

The target system of this master's thesis is a 1-degree of freedom (DOF) flexible beam attached to a rigid base structure. A hydraulic cylinder is used to actuate the rotating joint of the system. The flexible beam is modeled using the FEM and connected to a model of the hydraulic circuit. A dynamic controller is developed for driving the system, while simultaneously dampening vibrations. For this, the VDC approach is applied. The stability of the control system is proven via the VDC theory. The goal of this thesis is to apply the VDC approach to the target system and effectively control the tip position of the flexible beam, while guaranteeing the L_2 and L_∞ stability of the system. Due to the complexity of the controller, simulation is used in the development.

In scope of this thesis, parameter adaption in the VDC formulation is not implemented. Furthermore, only the necessary presentations of the load distribution factor and internal force vector formulation, associated with the VDC, are given. The modeling of the hydraulic circuit, the cylinder and the servo valve, are not presented, as their presence in this thesis is trivial and their formulations are easily found in the literature. Despite this, the hydraulics are modeled in the context of the VDC formulation.

The structure of the thesis is outlined as follows: The studied system is first introduced, followed by the presentation of mathematical preliminaries necessary to understand this thesis. The modeling of the system for simulation purposes is then formulated using the FEM procedure. After this, the VDC approach is applied to the system. The virtual stability of the system is also shown. Results are then presented, along with discussion. Finally, a conclusion is given.

2. TARGET SYSTEM

The target system of this thesis is presented in Fig. 2.1. A single beam of steel, 4.5 meters in total length, is attached to the base structure that is assumed rigid. The type of steel used is Strenx Tube 700MH, manufactured by SSAB, which is a high frequency welded cold-formed structural hollow section made of hot-rolled high-strength steel with a minimum yield strength of 700 MPa. The dimensions of the beam cross-section are $60 \times 60 \times 3$ mm. A load mass of 60 kg is bolted near the tip end. The system is interpreted as a single-link flexible manipulator.

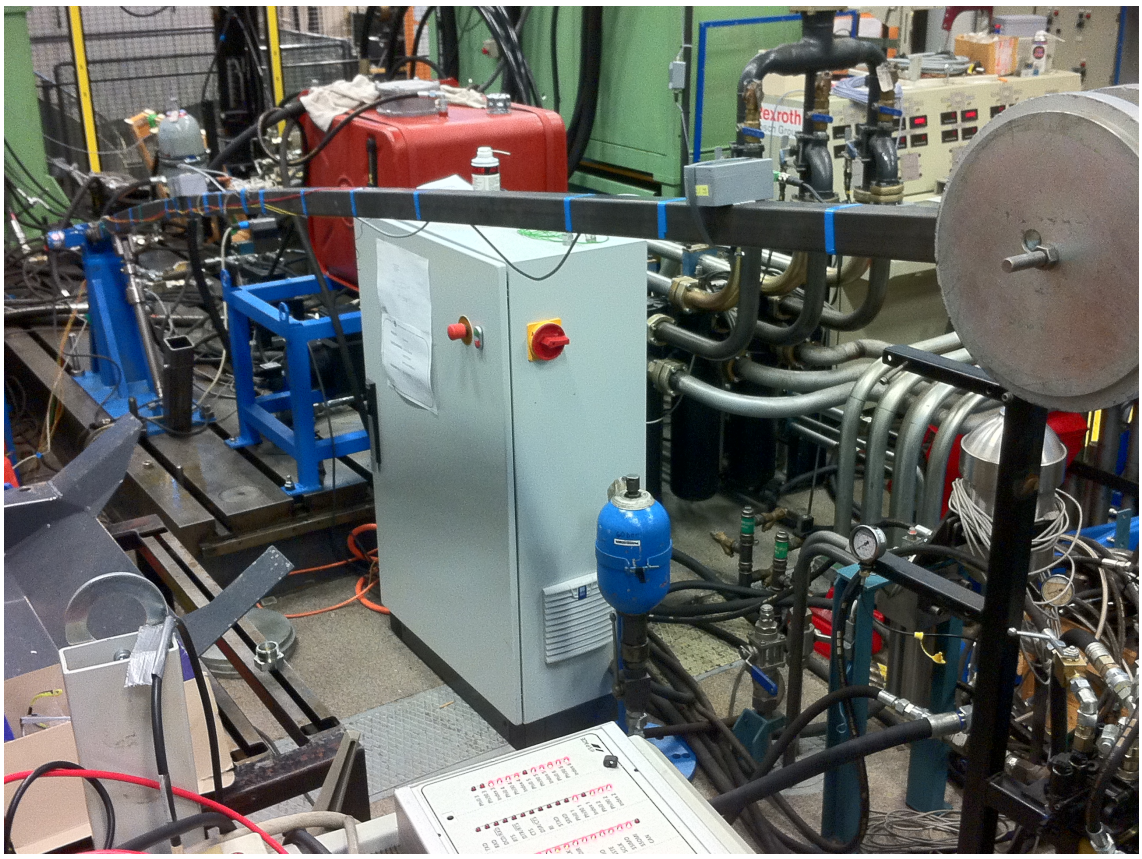

Figure 2.1 *The 1-DOF boom.*

The dimensions of the base structure are given in Fig. 2.2. Unlike in the figure, the boom can not reach a fully horizontal level. The minimum length of the hydraulic cylinder is 570 mm, which leads to a boom angle of 22.68° at rest.

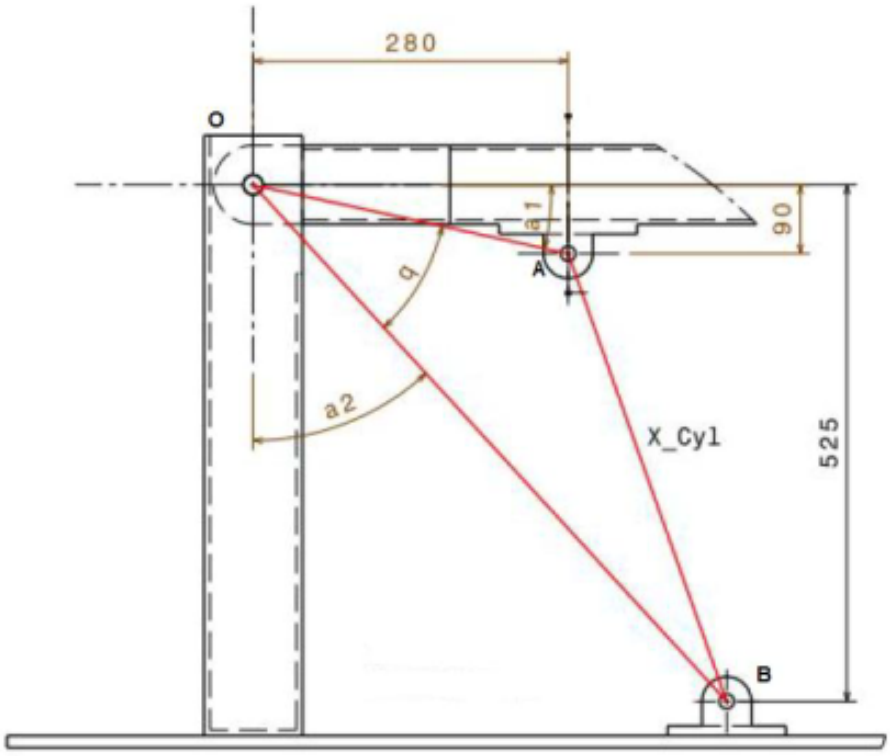

Figure 2.2 *Geometric dimensions of the base structure.*

Table 2.1 presents the numerical values of the angles. The hydraulics are composed of a hydraulic cylinder of size $\oslash 35/25-300$ mm, manufactured by Konepaja Ketola. The servo valve used is model 4WRPEH by Bosch Rexroth, with nominal flow of $2-40$ l/min at $\Delta p = 70$ bar and a maximum supply pressure of 315 bar.

Table 2.1 *Base structure angles.*

a_1	a_2	q
17.82°	40.16°	32.02°

The hydraulics are powered by a machinery by Bosch Rexroth, composed of three 200 kW pumps. Only one of the pumps is in the same circuit with the target system. The

maximum supply pressure of the machinery is 320 bar, while the maximum produced flow is 260 l/min. A pressure relief valve is also part of the machinery.

3. MATHEMATICAL PRELIMINARIES

In this chapter the most important mathematical concepts are introduced and defined, which are used throughout this thesis. These concepts are mainly used in formulating the VDC, hence this chapter is based heavily on [16] and [6].

First, a basic coordinate system is introduced along with vectors, followed by expressing orientation via rotation matrix. Then, definitions for linear/angular velocity and force/moment vectors in a body frame are given. The duality of these vectors is also established. Next, the formulation for rigid body dynamics is given, along with a linear parametrized form. After that, *virtual cutting points* and oriented graphs are introduced. Finally, the concept of virtual stability is explored.

3.1 Frames and orientation

For simplicity, the coordinate systems used in this thesis are called frames. These frames are constructed by three mutually orthogonal three-dimensional unit vectors as bases. Such a frame can be represented as $\{\mathbf{A}\} = [\vec{x},\ \vec{y},\ \vec{z}]$. [16, p. 24].

Rotation matrices are used for coordinate transformations and in this thesis frames are needed to rotate only about their $\vec{z}$-axis. This type of rotation matrix is defined as [5, p. 36]

$$ {}^{\mathbf{A}}\mathbf{R}_{\mathbf{B}} = \begin{bmatrix} \cos(\theta) & -\sin(\theta) & 0 \\ \sin(\theta) & \cos(\theta) & 0 \\ 0 & 0 & 1 \end{bmatrix}, \tag{3.1} $$

which describes the rotation of frame $\{\mathbf{B}\}$ with respect to frame $\{\mathbf{A}\}$. The θ denotes the orientation angle between the two frames.

3.2 Linear/angular and force/moment vectors

Let ${}^{\mathbf{A}}v \in \mathbb{R}^3$ and ${}^{\mathbf{A}}\omega \in \mathbb{R}^3$ be the linear and angular velocity vectors of frame $\{\mathbf{A}\}$, also expressed in frame $\{\mathbf{A}\}$. Similarly, let ${}^{\mathbf{A}}f \in \mathbb{R}^3$ and ${}^{\mathbf{A}}m \in \mathbb{R}^3$ be the linear force and moment vectors applied to frame $\{\mathbf{A}\}$. The linear/angular velocity and force/moment vectors of frame $\{\mathbf{A}\}$ are now defined as follows [16, pp. 28-29]:

$$ {}^{\mathbf{A}}V = \begin{bmatrix} {}^{\mathbf{A}}v \\ {}^{\mathbf{A}}\omega \end{bmatrix} \in \mathbb{R}^6, \quad {}^{\mathbf{A}}F = \begin{bmatrix} {}^{\mathbf{A}}f \\ {}^{\mathbf{A}}m \end{bmatrix} \in \mathbb{R}^6. \tag{3.2} $$

Vectors of these formats are used throughout the VDC formulation.

3.3 The duality of linear/angular velocity and force/moment transformations

Consider a rigid body moving freely and being subject to a pair of physical force and moment vectors. Also, let frame $\{\mathbf{A}\}$ and frame $\{\mathbf{B}\}$ be fixed to the rigid body. The dual nature of the linear/angular and force/moment transformations entails that

$$ {}^{\mathbf{B}}V = {}^{\mathbf{A}}\mathbf{U}_B^T {}^{\mathbf{A}}V \tag{3.3} $$

$$ {}^{\mathbf{A}}F = {}^{\mathbf{A}}\mathbf{U}_B {}^{\mathbf{B}}F \tag{3.4} $$

hold. Here

$$ {}^{\mathbf{A}}\mathbf{U}_{\mathbf{B}} = \begin{bmatrix} {}^{\mathbf{A}}\mathbf{R}_{\mathbf{B}} & \mathbf{0}_{3\times3} \\ ({}^{\mathbf{A}}\mathbf{r}_{\mathbf{AB}}\times){}^{\mathbf{A}}\mathbf{R}_{\mathbf{B}} & {}^{\mathbf{A}}\mathbf{R}_{\mathbf{B}} \end{bmatrix} \in \mathbb{R}^{6\times6} \tag{3.5} $$

is a transformation matrix that transforms the force/moment vector measured and expressed in frame $\{\mathbf{B}\}$ to the corresponding force/moment vector measured and expressed in frame $\{\mathbf{A}\}$. The expression $({}^{\mathbf{A}}\mathbf{r}_{\mathbf{AB}}\times)$ denotes a skew-symmetric matrix that is defined as follows:

$$ ({}^{\mathbf{A}}r_{\mathbf{AB}}\times) = \begin{bmatrix} 0 & -{}^{\mathbf{A}}r_z & {}^{\mathbf{A}}r_y \\ {}^{\mathbf{A}}r_z & 0 & -{}^{\mathbf{A}}r_x \\ -{}^{\mathbf{A}}r_y & {}^{\mathbf{A}}r_x & 0 \end{bmatrix}, \quad {}^{\mathbf{A}}r_{\mathbf{AB}} \in \mathbb{R}^3. \tag{3.6} $$

The denotation ${}^{\mathbf{A}}r_{\mathbf{AB}}$ depicts a vector from the origin of frame $\{\mathbf{A}\}$ to the origin of frame $\{\mathbf{B}\}$, expressed in frame $\{\mathbf{A}\}$. [16, p. 26-29]

3.4 Rigid body dynamics in a body frame

First, similar to (3.2), the net (summation) force/moment vector measured and expressed in frame $\{\mathbf{A}\}$ is defined as

$$^{\mathbf{A}}F^* = \begin{bmatrix} ^{\mathbf{A}}f^* \\ ^{\mathbf{A}}m^* \end{bmatrix} \in \mathbb{R}^6, \tag{3.7}$$

where $^{\mathbf{A}}f^*$ and $^{\mathbf{A}}m^*$ are the net force and moment vectors that are applied to the rigid body. Again, let frames $\{\mathbf{A}\}$ and $\{\mathbf{B}\}$ be fixed to a rigid body. The dynamics of the rigid body are expressed in frame $\{\mathbf{A}\}$, while frame $\{\mathbf{B}\}$ is located at the center of mass of the body. [16, p. 30] The equation for rigid body dynamics using the net force is written as:

$$^{\mathbf{A}}F^* = \mathbf{M}_{\mathbf{A}}\frac{d}{dt}(^{\mathbf{A}}V) + \mathbf{C}_{\mathbf{A}}(^{\mathbf{A}}\omega)^{\mathbf{A}}V + \mathbf{G}_{\mathbf{A}}, \tag{3.8}$$

where $\mathbf{M}_{\mathbf{A}}$ denotes the mass matrix, $\mathbf{C}_{\mathbf{A}}(^{\mathbf{A}}\omega)$ denotes the centrifugal and Coriolis forces and $\mathbf{G}_{\mathbf{A}}$ denotes gravity terms of the rigid body. The mass matrix is formulated as

$$\mathbf{M}_{\mathbf{A}} = \begin{bmatrix} m_{\mathbf{A}}\mathbf{I}_3 - m_{\mathbf{A}}(^{\mathbf{A}}r_{\mathbf{AB}}\times) & -m_{\mathbf{A}}(^{\mathbf{A}}r_{\mathbf{AB}}\times) \\ m_{\mathbf{A}}(^{\mathbf{A}}r_{\mathbf{AB}}\times) & \mathbf{I}_{\mathbf{A}} - m_{\mathbf{A}}(^{\mathbf{A}}r_{\mathbf{AB}}\times)^2 \end{bmatrix} \in \mathbb{R}^{6\times 6}, \tag{3.9}$$

$$\mathbf{I}_{\mathbf{A}} = ^{\mathbf{A}}\mathbf{R}_{\mathbf{I}}\mathbf{I}_o(t)^{\mathbf{I}}\mathbf{R}_{\mathbf{A}} \tag{3.10}$$

in which $\mathbf{I}_3$ denotes a 3×3 identity matrix and $m_{\mathbf{A}} \in \mathbb{R}$ denotes the mass of the rigid body. The moment of inertia expressed in frame $\{\mathbf{A}\}$ is defined in (3.10), where the moment of inertia matrix around the center mass is denoted by $\mathbf{I}_o(t) \in \mathbb{R}^{3\times 3}$. The centrifugal and Coriolis terms are derived as follows:

$$\mathbf{C}_{\mathbf{A}}(^{\mathbf{A}}\omega) = \begin{bmatrix} C_{11} & C_{12} \\ C_{21} & C_{22} \end{bmatrix} \in \mathbb{R}^{6\times 6}, \tag{3.11}$$

where

$$\begin{aligned} C_{11} &= m_{\mathbf{A}}(^{\mathbf{A}}\omega\times) \\ C_{12} &= -m_{\mathbf{A}}(^{\mathbf{A}}\omega\times)(^{\mathbf{A}}r_{\mathbf{AB}}\times) \\ C_{21} &= m_{\mathbf{A}}(^{\mathbf{A}}r_{\mathbf{AB}}\times)(^{\mathbf{A}}\omega\times) \\ C_{22} &= (^{\mathbf{A}}\omega\times)\mathbf{I}_{\mathbf{A}} + \mathbf{I}_{\mathbf{A}}(^{\mathbf{A}}\omega\times) - m_{\mathbf{A}}(^{\mathbf{A}}r_{\mathbf{AB}}\times)(^{\mathbf{A}}\omega\times)(^{\mathbf{A}}r_{\mathbf{AB}}\times). \end{aligned}$$

Here $({}^{\mathbf{A}}\boldsymbol{\omega}\times) \in \mathbb{R}^{3\times3}$ is a skew-symmetric matrix containing angular velocities. The gravity terms are presented as

$$\mathbf{G_A} = \begin{bmatrix} m_{\mathbf{A}}{}^{\mathbf{A}}\mathbf{R_I}\, g \\ m_{\mathbf{A}}({}^{\mathbf{A}}r_{\mathbf{AB}}\times){}^{\mathbf{A}}\mathbf{R_I}\, g \end{bmatrix} \in \mathbb{R}^6, \tag{3.12}$$

where $g = [0;\ 9.81;\ 0]^T \in \mathbb{R}^3$. The gravity vector may vary, depending on how the frames are chosen. Finally, a linear parametrized expression, based on (3.8), is defined:

$$\mathbf{Y_A}\Theta_\mathbf{A} = \mathbf{M_A}\frac{d}{dt}({}^{\mathbf{A}}V_r) + \mathbf{C_A}({}^{\mathbf{A}}\boldsymbol{\omega}){}^{\mathbf{A}}V_r + \mathbf{G_A}, \tag{3.13}$$

where ${}^{\mathbf{A}}V_r \in \mathbb{R}^6$ is the required vector of ${}^{\mathbf{A}}V \in \mathbb{R}^6$. [16, pp. 31-32] Velocity vectors and their required counterparts are a key aspect in the design of the VDC. The regressor matrix $\mathbf{Y_A} \in \mathbb{R}^{6\times13}$ and the parameter vector $\Theta_\mathbf{A} \in \mathbb{R}^{6\times13}$ are detailed later in the virtual decomposition control chapter.

3.5 Virtual cutting points and oriented graphs

According to Zhu [16, p. 34]: "The concept of the virtual *cutting point* is central to the VDC approach." Practically this concept means that a complex robot is divided into subsystems by placing virtual *cutting points* in suitable positions along the robot. The precise definition for a virtual *cutting point* is given by Zhu in [16, p. 34]:

Definition 3.1. *A cutting point is a directed separation interface that conceptually cuts trough a rigid body. At the cutting point, the two parts resulting from the virtual cut maintain equal position and orientation. The cutting point is interpreted as a driving cutting point by one part and is simultaneously interpreted as a driven cutting point by another part. A force vector $\boldsymbol{f} \in \mathbb{R}^3$ and a moment vector $\boldsymbol{m} \in \mathbb{R}^3$ are exerted from one part to which the cutting point is interpreted as a driving cutting point to the other part to which the cutting point is interpreted as a driven cutting point.*

In other words, the robot is virtually decomposed into sub-domains that all have their own dynamics and control equations. This will be shown later in the virtual decomposition chapter. After a robot is virtually cut into subsystems, the entire system's structure is depicted by using a simple oriented graph, which represents the topological structure and control relations of the system. The concept of a simple oriented graph is an important aspect of the VDC formulation and its definition is also given by Zhu in [16, p. 34]:

Definition 3.2. *A graph consists of nodes and edges. A directed graph is a graph in which all the edges have directions. An oriented graph is a directed graph in which each edge has a unique direction. A simple oriented graph is an oriented graph in which no loop is formed.*

A node represents a subsystem and a directed edge represents a *cutting point*. The direction of an edge defines the reference direction of forces and moments passing through the corresponding *cutting point*. The forces and moments are exerted from the subsystem of which the *cutting point* is interpreted as a *driving cutting point* to the adjacent subsystem to which the *cutting point* is interpreted as a *driven cutting point*. Some nodes also act as source or sink nodes, which only have pointing-away or pointing-to edges, respectively. [16, pp. 34-35]

3.6 Virtual stability

Being divided into subsystems, the stability of the entire complex system becomes a concern. Suitable properties for each subsystem must be determined in order to achieve stability of the entire system. In this section *virtual stability*, which is another central concept of the VDC approach, is defined.

First, Lebesgue space is introduced, followed by non-negative accompanying functions. *Virtual power flows* are then presented, along with the *virtual stability*. In scope of this thesis, only shortened versions of the concepts necessary for understanding the VDC approach are presented.

3.6.1 Lebesgue space

Two definitions concerning Lebesgue space are given by Zhu in [16, p. 15]:

Definition 3.3. *Lebesgue space, denoted as L_p with p being a positive integer, contains all Lebesgue measurable and integrable functions $f(t)$ subject to*

$$\|f\|_p = \lim_{T\to\infty}\left[\int_0^T |f(t)|^p d\tau\right]^{\frac{1}{p}} < +\infty. \tag{3.14}$$

Two important cases are given:

(a) A Lebesgue measurable function $f(t)$ belongs to L_2 if and only if $\lim_{T\to\infty}\int_0^T |f(t)|^2 d\tau < +\infty$.

(b) A Lebesgue measurable function $f(t)$ belongs to L_∞ if and only if $\max_{t\in[0,\infty)]} |f(t)| < +\infty$.

Definition 3.4. *A vectored Lebesgue measurable function*

$$\mathbf{f}(t) = [f_1(t), f_2(t), ..., f_n(t)]^T \in L_p,\ p = 1,2,...,\infty,\ implies\ f_i(t) \in L_p \tag{3.15}$$

for all $i \in \{1,n\}$.

Lebesgue spaces, namely L_2 and L_∞, have substantive roles in the concept of *virtual stability*.

3.6.2 Non-negative accompanying functions

Non-negative accompanying functions are used as a tool in stability and convergence analysis. Zhu provides the following definition in [16, p. 35]:

Definition 3.5. *A non-negative accompanying function* $\nu(t) \in \mathbb{R}$ *is a piecewise differentiable function possessing the following properties:*

(i) $\nu(t) \geq 0$ *for* $t > 0$, *and*

(ii) $\dot{\nu}(t)$ *exists almost everywhere*.

Every subsystem (or node in a simple oriented graph) is assigned a non-negative accompanying function.

3.6.3 Virtual power flow

The definition of *virtual power flow* is presented by Zhu in [16, p. 35]:

Definition 3.6. *With respect to frame* $\{\boldsymbol{A}\}$, *the virtual power flow (VPF) is defined as the inner product of the linear/angular velocity vector error and the force/moment vector error, that is*

$$p_{\mathbf{A}} = ({}^{\mathbf{A}}V_r - {}^{\mathbf{A}}V)^T - ({}^{\mathbf{A}}F_r - {}^{\mathbf{A}}F), \tag{3.16}$$

where ${}^{\boldsymbol{A}}V_r \in \mathbb{R}^6$ *and* ${}^{\boldsymbol{A}}F_r \in \mathbb{R}^6$ *represent required (design) vectors of* ${}^{\boldsymbol{A}}V \in \mathbb{R}^6$ *and* ${}^{\boldsymbol{A}}F \in \mathbb{R}^6$*, respectively.*

Again, let two frames $\{\mathbf{A}\}$ and $\{\mathbf{B}\}$ be attached to a rigid body. Assuming that the required linear/angular velocity and force/moment vectors are subject to the same constraints as the linear/angular and force/moments, it is evident that

$$ {}^{\mathbf{B}}V_r = {}^{\mathbf{A}}\mathbf{U}_B^T {}^{\mathbf{A}}V_r \tag{3.17} $$

$$ {}^{\mathbf{A}}F_r = {}^{\mathbf{A}}\mathbf{U}_B {}^{\mathbf{B}}F_r \tag{3.18} $$

hold. From (3.3), (3.4) and (3.16)-(3.18) it follows that

$$ p_{\mathbf{A}} = p_{\mathbf{B}} \tag{3.19} $$

also holds.

3.6.4 Virtual stability analysis

Considering the Lebesgue spaces, non-negative accompanying functions and VPFs, Zhu presents the following definition for *virtual stability* [16, p. 36]:

Definition 3.7. *A subsystem that is virtually decomposed from a complex robot is said to be virtually stable with its affiliated vector* $\boldsymbol{x}(t)$ *being a virtual function in* L_∞ *and its affiliated vector* $\boldsymbol{y}(t)$ *being a virtual function in* L_2*, if and only if there exists a non-negative accompanying function*

$$ v(t) \geq \frac{1}{2}\mathbf{x}(t)^T \mathbf{P}\mathbf{x}(t) \tag{3.20} $$

such that

$$ \dot{v}(t) \leq -\mathbf{y}(t)^T \mathbf{Q}\mathbf{y}(t) - s(t) + \sum_{\{\mathbf{A}\}\in\boldsymbol{\Phi}} p_{\mathbf{A}} - \sum_{\{\mathbf{C}\}\in\boldsymbol{\Psi}} p_{\mathbf{C}} \tag{3.21} $$

holds, subject to

$$ \int_0^\infty s(t)d\tau \geq -\gamma_s \tag{3.22} $$

with $0 \leq \gamma_s < \infty$*, where* $\boldsymbol{P}$ *and* $\boldsymbol{Q}$ *are two block-diagonal positive-definite matrices, set* $\boldsymbol{\Phi}$ *contains frames being placed at the driven cutting points of this subsystem and set* $\boldsymbol{\Psi}$ *contains frames being placed at the driving cutting points of this subsystem, and* $p_{\boldsymbol{A}}$ *and* $p_{\boldsymbol{C}}$ *denote the virtual power flows in Definition 3.6.*

The definition is followed by a lemma, which shows that two adjacent subsystems that are *virtually stable* are equivalent to a single subsystem that is *virtually stable*.

Lemma 3.1. *Every two adjacent subsystems that are virtually stable can be equivalent to a single subsystem that is virtually stable in the sense of Definition 3.7. Every virtual function in L_p affiliated with any one of the two adjacent subsystems remains to be a virtual function in L_p affiliated with the equivalent subsystem for $p = 2, \infty$.*

Lemma 3.1 and proof for it can be found in [16, p. 37]. If every subsystem of a complex robot is *virtually stable* with regard to Definition 3.7, the following thorem, presented by Zhu in [16, p. 38] with proof, ensures that the L_2 and L_∞ stability of the entire complex robot can be guaranteed.

Theorem 3.1. *Consider a complex robot that is virtually decomposed into subsystems and is represented by a simple oriented graph as in Definition 3.2. If every subsystem is virtually stable in the sense of Definition 3.7, then all virtual functions in L_2 are functions in L_2 and all virtual functions in L_∞ are functions in L_∞.*

The theoretical background for proving the *virtual stability* of a VDC-type controller is now given. The *virtual stability* of each subsystem will be proven individually, which leads to the *virtual stability* of the entire system.

4. MODELING THE FLEXIBLE BEAM

This chapter presents the procedure of modeling the target system as a flexible structure. The FEM along with the Euler-Bernoulli beam theory are used to derive the system equations for the rotating flexible beam.

The chapter is sectioned as follows: firstly, the FEM is described at a general level. Then, the mathematical equations for modeling a rotating flexible beam are given, followed by the system matrix formulation and diagonalization. Finally, the system equations are expanded by adding gravity and damping to the model.

4.1 The finite element method

Modeling systems is an essential aspect of modern engineering science. Mathematical equations are derived in order to model a system's behavior. With complex systems, these are often partial differential equations, which are challenging to solve. Along with modern computational power, different numerical solution techniques have been developed in attempt to solve these equations. The FEM is one such technique and it is a popular and powerful tool in analyzing systems. Most often the FEM is used for deformation and stress analysis of all kinds of mechanical structures, for example buildings, bridges, cars and aircraft. Another type of application is field analysis that includes fluid flow, magnetic flux and other problems related to flow. [1, p. 1]

The fundamental idea of the FEM is to discretize a complex region defining a continuum into simple geometric shapes called finite elements. The material properties, such as density and elasticity, along with governing relationships are considered over the elements and expressed in terms of unknown values at element corners. The element corners are also called nodes. Global governing equations are formed by assembling the elements together, while considering loading and constraints of the system. The solution of the global governing equations give an approximate behavior of the continuum. [1, p. 1]

A major advantage of the FEM is that its formulation can be developed into a general purpose software [8, p. 1]. For example ANSYS and Autodesk Software are such programs. In this thesis, however, a general purpose software is not used. Instead, the modeling and the FE procedure are conducted using Matlab, since from a structural point of view the target system is quite simple.

4.2 Euler-Bernoulli beam

The flexible beam of the target system is modeled by using Euler-Bernoulli beam theory, which incorporates the following assumptions [16, p. 354]:

- The beam is slender with uniform geometric and inertial characteristics.
- The beam is flexible in the lateral direction and stiff with respect to the axial force and to the axial torsion.
- The beam has no shear deformation or distributed moment of inertia.
- The beam is restricted in a plane with no motion in the x-axis.
- No gravity is considered.

The beam is divided into elements that each has two nodes, one at each end. A single beam element is presented in Fig. 4.1. Slope ϑ , also called rotation angle, and vertical

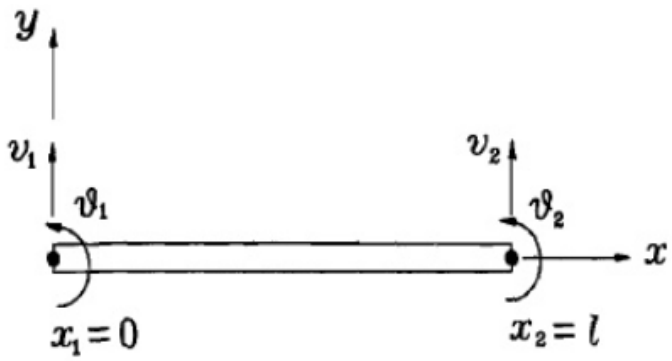

Figure 4.1 *A beam element [8, p. 236].*

deformation υ are the nodal variables. This ensures that any two neighboring elements have a continuous slope and deflection between them, which is a requirement from a

theoretical standpoint [1, p. 242]. The nodal variables contain the information of the magnitude of the beam's deformation. Equations for a rotating Euler-Bernoulli beam are presented in the next section.

4.3 Rotating flexible beam

Modeling of the beam and applying the FEM is done in accordance with [8, pp. 465-467]. A rotating flexible beam in planar coordinates can be described by its equations of motion:

$$I_c\ddot{\theta} + \int_{l_0}^{l} \rho x(\ddot{w} + x\ddot{\theta})dx + m_{tip}l(l\ddot{\theta} + \ddot{w}(l,t)) + I_t(\ddot{\theta} + \ddot{w}'(l,t)) = u \tag{4.1}$$

$$\rho(\ddot{w} + x\ddot{\theta}) + EI\frac{\partial^4 w}{\partial x^4} = 0, \tag{4.2}$$

where ρ denotes mass per unit length, E denotes Young's modulus, I denotes cross-sectional area moment of inertia of the beam about its neutral axis, θ denotes the beam angle, I_c and I_t are the moments of inertia of the center body and tip mass, l_θ is the radius of the center body, l is the length of the beam excluding the center body and m_{tip} is the load mass. The boundary condition for the beam end with rotating joint is

$$w = \frac{\partial w}{\partial x} = 0, \; at \; x = l_0 \tag{4.3}$$

and for the tip respectively

$$EI\frac{\partial^2 w}{\partial x^2} = -I_t(\ddot{\theta} + \ddot{w}'), \; EI\frac{\partial^3 w}{\partial x^3} = m_{tip}(l\ddot{\theta} + \ddot{w}), \; at \; x = l. \tag{4.4}$$

The denotation $\dot{()}$ is a partial derivative with respect to time t and $()'$ is a partial derivative with respect to spatial variable x. The extended Hamilton's principle is applied for each element [8, p. 465]

$$\int_{t_1}^{t_2} (\delta L + \delta W)dt = 0, \tag{4.5}$$

where $L = T_e$-V_e is the Lagrangian for an element, which is the difference between kinetic and potential energies. External work done in the system is denoted by W. The kinetic

energy T_e and potential energy K_e can be presented as follows

$$T_e = \int_{x_e}^{x_e+h} \rho(\dot{w}_e + x\dot{\theta})^2 dx \tag{4.6}$$

$$K_e = \int_{x_e}^{x_e+h} EI\Big(\frac{\partial^2 w}{\partial x^2}\Big)^2 dx, \tag{4.7}$$

where h denotes the length of an element and w denotes a cubic polynomial function that is used for spatial interpolation of the transverse deflection of the beam. This function can be written as

$$w_e(x,t) = \Phi_1(x)q_1(t) + \Phi_2(x)q_2(t) + \Phi_3(x)q_3(t) + \Phi_4(x)q_4(t), \tag{4.8}$$

where q_1 and q_3 denote the vertical displacements at the left-end and right-end of the element. Similarly, q_2 and q_4 denote the slopes, or rotations, of the element at each end. The shape functions $\Phi_n, n \in [1,4]$ are known as Hermite polynomials and are defined as follows:

$$\Phi_1(x) = 1 - \frac{3x^2}{h^2} + \frac{2x^3}{h^3} \tag{4.9}$$

$$\Phi_2(x) = x - \frac{2x^2}{h} + \frac{x^3}{h^2} \tag{4.10}$$

$$\Phi_3(x) = \frac{3x^2}{h^2} - \frac{2x^3}{h^3} \tag{4.11}$$

$$\Phi_4(x) = -\frac{x^2}{h} + \frac{x^3}{h^2}. \tag{4.12}$$

Substituting the Hermite polynomials into (4.6) and (4.7) and integrating by parts gives

$$\mathbf{M}_e^i \ddot{q}_e + \mathbf{K}_e^i \dot{q}_e = 0 \tag{4.13}$$

for the i^{th} element. The element mass matrix is denoted by $\mathbf{M}_e$ and the element stiffness matrix by $\mathbf{K}_e$. This procedure can be applied to each element, which eventually leads to the global governing equations

$$\mathbf{M}\ddot{q} + \mathbf{K}\dot{q} = \mathbf{F}u, \text{ where } \quad q = [\theta, q_1, q_2, ..., q_{n-1}, q_n]^T. \tag{4.14}$$

The number of elements is denoted by N. The global mass and stiffness matrices take the following forms:

$$\mathbf{M} = \begin{bmatrix} I_c + M_{\theta\theta} & \vec{M}_{\theta q} \\ \vec{M}_{q\theta} & \mathbf{M}_{qq} \end{bmatrix} \tag{4.15}$$

$$\mathbf{K} = \begin{bmatrix} 0 & \vec{0} \\ \vec{0}^T & \mathbf{K}_{qq} \end{bmatrix}. \tag{4.16}$$

Here $\mathbf{M}_{qq}$ and $\mathbf{K}_{qq}$ denote the flexible terms, $\vec{M}_{q\theta}$ and $\vec{M}_{\theta q}$ denote the coupling terms and $I_c + M_{\theta\theta}$ denotes the rigid term. The flexible terms are the only non-zero terms in the global stiffness matrix. The vector $\vec{0}$ is of size $1 \times N$.

4.4 Element matrices and combining them

In this section the construction of element matrices and combining them to global matrices as in (4.15)-(4.16) is presented in view of [8, pp. 467-468]. Matrices for each element can be expressed as follows:

$$\mathbf{M}_e^i = \begin{bmatrix} M_{11}^i & M_{12}^i & M_{13}^i \\ M_{21}^i & M_{22}^i & M_{23}^i \\ M_{31}^i & M_{32}^i & M_{33}^i \end{bmatrix}, \ \mathbf{K}_e^i = \begin{bmatrix} 0 & 0 & 0 \\ 0 & K_{22}^i & K_{23}^i \\ 0 & K_{32}^i & K_{33}^i. \end{bmatrix}, \ \mathbf{M}_t = \begin{bmatrix} M_{11}^t & M_{12}^t \\ M_{21}^t & M_{22}^t \end{bmatrix}, \tag{4.17}$$

where $\mathbf{M}_t$ is a mass matrix associated to the rigid body portion of the beam. The matrix elements of the element mass matrix can be written as follows:

$$M_{11}^i = \frac{\rho}{3}(x_i + l_0)^2 + (x_i + l_0 + h)(x_i + l_0) + (x_i + l_0 + h)^2 \tag{4.18}$$

$$M_{12}^i = [M_{21}^i]^T = \rho h \begin{bmatrix} \frac{3}{20} + \frac{1}{2}(x_i + l_0) & \frac{1}{30}h^2 + \frac{1}{12}h(x_i + l_0) \end{bmatrix} \tag{4.19}$$

$$M_{13}^i = [M_{31}^i]^T = \rho h \begin{bmatrix} \frac{7}{20}h + \frac{1}{2}(x_i + l_0) & -\frac{1}{20}h^2 - \frac{1}{12}h(x_i + l_0) \end{bmatrix} \tag{4.20}$$

$$M_{22}^i = \frac{\rho h}{420} \begin{bmatrix} 156 & 22h \\ 22h & 4h^2 \end{bmatrix}, \ M_{33}^i = \frac{\rho h}{420} \begin{bmatrix} 156 & -22h \\ -22h & 4h^2 \end{bmatrix} \tag{4.21}$$

$$M_{23}^i = [M_{32}^i]^T = \frac{\rho h}{420} \begin{bmatrix} 54 & -13h \\ 13h & -3h^2 \end{bmatrix}. \tag{4.22}$$

The elements of the stiffness matrix can be written as:

$$K_{22}^i = \frac{EI}{h^3}\begin{bmatrix} 12 & 6h \\ 6h & 4h^2 \end{bmatrix},\ K_{33}^i = \frac{EI}{h^3}\begin{bmatrix} 12 & -6h \\ -6h & 4h^2 \end{bmatrix} \tag{4.23}$$

$$M_{12}^i = [M_{21}^i]^T = \frac{EI}{h^3}\begin{bmatrix} -12 & 6h \\ -6h & 2h^2 \end{bmatrix}. \tag{4.24}$$

Finally, the elements of the rigid mass matrix can be expressed as

$$M_{11}^t = J_t + m_t(l_0+l)^2,\ M_{12}^t = [M_{21}^t]^T \begin{bmatrix} m_{tip}(l_0+l) & I_t \end{bmatrix} \tag{4.25}$$

$$M_{22}^t = \begin{bmatrix} m_{tip} & 0 \\ 0 & I_t \end{bmatrix}. \tag{4.26}$$

After forming the elements as described, they are combined to global governing matrices. First, the rigid term of the global mass matrix given in Eq. (4.14) is as follows:

$$M_{\theta\theta} = \sum_{i=1}^{N} M_{11}^i + M_{11}^t. \tag{4.27}$$

Then, the coupling terms of the global mass matrix are formulated as

$$M_{\theta q} = \begin{bmatrix} M_{13}^1 + M_{12}^2 & M_{13}^2 + M_{12}^3 & \cdots & M_{13}^{N-1} + M_{12}^N & M_{13}^N + M_{12}^t \end{bmatrix} \tag{4.28}$$

$$M_{q\theta} = [M_{\theta q}]^T. \tag{4.29}$$

Finally, the flexible terms are assembled in the following way

$$M_{qq} = \begin{bmatrix} M_{33}^1 + M_{22}^2 & M_{23}^2 & & & & & \\ M_{32}^2 & M_{33}^2 + M_{22}^3 & M_{23}^3 & & & & \\ & M_{32}^3 & M_{33}^3 + M_{22}^4 & M_{23}^4 & & & \\ & & & \ddots & & & \\ & & & & M_{32}^{N-1} & \bar{M} & M_{23}^N \\ & & & & & M_{32}^N & M_{33}^N \end{bmatrix} \tag{4.30}$$

where $\bar{M} = M_{33}^{N-1} + M_{22}^N$. The formulation is the same for both mass and stiffness; stiffness is acquired by substituting M with K in (4.30). The global mass and stiffness matrices for a rotating flexible beam are now known.

4.5 Mass matrix diagonalization

The solution to the FEM problem is acquired by solving the nodal acceleration vector from (4.15), which is integrated in order to obtain nodal velocities and positions. Solving the equation requires inverting the global mass matrix $\mathbf{M}$. For simulation purposes, the flexible terms $\mathbf{M}_{qq}$ of $\mathbf{M}$ are diagonalized with the following steps [8, p. 241]:

(a) The diagonal components of the consistent mass matrix associated with translational degrees of freedom, vertical deformation in this case, are summed together.

(b) Each diagonal component is then divided by the sum and multiplied by the element's total mass.

(c) All off-diagonal components are set to zero.

This matrix is called the diagonal mass matrix, which conserves the mass for the translational degrees of freedom. The procedure is conducted in order to achieve an easily invertible global mass matrix $\mathbf{M}$. In accordance with the steps described, the sum of respective diagonal components is first calculated:

$$S_{diag} = \sum M_{qq}^{ii},\ i = 1,3,5,\ldots,2N-1 \tag{4.31}$$

Then, according to step two, division and multiplication is applied to the diagonals:

$$M_{qqd}^{ii} = \frac{S_{diag} M_{qq}^{ii}}{m_e},\ i = 1,3,5,\ldots,2N-1 \tag{4.32}$$

The element's total mass is denoted by m_e. Finally, the third step of the diagonalization is seen through by setting all off-diagonal components to zero.

4.6 Force vectors and damping

To make the model more accurate, damping and gravity terms are added to the equation of motion (4.14) and then the equation is solved with respect to acceleration:

$$\ddot{q} = \mathbf{M}^{-1}(F - G - \mathbf{K}q - \mathbf{C}\dot{q}), \tag{4.33}$$

where G denotes the gravity vector and $\mathbf{C}$ denotes the damping matrix. The force vector F has two non-zero components; a positive force at the cylinder attachment point and a negative force caused by the load mass near the tip of the boom.

Gravity is incorporated to the model as a uniform pressure load for each element [8, p. 238]

$$G_e = \frac{m_e g}{12}\begin{bmatrix} 6h & h & 6h & -h^2 \end{bmatrix}^T, \tag{4.34}$$

where g denotes gravitational acceleration. The alignment of the gravity vector for each element is adjusted for each time step. The global gravity vector is then assembled as a standard finite element procedure.

Damping is also incorporated to the model, otherwise the system would not naturally compensate any vibration. Rayleigh damping is used [8, p. 406], in which the damping matrix is formulated as follows:

$$\mathbf{C} = \alpha_{ray}\mathbf{M} + \beta_{ray}\mathbf{K}. \tag{4.35}$$

The two constants α_{ray} and β_{ray} are called Rayleigh damping coefficients. As can be seen from (4.35), in this method the damping is proportional; the damping matrix is a linear combination of the system mass and stiffness matrices. Having only two constant variables results in this method being convenient and easy to configure.

Boundary conditions of the FE model are realized by setting the nodal acceleration at the cylinder attachment point to zero. This forces the transverse deflection and slope to zero at this point. This implies that the beam model is flexible from the first nodal point after the attachment point till the boom tip.

5. VIRTUAL DECOMPOSITION CONTROL

In this chapter the full formulation of the VDC approach is applied to the studied system. The VDC approach is a nonlinear, subsystem based control method that utilizes the dynamics of these subsystems. An important feature of the VDC approach is maintaining the L_2 and L_∞ stability and convergence of the entire complex robot, which leads into a stability-guaranteed system. Especially with hydraulic robots, there has been a lack of stability proof for proposed control laws, when nonlinear and model-based control are considered [7, p. 1]. The idea is to enable decentralized control of complex robots by forming dynamics and designing control equations for each subsystem separately. Practically this means that if an electric actuator is substituted for a hydraulic one, only the dynamics and respective control equations of the given actuator subsystem would need to be changed. This also opens up a possibility for modularity in the controller design. [16, p. 9]

The first step in this process is to virtually decompose the system into subsystems, i.e., *open chains* and *objects*, by placing conceptual *virtual cutting points*. An *object* is a rigid body on which the motion and force control specifications are given. An *object* also connects with multiple *open chains* and can be in contact with the environment. An *open chain* comprises of rigid links and connects with two *objects* at most. In contrast with *objects*, *open chains* may not be in touch with the environment. [16, p. 64, 68]

Virtual power flows are then used to define the dynamic interactions between subsystems and are in a key role in the definition of *virtual stability*. The ultimate control objective in the VDC approach is to design a velocity controller that takes care of the dynamics of the entire system [7, p. 2]. Other control objectives, such as motion control, internal force control or optimizations can easily be implemented into the control laws, without restrictions on the target system. [16, p. 9]

5.1 Decomposing the target system

The decomposed structure is presented in Fig. 5.1. The hydraulic actuator is separated from the rest of the manipulator by placing *virtual cutting points* to both ends of the actuator. The actuator itself consists of two rigid links, cylinder and piston, while the actuator assembly also consists of two rigid links that are connected by the hydraulic cylinder.

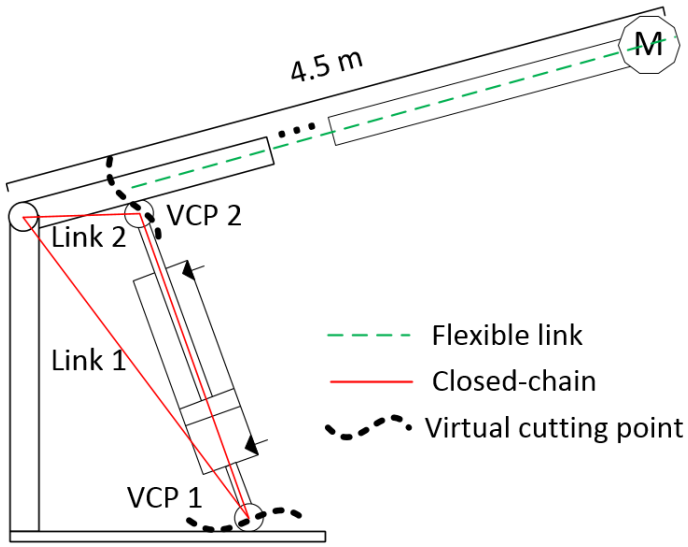

Figure 5.1 *Decomposed structure of the boom.*

As can be seen, the target system is virtually decomposed into two main components: a *closed chain* and a *flexible link*. The *closed chain* is composed of four rigid links and has three unactuated rotational joint and one actuated prismatic joint. In hydraulics, the friction is mostly dominated by the friction between the piston seal and the cylinder [16, p. 169]. Thus the friction torques of the unactuated rotational joints are assumed to be zero, for simplicity. Modeling of the *flexible link* in the context of the VDC formulation is based on the Euler-Bernoulli beam theory.

The *closed chain* structure needs to be further decomposed into open-chains as described Fig. 5.2. This is achieved by adding two zero-mass *objects* to the system, along with four subsidiary *cutting points*. No motion control specifications are derived for the zero-mass *objects*; they are merely tools used in decomposing the *closed chain*.

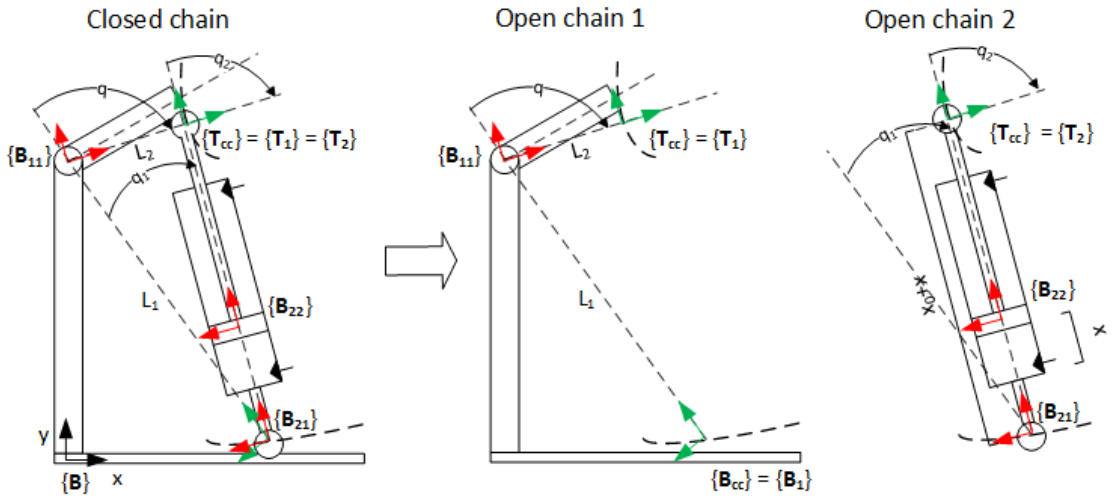

Figure 5.2 *Decomposing closed-chain into open-chains.*

Frames $\{\mathbf{T}_{cc}\}$, $\{\mathbf{T}_1\}$ and $\{\mathbf{T}_2\}$ are coinciding with each other. Frame $\{\mathbf{B}_{22}\}$ is attached to the piston. Respectively, frames $\{\mathbf{B}_{cc}\}$, $\{\mathbf{B}_1\}$ and $\{\mathbf{B}_2\}$ coincide with each other. Frame $\{\mathbf{B}\}$ denotes the inertial frame. Link lengths of the actuator assembly are denoted by L_1 and L_2. The initial cylinder length is denoted by x_0 and the cylinder stroke by x. Angles q, q_1 and q_2 denote the *closed chain* angles. Due to geometry, for a given x, all q, q_1 and q_2 can be computed. Alternatively, for a given q, all x, q_1 and q_2 can be computed. A simple oriented graph of the system is given in Fig. 5.3.

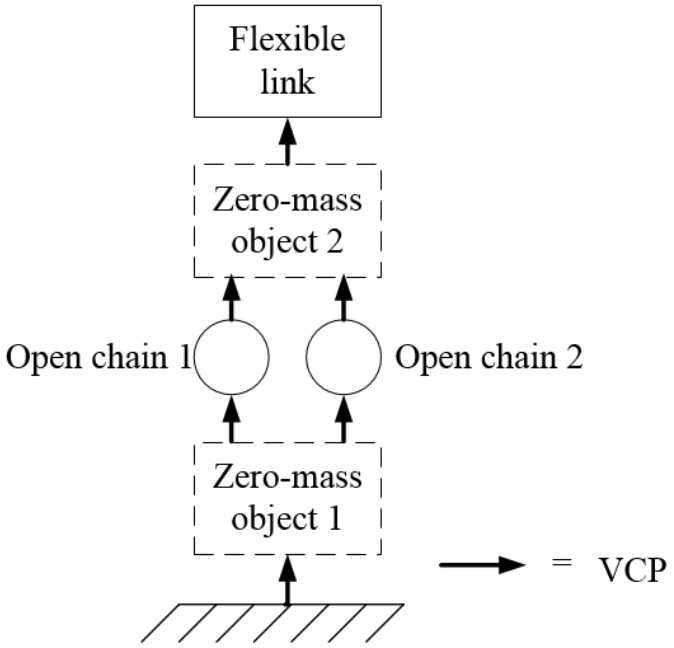

Figure 5.3 *A simple oriented graph of the boom.*

Based on Figs. 5.1, 5.2 and 5.3, the *virtual cutting points* of the system are as follows:

- The zero-mass *object* 1 has one *driven cutting point* associated with frame $\{\mathbf{B}_{cc}\}$ and two *driving cutting points* associated with frames $\{\mathbf{B}_1\}$ and $\{\mathbf{B}_2\}$
- The jth *open chain* has one *driven cutting point* associated with frame $\{\mathbf{B}_j\}$ and one *driving cutting point* associated with frame $\{\mathbf{T}_j\}$, for all $j \in \{1,2\}$.
- The zero-mass *object* 2 has two *driven cutting points* associated with frames $\{\mathbf{T}_1\}$ and $\{\mathbf{T}_2\}$ and one *driving cutting point* associated with frame $\{\mathbf{T}_{cc}\}$.

5.2 Flexible link

Being a fully model-based control method, the VDC approach uses the Euler-Bernoulli beam theory in modeling the *flexible link*; the assumptions presented in Section 4.2 stand. However, the equations differ from the ones used in the finite element modeling, because here rotating of the beam is neglected. The *flexible link*, virtually decomposed as in Fig. 5.1, is depicted in Fig. 5.4.

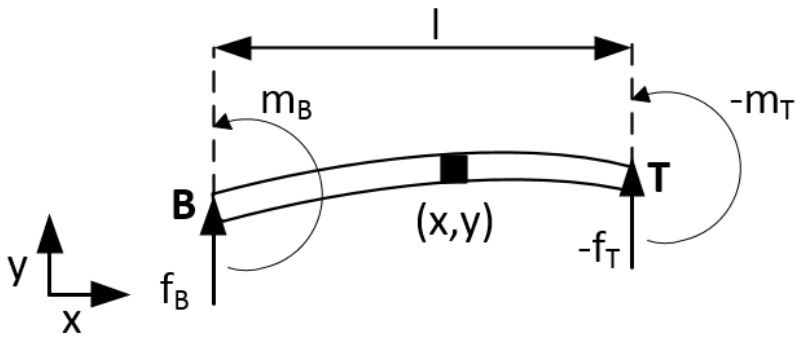

Figure 5.4 *A flexible link virtually decomposed from a planar flexible robot.*

According to the figure, there is a *virtual cutting point* at each end of the *flexible link*. The *cutting point* at point **B** is interpreted as the *driven cutting point* of the link and the *cutting point* at point **T** is interpreted as the *driving cutting point* of the link, respectively. Applied shear force at point **B** is denoted by f_B and bending moment by m_B. Similarly, applied shear force at point **T** is denoted by f_T and bending moment by m_T. Link length is denoted by l. [16, p. 339] The load mass situated at the boom tip is incorporated into f_T and m_T.

5.2.1 Dynamics

Following the Euler-Bernoulli beam theory, the energy equations for the *flexible link* are written in view of [16, pp. 339-340] as follows:

$$E_K = \frac{1}{2}\int_0^l \rho \dot{y}(x,t)^2 dx \tag{5.1}$$

$$E_P = \frac{1}{2}\int_0^l EIy''(x,t)^2 dx, \tag{5.2}$$

where E_K denotes the kinetic energy and E_P denotes the potential energy.

Applying (5.1) and (5.2) to the extended Hamilton's principle (4.5) eventually yields the *flexible link* dynamic equation as

$$\rho \ddot{y}(x,t) + EIy''''(x,t) = 0, \quad \text{for all } x \in [0,l], \tag{5.3}$$

subject to the following boundary conditions:

$$f_B = EIy'''(0,t) \tag{5.4}$$
$$m_B = -EIy''(0,t) \tag{5.5}$$
$$f_T = EIy'''(l,t) \tag{5.6}$$
$$m_T = -EIy''(l,t). \tag{5.7}$$

5.2.2 Control equations

In view of (5.3)-(5.7) and [16, p. 341], the model based control for the flexible link is designed as:

$$\rho\ddot{y}_r(x,t) + EIy_r''''(x,t) + k_v[\dot{y}_r(x,t) - \dot{y}(x,t)] = 0, \tag{5.8}$$

for all $x \in [0,l]$ and $k_v \geq 0$ being a velocity gain. The design is subject to the following boundary conditions:

$$f_{Br} = EIy_r'''(0,t) \tag{5.9}$$
$$m_{Br} = -EIy_r''(0,t) \tag{5.10}$$
$$f_{Tr} = EIy_r'''(l,t) \tag{5.11}$$
$$m_{Tr} = -EIy_r''(l,t). \tag{5.12}$$

5.2.3 Control implementation

The control implementation is conducted in view of [17, pp. 4-5]. The goal of the control algorithm is to obtain f_{Br} and m_{Br} from given f_{Tr} and m_{Tr}, which is equivalent to finding $y_r(0,t)$, $y_r'(0,t)$, $y_r''(0,t)$ and $y_r'''(0,t)$ from given $y_r(l,t)$, $y_r'(l,t)$, $y_r''(l,t)$ and $y_r'''(l,t)$, subject to the control equation (5.8). Having knowledge of $y_r''(0,t)$ and $y_r'''(0,t)$, f_{Br} and m_{Br} are given by (5.9)-(5.10). Respectively, knowing f_{Tr} and m_{Tr} gives $y_r''(l,t)$ and $y_r'''(l,t)$ from (5.11)-(5.12).

The *flexible link* is divided into $N > 0$ discrete sections with the following limits: $x(0) = 0$ and $x(N) = l$. Backward differentiation is utilized for calculating derivatives of both time

and spatial variables:

$$\dot{y}(x,k) = \frac{y(x,k) - y(x,k-1)}{\Delta T} \tag{5.13}$$

$$y'(x(j),t) = \frac{y(x(j),t) - y(x(j-1),t)}{\Delta x}, \tag{5.14}$$

where ΔT denotes the sampling period, k is a positive integer and $\Delta x = l/N$ denotes the length of a discrete section with $j \in \{1,N\}$. The main computational algorithm is presented as follows:

Step 1: Using (5.8) and a given $\ddot{y}_r(l,k)$, compute

$$y_r''''(l,k) = -\frac{\rho \ddot{y}_r(l,k) + k_v[\dot{y}_r(l,k) - \dot{y}(l,k)]}{EI}. \tag{5.15}$$

Step 2: For given $y_r(l,t)$, $y_r'(l,t)$, $y_r''(l,t)$ and $y_r'''(l,t)$, compute

$$y_r'''(x(N-1),k) = y_r'''(x(N),k) - \Delta x y_r''''(x(N),k) \tag{5.16}$$

$$y_r''(x(N-1),k) = y_r''(x(N),k) - \Delta x y_r'''(x(N),k) \tag{5.17}$$

$$y_r'(x(N-1),k) = y_r'(x(N),k) - \Delta x y_r''(x(N),k) \tag{5.18}$$

$$y_r(x(N-1),k) = y_r(x(N),k) - \Delta x y_r'(x(N),k). \tag{5.19}$$

Step 3: Update the required velocity and acceleration at $x(N-1)$ by computing

$$\dot{y}_r(x(N-1),k) = \frac{y_r(x(N-1),k) - y_r(x(N-1),k,1)}{\Delta T} \tag{5.20}$$

$$\ddot{y}_r(x(N-1),k) = \frac{\dot{y}_r(x(N-1),k) - \dot{y}_r(x(N-1),k,1)}{\Delta T}. \tag{5.21}$$

Step 4: In an iterative manner, repeat steps 1-3 from $x(N-1)$ to $x(0)$ to determine $y_r(0,t)$, $y_r'(0,t)$, $y_r''(0,t)$ and $y_r'''(0,t)$. Then f_{Br} and m_{Br} can finally be obtained from (5.9)-(5.10).

5.2.4 Control objective

First, an arc approximation for the boom tip position is defined as [15, p. 2]

$$p = L\theta + y_t, \tag{5.22}$$

where L denotes the length of the flexible beam, θ denotes the rotation angle of an undeformed beam, y_t denotes tip deflection with respect to the undeformed beam and p

denotes the arc approximation of the tip position.

In this case it is assumed that only the tip positions, $y(0,t)$ and $y(l,t)$, and angles, $y'(0,t)$ and $y'(l,t)$ are measurable. The velocity gain k_v in (5.8) is zero, as $\dot{y}(x,t)$ for $x \in (0,l)$ is not available. In view of [17, p. 4], equations for controlling the tip position and the tip angle are as follows:

$$\dot{y}_r(l,t) = \dot{y}_d(l,t) + \lambda_f[y_r(l,t) - y(l,t)] \tag{5.23}$$

$$\dot{y}'_r(l,t) = \dot{y}'_d(l,t) + \lambda_m[y'_r(l,t) - y'(l,t)], \tag{5.24}$$

where $\lambda_f > 0$ and $\lambda_m > 0$ are two control parameters, $\dot{y}_d(l,t)$ is the desired velocity and $\dot{y}'_d(l,t)$ is the desired angular velocity. The desired values at the boom tip are obtained from a designed reference trajectory. Based on the *virtual power flows*, the fact that f_T and m_T are measurable and that f_B and m_B are controllable, the boundary conditions given earlier can be expressed in the following form:

$$f_{Tr} = k_{fv}[\dot{y}_r(l,t) - \dot{y}(l,t)] + k_{fI}\int_0^t [\dot{y}_r(l,t) - \dot{y}(l,t)]dt \tag{5.25}$$

$$m_{Tr} = k_{mv}[\dot{y}'_r(l,t) - \dot{y}'(l,t)] + k_{mI}\int_0^t [\dot{y}'_r(l,t) - \dot{y}'(l,t)]dt \tag{5.26}$$

$$f_B = f_{Br} + k_{fB}[\dot{y}_r(0,t) - \dot{y}(0,t)] \tag{5.27}$$

$$m_B = m_{Br} + k_{mB}[\dot{y}'_r(0,t) - \dot{y}'(0,t)], \tag{5.28}$$

where $k_{fv} > 0$, $k_{fI} > 0$, $k_{mv} > 0$, $k_{mI} > 0$, $k_{fB} > 0$ and $k_{mB} > 0$ are six control parameters. The force/moment vector and its required counterpart in frame $\{\mathbf{B}_3\}$ are formulated as

$${}^{B_3}F = \begin{bmatrix} 0 \\ f_B \\ 0 \\ 0 \\ 0 \\ m_B \end{bmatrix}, \quad {}^{B_3}F_r = \begin{bmatrix} 0 \\ f_{Br} \\ 0 \\ 0 \\ 0 \\ m_{Br} \end{bmatrix}. \tag{5.29}$$

In view of (3.4) the force/moment vector of frame $\{\mathbf{B}_3\}$ is expressed in frame $\{\mathbf{T}_{cc}\}$, which is situated at the *driving cutting point* of the *closed chain*:

$${}^{T_{cc}}F = {}^{\mathbf{T}_{cc}}\mathbf{U}^{B_3}_{\mathbf{B}_3}F \tag{5.30}$$

$${}^{T_{cc}}F_r = {}^{\mathbf{T}_{cc}}\mathbf{U}^{B_3}_{\mathbf{B}_3}F_r \tag{5.31}$$

The transformation matrix, ${}^{\mathbf{T}_{cc}}\mathbf{U}_{\mathbf{B}_3}$, in this case is constant due to the mechanical structure.

5.3 Closed chain - kinematics and dynamics

5.3.1 Kinematics

Kinematics of the *closed chain* are presented in view of [16, pp. 170-172]. The first step is to determine the *closed chain* angles q, q_1 and q_2. The boom angle, θ, with respect to the inertial frame $\{\mathbf{B}\}$ is measured, which is converted into q as follows:

$$q = \Phi_q + \theta \tag{5.32}$$

$$\dot{q} = \dot{\theta}, \tag{5.33}$$

where Φ_q is a conversion factor based on geometry. The angular velocity $\dot{q}$ is obtained simply by taking the time derivative of θ. Knowing q, the rest of *closed chain* variables can also be obtained by using the law of cosines:

$$x = \sqrt{L_1^2 + L_2^2 + 2L_1L_2\cos(q)} - x_0 \tag{5.34}$$

$$q_1 = -\cos^{-1}\left(\frac{L_2^2 - (x+x_0)^2 - L_1^2}{-2(x+x_0)L_1}\right) \tag{5.35}$$

$$q_2 = -\cos^{-1}\left(\frac{L_1^2 - (x+x_0)^2 - L_2^2}{-2(x+x_0)L_2}\right). \tag{5.36}$$

Respective joint velocities are obtained by taking the time derivatives of (5.34)-(5.36):

$$\dot{x} = -\frac{L_1L_2\sin(q)}{(x+x_0)}\dot{q} \tag{5.37}$$

$$\dot{q_1} = -\frac{(x+x_0) - L_1\cos(q_1)}{(x+x_0)L_1\sin(q_1)}\dot{x} \tag{5.38}$$

$$\dot{q_2} = -\frac{(x+x_0) - L_2\cos(q_2)}{(x+x_0)L_2\sin(q_2)}\dot{x}. \tag{5.39}$$

Again, only $\dot{x}$ or $\dot{q}$ is needed to solve all of the *closed chain* velocities. As can be seen from (5.37)-(5.39), it is possible for the denominators to reach zero values, which would cause singularities. To avoid this, the motion trajectory should be planned so that q, q_1 and q_2 never reach zero.

In view of (3.3) and Fig. 5.2, the linear/angular velocity vectors of the *closed chain* can

be written as follows:

$$^{\mathbf{B}_{cc}}V = {}^{\mathbf{B}_1}V = {}^{\mathbf{B}_2}V \tag{5.40}$$

$$^{\mathbf{B}_{11}}V = {}^{\mathbf{B}_1}\mathbf{U}^T_{\mathbf{B}_{11}}\,{}^{\mathbf{B}_1}V + \mathbf{z}_\tau\dot{q} \tag{5.41}$$

$$^{\mathbf{T}_1}V = {}^{\mathbf{B}_{11}}\mathbf{U}^T_{\mathbf{T}_1}\,{}^{\mathbf{B}_{11}}V \tag{5.42}$$

$$^{\mathbf{B}_{21}}V = {}^{\mathbf{B}_2}\mathbf{U}^T_{\mathbf{B}_{21}}\,{}^{\mathbf{B}_2}V + \mathbf{z}_\tau\dot{q}_1 \tag{5.43}$$

$$^{\mathbf{B}_{22}}V = {}^{\mathbf{B}_{21}}\mathbf{U}^T_{\mathbf{B}_{22}}\,{}^{\mathbf{B}_{21}}V + \mathbf{x}_f\dot{x} \tag{5.44}$$

$$^{\mathbf{T}_2}V = {}^{\mathbf{B}_{22}}\mathbf{U}^T_{\mathbf{T}_2}\,{}^{\mathbf{B}_{22}}V + \mathbf{z}_\tau\dot{q}_2 \tag{5.45}$$

$$^{\mathbf{T}_{cc}}V = {}^{\mathbf{T}_1}V = {}^{\mathbf{T}_2}V, \tag{5.46}$$

where

$$\mathbf{x}_f = [1,0,0,0,0,0]^T \in \mathbb{R}^6 \tag{5.47}$$

$$\mathbf{z}_\tau = [0,0,0,0,0,1]^T \in \mathbb{R}^6. \tag{5.48}$$

Notably, frame $\{\mathbf{B}_{cc}\}$ is fixed and cannot move, which gives $^{\mathbf{B}_{cc}}V = \vec{0} \in \mathbb{R}^6$.

5.3.2 Dynamics

In this subsection the dynamics of the *closed chain* are presented in view of [16, pp. 172-173]. In uniform with (3.8), the dynamics of the four rigid links of the *closed chain* are expressed as follows:

$$^{\mathbf{B}_1}F^* = \mathbf{M}_{\mathbf{B}_1}\frac{d}{dt}(^{\mathbf{B}_1}V) + \mathbf{C}_{\mathbf{B}_1}(^{\mathbf{B}_1}\omega)^{\mathbf{B}_1}V + \mathbf{G}_{\mathbf{B}_1} \tag{5.49}$$

$$^{\mathbf{B}_{11}}F^* = \mathbf{M}_{\mathbf{B}_{11}}\frac{d}{dt}(^{\mathbf{B}_{11}}V) + \mathbf{C}_{\mathbf{B}_{11}}(^{\mathbf{B}_{11}}\omega)^{\mathbf{B}_{11}}V + \mathbf{G}_{\mathbf{B}_{11}} \tag{5.50}$$

$$^{\mathbf{B}_{21}}F^* = \mathbf{M}_{\mathbf{B}_{21}}\frac{d}{dt}(^{\mathbf{B}_{21}}V) + \mathbf{C}_{\mathbf{B}_{21}}(^{\mathbf{B}_{21}}\omega)^{\mathbf{B}_{21}}V + \mathbf{G}_{\mathbf{B}_{21}} \tag{5.51}$$

$$^{\mathbf{B}_{22}}F^* = \mathbf{M}_{\mathbf{B}_{22}}\frac{d}{dt}(^{\mathbf{B}_{22}}V) + \mathbf{C}_{\mathbf{B}_{22}}(^{\mathbf{B}_{22}}\omega)^{\mathbf{B}_{22}}V + \mathbf{G}_{\mathbf{B}_{22}}. \tag{5.52}$$

The force resultant equation of the zero-mass *object* 2, located at the *virtual cutting point* 2, can be written as:

$$^{\mathbf{T}_{cc}}F = {}^{\mathbf{T}_1}F + {}^{\mathbf{T}_2}F, \tag{5.53}$$

where $^{\mathbf{T}_1}F$ and $^{\mathbf{T}_2}F$ are the forces exerted from the *open chains*. Let $^{\mathbf{T}_{cc}}\eta \in \mathbb{R}^6$ be the internal force/moment vector between *open chain* 1 and 2, having its reference direction

pointing from the cylinder to link 2, expressed in frame $\{\mathbf{T}_{cc}\}$. From (5.53) it follows that

$$^{\mathbf{T}_1}F = \alpha_1 {}^{\mathbf{T}_{cc}}F + {}^{\mathbf{T}_{cc}}\eta \tag{5.54}$$

$$^{\mathbf{T}_2}F = \alpha_2 {}^{\mathbf{T}_{cc}}F - {}^{\mathbf{T}_{cc}}\eta \tag{5.55}$$

hold with $\alpha_1 + \alpha_2 = 1$, where α_1 and α_2 are called load distribution factors. Equations for both internal force/moment vector and load distribution factors will be provided in the next section. The force resultant equations associated with the rigid bodies in the *open chain* 1 are formulated as

$$^{\mathbf{B}_{11}}F = {}^{\mathbf{B}_{11}}F^* + {}^{\mathbf{B}_{11}}\mathbf{U}_{\mathbf{T}_1} {}^{\mathbf{T}_1}F \tag{5.56}$$

$$^{\mathbf{B}_1}F = {}^{\mathbf{B}_1}F^* + {}^{\mathbf{B}_1}\mathbf{U}_{\mathbf{B}_{11}} {}^{\mathbf{B}_{11}}F. \tag{5.57}$$

Respectively, the force resultant equations of the rigid bodies affiliated with the *open chain* 2 are written as

$$^{\mathbf{B}_{22}}F = {}^{\mathbf{B}_{22}}F^* + {}^{\mathbf{B}_{22}}\mathbf{U}_{\mathbf{T}_2} {}^{\mathbf{T}_2}F \tag{5.58}$$

$$^{\mathbf{B}_{21}}F = {}^{\mathbf{B}_{21}}F^* + {}^{\mathbf{B}_{21}}\mathbf{U}_{\mathbf{B}_{22}} {}^{\mathbf{B}_{22}}F. \tag{5.59}$$

Furthermore, the force resultant equation in frame $\{\mathbf{B}_2\}$ is formulated as

$$^{\mathbf{B}_2}F = {}^{\mathbf{B}_2}\mathbf{U}_{\mathbf{B}_{21}} + {}^{\mathbf{B}_{21}}F. \tag{5.60}$$

Finally, the force resultant equation of the zero-mass *object* 1 is

$$^{\mathbf{B}_{cc}}F = {}^{\mathbf{B}_1}F + {}^{\mathbf{B}_2}F. \tag{5.61}$$

The actuation force of the cylinder is expressed by using the force in frame $\{\mathbf{B}_{22}\}$, which is attached to the piston, as

$$f_c = \mathbf{x}_f^T {}^{\mathbf{B}_{22}}F. \tag{5.62}$$

Assuming the frictions of the three unactuated rotational joints as zero, the constraints can be written as follows:

$$\mathbf{z}_\tau^T {}^{\mathbf{T}_2}F = 0 \tag{5.63}$$

$$\mathbf{z}_\tau^T {}^{\mathbf{B}_{11}}F = 0 \tag{5.64}$$

$$\mathbf{z}_\tau^T {}^{\mathbf{B}_{21}}F = 0. \tag{5.65}$$

The constraint equations are essential in deriving the internal force vector. The moment element ${}^{\mathbf{T}_{cc}}\eta_z$ is obtained from (5.63), while the force elements ${}^{\mathbf{T}_{cc}}\eta_x$ and ${}^{\mathbf{T}_{cc}}\eta_y$ are obtained from (5.64)-(5.65). [16, p. 173]

5.4 Closed chain - load distribution factors and internal force vector

In this section the equations for determining the load distribution factors and the internal force vector are given in view of [6, Appendix D and Appendix E]. In scope of this thesis, only the necessary equations are presented.

5.4.1 Load distribution factors

The load distribution factors are two coefficients that define the magnitudes of the forces exerted from rigid links. In case of a *closed chain*, the load distribution between *open chains* 1 and 2 is needed. The distribution itself is dependent on the current geometrical configuration of the *closed chain* and is bound to change as the piston moves.

First, the direction of the reaction force $-{}^{\mathbf{T}_{cc}}F \in \mathbb{R}^6$ is computed as follows:

$$\beta_{ld} = \tan^{-1}\left(\frac{{}^{\mathbf{T}_{cc}}F(2)}{{}^{\mathbf{T}_{cc}}F(1)}\right), \tag{5.66}$$

where ${}^{\mathbf{T}_{cc}}\mathbf{F}(n)$ denotes the n^{th} element of ${}^{\mathbf{T}_{cc}}\mathbf{F}$. Next, two additional angles are defined as

$$\gamma_{ld} = \text{sign}(\beta_{ld})|q_2| \tag{5.67}$$

$$\Delta_{ld} = \pi - \gamma_{ld}. \tag{5.68}$$

Considering a case, in which the direction angle $\beta_{ld} \geq 0$, the load distribution factors are derived as

$$\theta_{ld} = \gamma_{ld} - \beta_{ld} \tag{5.69}$$

$$\alpha_1 = \cos(\beta_{ld})\frac{\sin(\theta_{ld})}{\sin(\Delta_{ld})} \tag{5.70}$$

$$\alpha_2 = \cos(\theta_{ld})\frac{\sin(\beta_{ld})}{\sin(\Delta_{ld})}. \tag{5.71}$$

Considering a case, where the direction angle $\beta_{ld} < 0$, the load distribution factors are derived as

$$\theta_{ld} = -\pi - \gamma_{ld} - \beta_{ld} \tag{5.72}$$

$$\alpha_1 = \cos(\beta_{ld}) \frac{\sin(\theta_{ld})}{\sin(\gamma_{ld})} \tag{5.73}$$

$$\alpha_2 = \cos(\theta_{ld}) \frac{\sin(\beta_{ld})}{\sin(\gamma_{ld})}. \tag{5.74}$$

For an appropriately defined *closed chain* structure, only the equations presented above are needed for solving the load distribution factors. Thorough formulation can be found in [6, Appendix D].

5.4.2 Internal force/moment vector

Having specified the load distribution factors and using (5.55) and (5.63), the moment element ${}^{\mathbf{T}_{cc}}\eta_z$ of the internal force vector can be expressed as follows:

$${}^{\mathbf{T}_{cc}}\eta_z = \alpha_2 \mathbf{z}_\tau^T {}^{\mathbf{T}_{cc}}F. \tag{5.75}$$

After ${}^{\mathbf{T}_{cc}}\eta_z$ is solved, the force element ${}^{\mathbf{T}_{cc}}\eta_y$ is obtained through (5.50), (5.54), (5.56) and (5.64) as

$${}^{\mathbf{B}_{11}}\mathbf{U}_{\mathbf{T}_1}{}^{\mathbf{T}_{cc}}\eta = -{}^{\mathbf{B}_{11}}F^* - \alpha_1 {}^{\mathbf{B}_{11}}\mathbf{U}_{\mathbf{T}_1}{}^{\mathbf{T}_{cc}}F = F_{\eta y} \tag{5.76}$$

$${}^{\mathbf{T}_{cc}}\eta_y = \frac{F_{\eta y}(6) - {}^{\mathbf{T}_{cc}}\eta_z}{{}^{\mathbf{B}_{11}}\mathbf{U}_{\mathbf{T}_1}(6,2)}, \tag{5.77}$$

where ${}^{\mathbf{B}_{11}}\mathbf{U}_{\mathbf{T}_1}(x,y)$ denotes a matrix element located at (x,y). Having ${}^{\mathbf{T}_{cc}}\eta_z$ and ${}^{\mathbf{T}_{cc}}\eta_y$ solved, the force element ${}^{\mathbf{T}_{cc}}\eta_x$ can now be acquired from (5.54), (5.58), (5.59) and (5.65) as

$${}^{\mathbf{B}_{21}}\mathbf{U}_{\mathbf{B}_{22}}{}^{\mathbf{B}_{22}}\mathbf{U}_{\mathbf{T}_2}{}^{\mathbf{T}_{cc}}\eta = {}^{\mathbf{B}_{21}}F^* + {}^{\mathbf{B}_{21}}\mathbf{U}_{\mathbf{B}_{22}}{}^{\mathbf{B}_{22}}F^* + \alpha_2 {}^{\mathbf{B}_{21}}\mathbf{U}_{\mathbf{B}_{22}}{}^{\mathbf{B}_{22}}\mathbf{U}_{\mathbf{T}_2}{}^{\mathbf{T}_{cc}}F = F_{\eta x} \tag{5.78}$$

$${}^{\mathbf{T}_{cc}}\eta_x = \frac{F_{\eta x}(6) - {}^{\mathbf{T}_{cc}}\eta_z - ({}^{\mathbf{B}_{21}}\mathbf{U}_{\mathbf{B}_{22}}{}^{\mathbf{B}_{22}}\mathbf{U}_{\mathbf{T}_2})(6,2){}^{\mathbf{T}_{cc}}\eta_y}{({}^{\mathbf{B}_{21}}\mathbf{U}_{\mathbf{B}_{22}}{}^{\mathbf{B}_{22}}\mathbf{U}_{\mathbf{T}_2})(6,1)}. \tag{5.79}$$

The internal force vector can now be expressed as

$$ {}^{\mathbf{T}_{cc}}\eta = \begin{bmatrix} {}^{\mathbf{T}_{cc}}\eta_x \\ {}^{\mathbf{T}_{cc}}\eta_y \\ 0 \\ 0 \\ 0 \\ {}^{\mathbf{T}_{cc}}\eta_z \end{bmatrix} \in \mathbb{R}^6. \tag{5.80} $$

The complete formulation with more detail can be found in [6, Appendix E].

5.5 Closed chain - control equations

5.5.1 Required velocities

In accordance with (5.37)-(5.39), the required velocities of the kinematic structure can be expressed as

$$ \dot{x}_r = -\frac{L_1 L_2 \sin(q)}{(x+x_0)} \dot{q}_r \tag{5.81} $$

$$ \dot{q}_{1r} = -\frac{(x+x_0) - L_1\cos(q_1)}{(x+x_0)L_1\sin(q_1)} \dot{x}_r \tag{5.82} $$

$$ \dot{q}_{2r} = -\frac{(x+x_0) - L_2\cos(q_2)}{(x+x_0)L_2\sin(q_2)} \dot{x}_r. \tag{5.83} $$

Respectively, the required velocity transformations can be written in accordance with (5.40)-(5.46) as

$$ {}^{\mathbf{B}_{cc}}V_r = {}^{\mathbf{B}_1}V_r = {}^{\mathbf{B}_2}V_r \tag{5.84} $$

$$ {}^{\mathbf{B}_{11}}V_r = {}^{\mathbf{B}_1}\mathbf{U}^T_{\mathbf{B}_{11}}\,{}^{\mathbf{B}_1}V_r + \mathbf{z}_\tau \dot{q}_r \tag{5.85} $$

$$ {}^{\mathbf{T}_1}V_r = {}^{\mathbf{B}_{11}}\mathbf{U}^T_{\mathbf{T}_1}\,{}^{\mathbf{B}_{11}}V_r \tag{5.86} $$

$$ {}^{\mathbf{B}_{21}}V_r = {}^{\mathbf{B}_2}\mathbf{U}^T_{\mathbf{B}_{21}}\,{}^{\mathbf{B}_2}V_r + \mathbf{z}_\tau \dot{q}_{1r} \tag{5.87} $$

$$ {}^{\mathbf{B}_{22}}V_r = {}^{\mathbf{B}_{21}}\mathbf{U}^T_{\mathbf{B}_{22}}\,{}^{\mathbf{B}_{21}}V_r + \mathbf{x}_f \dot{x} \tag{5.88} $$

$$ {}^{\mathbf{T}_2}V_r = {}^{\mathbf{B}_{22}}\mathbf{U}^T_{\mathbf{T}_2}\,{}^{\mathbf{B}_{22}}V_r + \mathbf{z}_\tau \dot{q}_{2r} \tag{5.89} $$

$$ {}^{\mathbf{T}_{cc}}V_r = {}^{\mathbf{T}_1}V_r = {}^{\mathbf{T}_2}V_r. \tag{5.90} $$

Frame $\{\mathbf{B}_{cc}\}$ is non-moving, which gives ${}^{\mathbf{B}_{cc}}V_r = \vec{0} \in \mathbb{R}^6$. Having $\dot{q}_r \in \mathbb{R}$ or $\dot{x}_r \in \mathbb{R}$ and ${}^{\mathbf{B}_{cc}}V_r \in \mathbb{R}^6$ specified, all of the linear/angular velocity vectors of the *closed chain* assembly

can be determined from (5.81)-(5.90). [16, pp. 173-174]

5.5.2 Regressor matrix and parameter vector

Consider the fact that the target system and its frames are restricted to an xy-plane, while all rotational movement is about z-axis. From this it follows that any velocity vector in the system, denoted by ${}^{\mathbf{A}}\mathbf{V} \in \mathbb{R}^6$, will always have three zero values, namely ${}^{\mathbf{A}}\mathbf{V}(j) = 0$ for $j \in \{3,4,5\}$. Due to this the regressor matrix and parameter vector can be simplified to cover only 2-DOF (degree-of-freedom) movement. The simplification is presented by Koivumäki in [6, Appendix B].

Let frame $\{\mathbf{A}\}$ be attached to a rigid body. The 2-DOF regressor matrix takes the following form:

$$\mathbf{Y_A} = \begin{bmatrix} y_{\mathbf{A}}(1,1) & y_{\mathbf{A}}(1,2) & y_{\mathbf{A}}(1,3) & 0 & 0 & 0 \\ y_{\mathbf{A}}(2,1) & y_{\mathbf{A}}(2,2) & y_{\mathbf{A}}(2,3) & 0 & 0 & 0 \\ 0 & 0 & 0 & 0 & 0 & 0 \\ 0 & 0 & 0 & 0 & 0 & 0 \\ 0 & 0 & 0 & 0 & 0 & 0 \\ 0 & y_{\mathbf{A}}(6,2) & y_{\mathbf{A}}(6,3) & y_{\mathbf{A}}(6,4) & y_{\mathbf{A}}(6,5) & y_{\mathbf{A}}(6,6) \end{bmatrix} \in \mathbb{R}^{6\times 6}, \quad (5.91)$$

where the nonzero matrix elements are given as

$$y_{\mathbf{A}}(1,1) = \frac{d}{dt}({}^{\mathbf{A}}V_r)(1) - {}^{\mathbf{A}}V(6){}^{\mathbf{A}}V_r(2) + {}^{\mathbf{A}}g(1) \tag{5.92}$$

$$y_{\mathbf{A}}(1,2) = -{}^{\mathbf{A}}V(6){}^{\mathbf{A}}V_r(6) \tag{5.93}$$

$$y_{\mathbf{A}}(1,3) = -\frac{d}{dt}({}^{\mathbf{A}}V_r)(6) \tag{5.94}$$

$$y_{\mathbf{A}}(2,1) = \frac{d}{dt}({}^{\mathbf{A}}V_r)(2) - {}^{\mathbf{A}}V(6){}^{\mathbf{A}}V_r(1) + {}^{\mathbf{A}}g(2) \tag{5.95}$$

$$y_{\mathbf{A}}(2,2) = \frac{d}{dt}({}^{\mathbf{A}}V_r)(6) \tag{5.96}$$

$$y_{\mathbf{A}}(2,3) = -{}^{\mathbf{A}}V(6){}^{\mathbf{A}}V_r(6) \tag{5.97}$$

$$y_{\mathbf{A}}(6,2) = y_{\mathbf{A}}(2,1) \tag{5.98}$$

$$y_{\mathbf{A}}(6,3) = -y_{\mathbf{A}}(1,1) \tag{5.99}$$

$$y_{\mathbf{A}}(6,4) = y_{\mathbf{A}}(2,2) \tag{5.100}$$

$$y_{\mathbf{A}}(6,5) = -y_{\mathbf{A}}(1,3) \tag{5.101}$$

$$y_{\mathbf{A}}(6,6) = \frac{d}{dt}({}^{\mathbf{A}}V_r)(6). \tag{5.102}$$

Here ${}^{\mathbf{A}}g(n)$ denotes the n^{th} element of ${}^{\mathbf{A}}\mathbf{R}_{\mathbf{I}}g$, in which $g = [0\ 9.81\ 0]^T \in \mathbb{R}^3$ [16, p. 388]. The corresponding 2-DOF parameter vector is given as

$$\Theta_{\mathbf{A}} = \begin{bmatrix} m_{\mathbf{A}} \\ m_{\mathbf{A}}{}^{\mathbf{A}}r_{mx} \\ m_{\mathbf{A}}{}^{\mathbf{A}}r_{my} \\ m_{\mathbf{A}}{}^{\mathbf{A}}r_{mx}^2 \\ m_{\mathbf{A}}{}^{\mathbf{A}}r_{my}^2 \\ I_{\mathbf{A}zz} \end{bmatrix} \in \mathbb{R}^6, \tag{5.103}$$

where $m_{\mathbf{A}}$ denotes the mass of the rigid body, ${}^{\mathbf{A}}r_m = [{}^{\mathbf{A}}r_{mx}\ {}^{\mathbf{A}}r_{my}\ {}^{\mathbf{A}}r_{mz}]^T \in \mathbb{R}^3$ denotes a vector pointing from the origin of frame $\{\mathbf{A}\}$ toward the center of mass and expressed in frame $\{\mathbf{A}\}$ and $I_{\mathbf{A}zz}$ is an element of $\mathbf{I}_{\mathbf{A}}$ [16, p. 389].

From a simulating point of view, every simplification possible is desirable. This is due to the fact that in case of four rigid bodies, four regressor matrices and four parameter vectors need to be calculated during each time step. Because of this the matrix and vector have been designed as elemental as possible. Full 3-DOF regressor matrix and parameter vector formulations can be found in [16, Appendix A].

5.5.3 Required net force/moment vectors

Having the regressor matrix and parameter vector defined, the required net force/moment vectors of the rigid links are computed as

$$^{\mathbf{B}_1}F_r^* = \mathbf{Y}_{\mathbf{B}_1}\Theta_{\mathbf{B}_1} + \mathbf{K}_{\mathbf{B}_1}(^{\mathbf{B}_1}V_r - ^{\mathbf{B}_1}V) \tag{5.104}$$

$$^{\mathbf{B}_{11}}F_r^* = \mathbf{Y}_{\mathbf{B}_{11}}\Theta_{\mathbf{B}_{11}} + \mathbf{K}_{\mathbf{B}_{11}}(^{\mathbf{B}_{11}}V_r - ^{\mathbf{B}_{11}}V) \tag{5.105}$$

$$^{\mathbf{B}_{21}}F_r^* = \mathbf{Y}_{\mathbf{B}_{21}}\Theta_{\mathbf{B}_{21}} + \mathbf{K}_{\mathbf{B}_{21}}(^{\mathbf{B}_{21}}V_r - ^{\mathbf{B}_{21}}V) \tag{5.106}$$

$$^{\mathbf{B}_{22}}F_r^* = \mathbf{Y}_{\mathbf{B}_{22}}\Theta_{\mathbf{B}_{22}} + \mathbf{K}_{\mathbf{B}_{22}}(^{\mathbf{B}_{22}}V_r - ^{\mathbf{B}_{22}}V), \tag{5.107}$$

where $\mathbf{Y_A}\Theta_\mathbf{A} \in \mathbb{R}^6$ is a model-based feedforward term defined in (3.13) and $\mathbf{K_A} \in \mathbb{R}^{6\times 6}$ is a positive-definite gain matrix, with a given frame being substituted for frame $\{\mathbf{A}\}$. [16, p. 174]

5.5.4 Required force/moment vector transformations

In view of [16, p. 176], given a required force/moment vector, $^{\mathbf{T}_{cc}}F_r$, located at the *driving cutting point* of the *closed chain*, the required force/moment vectors at the two *driven cutting points* of the zero-mass *object* 2 can be formulated similarly to (5.54)-(5.55) as follows:

$$^{\mathbf{T}_1}F_r = \alpha_1\,^{\mathbf{T}_{cc}}F_r + ^{\mathbf{T}_{cc}}\eta_r \tag{5.108}$$

$$^{\mathbf{T}_2}F_r = \alpha_2\,^{\mathbf{T}_{cc}}F_r - ^{\mathbf{T}_{cc}}\eta_r, \tag{5.109}$$

where the load distribution factors α_1 and α_2 are obtained from (5.66)-(5.74) and the required internal force/moment vector from (5.75)-(5.80) by substituting force/moment vectors to required ones.

Next, the required force/moment vectors of the *open chain* 1 are formulated as

$$^{\mathbf{B}_{11}}F_r = ^{\mathbf{B}_{11}}F_r^* + ^{\mathbf{B}_{11}}\mathbf{U}_{\mathbf{T}_1}\,^{\mathbf{T}_1}F_r \tag{5.110}$$

$$^{\mathbf{B}_1}F_r = ^{\mathbf{B}_1}F_r^* + ^{\mathbf{B}_1}\mathbf{U}_{\mathbf{B}_{11}}\,^{\mathbf{B}_{11}}F_r \tag{5.111}$$

and the required force/moment vectors of the *open chain* 2 can be computed as

$$^{\mathbf{B}_{22}}F_r = ^{\mathbf{B}_{22}}F_r^* + ^{\mathbf{B}_{22}}\mathbf{U}_{\mathbf{T}_2}\,^{\mathbf{T}_2}F_r \tag{5.112}$$

$$^{\mathbf{B}_2}F_r = ^{\mathbf{B}_2}\mathbf{U}_{\mathbf{B}_{21}}\,^{\mathbf{B}_{21}}F_r^* + ^{\mathbf{B}_2}\mathbf{U}_{\mathbf{B}_{22}}\,^{\mathbf{B}_{22}}F_r. \tag{5.113}$$

The required force/moment vector, ${}^{\mathbf{T}_{cc}}F_r$, situated at the *driven cutting point* of the *closed chain* is now computed as

$${}^{\mathbf{B}_{cc}}F_r = {}^{\mathbf{B}_1}F_r + {}^{\mathbf{B}_2}F_r \tag{5.114}$$

In accordance with (5.62), the required actuation force of the hydraulic cylinder is expressed as

$$f_{cr} = \mathbf{x}_f^T {}^{\mathbf{B}_{22}}F_r. \tag{5.115}$$

Similar to (5.63)-(5.65), the *closed chain* is bound by the following constraints:

$$\mathbf{z}_\tau^T {}^{\mathbf{T}_2}F_r = 0 \tag{5.116}$$

$$\mathbf{z}_\tau^T {}^{\mathbf{B}_{11}}F_r = 0 \tag{5.117}$$

$$\mathbf{z}_\tau^T {}^{\mathbf{B}_{21}}F_r = \mathbf{z}_\tau^T {}^{\mathbf{B}_{21}}\mathbf{U}_{\mathbf{B}_2} {}^{\mathbf{B}_2}F_r = 0. \tag{5.118}$$

These constraint equations are applied, while deriving the required internal force vector ${}^{\mathbf{T}}\eta_r$.

5.6 Hydraulic cylinder dynamics and control

5.6.1 Friction model

The friction model for the hydraulic cylinder is given in view of [18, pp. 2-6]. First, a selective function is defined as

$$\varepsilon(x) = \begin{cases} 1, & \text{if } x > 0 \\ 0, & \text{if } x \leq 0 \end{cases} \tag{5.119}$$

and a differentiable function $g(z, z_{ss})$ as

$$g(z, z_{ss}) = \begin{cases} 1, & \text{if } z \geq z_{ss} \\ \frac{z}{z_{ss}}, & \text{if } 0 < z < z_{ss} \\ 0, & \text{if } z \leq 0, \end{cases} \tag{5.120}$$

where z denotes the average deformation of bristles in a friction model and $z_{ss} > 0$ is a constant. A Coulomb-viscous friction model with dc offset is used to model friction

during sliding motion and can be expressed as follows:

$$\begin{aligned} f_{cf} = k_{cp}g(z,z_{ss})\varepsilon(z) - k_{cn}g(-z,z_{ss})\varepsilon(-z) + k_0 \\ + [k_{vp}\varepsilon(\dot{x}) + k_{vn}\varepsilon(-\dot{x})]\Phi(\dot{x})\dot{x}. \end{aligned} \tag{5.121}$$

The two first terms on the right-hand side are affiliated with the Coulomb friction, while k_0 denotes the dc offset. The last term is associated with the Stribeck and viscous friction. The parameter $\Phi(\dot{x})$ is chosen as -1. The time derivative of z is written as

$$\dot{z} = \dot{x} - \frac{|\dot{x}|}{z_{ss}}z, \tag{5.122}$$

where $\dot{x}$ denotes the velocity. Friction during presliding motion can be formulated as a function of the output force:

$$f_{sf} = [k_{fp}\varepsilon(F_{out} + k_{fn}\varepsilon(-F_{out})]\varphi(F_{out}), \tag{5.123}$$

where F_{out} denotes the output force and φF_{out} is a monotonic function defined as

$$\varphi(F_{out}) = \frac{F_{out}}{1+\delta|F_{out|}}. \tag{5.124}$$

Here $\delta > 0$ is a constant. The total friction force of the piston can now be presented as

$$f_f = [1-\mathscr{L}(t)]f_{cf} + \mathscr{L}(t)f_{sf}, \tag{5.125}$$

in which $\mathscr{L}(t) \in [0,1]$ is a differentiable switching function, with $\mathscr{L}(t) \to 1$ for presliding motion and $\mathscr{L}(t) \to 0$ for sliding motion. In scope of this thesis, $\mathscr{L}(t)$ is defined in view of [18, p. 6] as

$$\mathscr{L}(t) = \frac{1}{1+(\delta_1\dot{\tilde{x}})^3}, \tag{5.126}$$

with

$$\ddot{\tilde{x}} = 10(|\dot{x}| - \dot{\tilde{x}}), \tag{5.127}$$

where $\delta_1 > 0$ and $\dot{\tilde{x}}(t) \geq 0$ if $\dot{\tilde{x}}(0) = 0$. The chamber pressure force of the cylinder can now be expressed as the sum of the piston friction force and the cylinder output force as

$$f_p = f_c + f_f. \tag{5.128}$$

A linearized parametrization form for the piston friction force is presented as

$$f_f = \mathbf{Y}_f \theta_f. \tag{5.129}$$

The differentiable regressor $\mathbf{Y}_f$ is given as

$$\mathbf{Y}_f = \begin{bmatrix} (1-\mathscr{L}(t))g(z,z_{ss})\varepsilon(z) \\ -(1-\mathscr{L}(t))g(-z,z_{ss})\varepsilon(-z) \\ (1-\mathscr{L}(t)) \\ (1-\mathscr{L}(t))\varepsilon(\dot{x})\Phi(\dot{x})\dot{x} \\ (1-\mathscr{L}(t))\varepsilon(-\dot{x})\Phi(\dot{x})\dot{x} \\ \varepsilon(F_d)\mathscr{L}(t)\varphi(F_d) \\ \varepsilon(-F_d)\mathscr{L}(t)\varphi(F_d) \end{bmatrix} \in \mathbb{R}^{1\times 7}, \tag{5.130}$$

where F_d is the desired output force. Finally, the parameter vector is defined as

$$\theta_f = [k_{cp} \quad k_{cn} \quad k_0 \quad k_{vp} \quad k_{vn} \quad k_{fp} \quad k_{fn}]^T \in \mathbb{R}^7 \tag{5.131}$$

Parameters k_{cp} and k_{vp} correspond to the positive velocity, while k_{cn} and k_{vn} correspond to the negative velocity, respectively.

5.6.2 Hydraulic fluid dynamics

In view of [16, p. 181], the control valve's spool position is considered to be proportional to its control voltage within a frequency range of interest. With this simplification it is recommended to use a high-bandwidth servo valve. The control arrangement of the cylinder used in this thesis is identical with [6, pp. 50-54], which differs from the arrangement presented in [16]. The differences are mainly in notation.

The valve used is a 4/3-servo valve, thus there are four control edges that can be modeled as orifices. Based on the Bernoulli's static flow equation, the rate of flow through an orifice is proportional to the product of the valve control voltage and the square root of the pressure drop across the orifice, which is written as

$$Q = c\sqrt{\Delta p u}, \tag{5.132}$$

where $c > 0$ is a constant flow coefficient, given by the valve specifications, $\Delta p = p_1 - p_2$ denotes the difference in pressure across the valve orifice and u is the valve control volt-

age. Fluid compressibility inside a cylinder chamber can be expressed as

$$\dot{p} = \frac{\beta}{v_c}(Q - \dot{v}_c), \tag{5.133}$$

in which β denotes the fluid bulk modulus, p denotes the chamber pressure, v_c denotes the chamber volume and Q denotes the rate of fluid flow flowing into the chamber.

A sign function is defined as

$$\text{sign}(x) = \begin{cases} 1, & \text{if } x > 0 \\ 0, & \text{if } x = 0 \\ -1, & \text{if } x < 0, \end{cases} \tag{5.134}$$

along with a pressure-drop related function

$$\upsilon(x) = \sqrt{|x|}\text{sign}(x). \tag{5.135}$$

Let Q_a and Q_b denote the rates of flows entering the respective cylinder chambers. Similarly, let p_a and p_b denote the chamber pressures. From (5.132) and applying (5.119) it follows that

$$Q_a = c_{p1}\upsilon(p_s - p_a)u\varepsilon(u) + c_{n1}\upsilon(p_a - p_r)u\varepsilon(-u) \tag{5.136}$$

$$Q_b = -c_{n2}\upsilon(p_b - p_r)u\varepsilon(u) - c_{p2}\upsilon(p_s - p_b)u\varepsilon(-u), \tag{5.137}$$

hold, where $c_{p1} > 0$, $c_{n1} > 0$, $c_{p2} > 0$ and $c_{n2} > 0$ are constants and $p_s > 0$ $p_r > 0$ denote supply and return line pressures. Note that $p_s \gg p_r$. Next, using (5.133) the dynamic equations for the pressure drop in each cylinder chamber is written as

$$\dot{p}_a = \frac{\beta}{A_a x}(Q_a - A_a\dot{x}) \tag{5.138}$$

$$\dot{p}_b = \frac{\beta}{A_b(l_0 - x)}(Q_b + A_b\dot{x}), \tag{5.139}$$

where A_a and A_b denote the piston areas at both sides of the cylinder chambers with $A_a > A_b$. Net pressure force of the cylinder can now be expressed as

$$f_p = A_a p_a - A_b p_b, \tag{5.140}$$

which is used for determining the current cylinder force by using pressure measurements.

Premultiplying A_a and A_b to (5.138)-(5.139), while using (5.136) ,(5.137) and (5.140) yields

$$\dot{f}_p = \beta \left[u_f - \left(\frac{A_a}{x} + \frac{A_b}{l_0 - x} \right) \dot{x} \right], \tag{5.141}$$

in which

$$\begin{aligned} u_f &= \frac{Q_a}{x} - \frac{Q_b}{l_0 - x} \\ &= \left(\frac{c_{p1} \upsilon (p_s - p_a)}{x} + \frac{c_{n2} \upsilon (p_b - p_r)}{l_0 - x} \right) u \varepsilon(u) \\ &+ \left(\frac{c_{n1} \upsilon (p_a - p_r)}{x} + \frac{c_{p2} \upsilon (p_s - p_b)}{l_0 - x} \right) u \varepsilon(-u) \\ &= \mathbf{Y}_v(u) \theta_v. \end{aligned} \tag{5.142}$$

Here

$$\mathbf{Y}_v(u) = \begin{bmatrix} \frac{\upsilon (p_s - p_a)}{x} u \varepsilon(u) \\ \frac{\upsilon (p_a - p_r)}{x} u \varepsilon(-u) \\ \frac{\upsilon (p_s - p_b)}{l_0 - x} u \varepsilon(-u) \\ \frac{\upsilon (p_b - p_r)}{l_0 - x} u \varepsilon(u) \end{bmatrix}^T \in \mathbb{R}^{1 \times 4} \tag{5.143}$$

and

$$\theta_v = [c_{p1} \quad c_{n1} \quad c_{p2} \quad c_{n2}]^T \in \mathbb{R}^4. \tag{5.144}$$

It is assumed that the following relationship holds: $0 < x < l_0$, which states that the piston will never reach either of its two ends. In view of this assumption and (5.142), univalence between u and u_f exists, if

$$\frac{c_{p1} \upsilon (p_s - p_a)}{x} + \frac{c_{n2} \upsilon (p_b - p_r)}{l_0 - x} > 0 \tag{5.145}$$

$$\frac{c_{n1} \upsilon (p_a - p_r)}{x} + \frac{c_{p2} \upsilon (p_s - p_b)}{l_0 - x} > 0 \tag{5.146}$$

hold. A unique valve control voltage for a given u_f can be expressed as

$$\begin{aligned} u = &\frac{1}{\frac{c_{p1} \upsilon (p_s - p_a)}{x} + \frac{c_{n2} \upsilon (p_b - p_r)}{l_0 - x}} u_f \varepsilon(u_f) \\ &+ \frac{1}{\frac{c_{n1} \upsilon (p_a - p_r)}{x} + \frac{c_{p2} \upsilon (p_s - p_b)}{l_0 - x}} u_f \varepsilon(-u_f), \end{aligned} \tag{5.147}$$

granted that (5.145)-(5.146) are satisfied.

5.6.3 Cylinder control equations

In view of (5.145)-(5.147) and [16, p. 184], for a given u_{fd} a unique valve control voltage u can be designed as

$$\begin{aligned} u = & \frac{1}{\frac{c_{p1}\upsilon(p_s-p_a)}{x}+\frac{c_{n2}\upsilon(p_b-p_r)}{l_0-x}}u_{fd}\varepsilon(u_{fd}) \\ & + \frac{1}{\frac{c_{n1}\upsilon(p_a-p_r)}{x}+\frac{c_{p2}\upsilon(p_s-p_b)}{l_0-x}}u_{fd}\varepsilon(-u_{fd}). \end{aligned} \tag{5.148}$$

Considering the friction model and the fluid dynamics defined by (5.141), the cylinder control equations are designed as follows:

$$\begin{aligned} u_{fd} = & \left(\frac{1}{\beta}\right)\dot{f}_{pr}+\left(\frac{A_a}{x}+\frac{A_b}{l_0-x}\right)\dot{x} \\ & + K_{Fp}(f_{pr}-f_p)+K_x(\dot{x}_r-\dot{x}) \\ & = \mathbf{Y}_c\theta_c + K_{Fp}(f_{pr}-f_p)+K_x(\dot{x}_r-\dot{x}), \end{aligned} \tag{5.149}$$

where

$$\dot{x}_r = \dot{x}_d + \lambda_x(x_d - x) \tag{5.150}$$

$$f_{pr} = f_{cr} + f_f \tag{5.151}$$

$$\mathbf{Y}_c = \begin{bmatrix} \dot{f}_{pr} & \frac{\dot{x}}{x} & \frac{\dot{x}}{l_0-x} \end{bmatrix} \in \mathbb{R}^{1\times 3} \tag{5.152}$$

$$\theta_c = \begin{bmatrix} \frac{1}{\beta} & A_a & A_b \end{bmatrix}^T \in \mathbb{R}^3. \tag{5.153}$$

Here f_{cr} is the required cylinder force obtained from (5.115), f_f is the friction force and f_{pr} is the required piston force, which takes the friction into account. Two feedback gains are denoted by $K_{Fp} > 0$ and $K_x > 0$. The piston velocity is denoted by $\dot{x}$ and its required counterpart by $\dot{x}_r$. Desired piston velocity and position are denoted by $\dot{x}_d$ and x_d, with $\lambda_x > 0$ being a control gain. It should be noted that the valve control voltage obtained from (5.148) may have to be scaled down, depending on where it is used.

5.7 Virtual stability analysis

Theorems 5.1-5.5 given in this section ensure the *virtual stability* of the *flexible link*, the zero-mass *objects* and the *open chains*, each combined with their respective control

equations, in the sense of Definition 3.7. Therefore, in view of Lemma 3.1, the entire system is *virtually stable*.

The stability analysis of the VDC approach is presented in detail in [16]. All the Theorems, Lemmas and equations are taken from the aforementioned book.

5.7.1 Flexible link

Theorem 5.1. *The uniform flexible beam described by the Euler-Bernoulli equation (5.3) subject to its boundary conditions (5.4)-(5.7), combined with its respective control equations (5.8)-(5.12), is virtually stable in the sense of Definition 3.7.*

Proof: Subtracting (5.3) from (5.8) yields

$$\begin{aligned}\rho[\ddot{y}_r(x,t)-\ddot{y}(x,t)]+EI[y_r''''(x,t)-y''''(x,t)]\\ +k_v[\dot{y}_r(x,t)-\dot{y}(x,t)]=0.\end{aligned} \tag{5.154}$$

Next, a non-negative accompanying function assigned to the *flexible link* is chosen as

$$v = v_K + v_V, \tag{5.155}$$

where

$$v_K = \frac{1}{2}\int_0^l \rho[\dot{y}_r(x,t)-\dot{y}(x,t)]^2 dx \tag{5.156}$$

$$v_V = EI\int_0^l \rho[y_r''(x,t)-y''(x,t)]^2 dx. \tag{5.157}$$

With integration by parts, it follows from (5.154) and (5.156) that

$$\begin{aligned}
\dot{v}_K =& \int_0^l \rho[\dot{y}_r(x,t)-\dot{y}(x,t)][\ddot{y}_r(x,t)-\ddot{y}(x,t)]dx \\
=& -\int_0^l [\dot{y}_r(x,t)-\dot{y}(x,t)]EI[y_r''''(x,t)-y''''(x,t)]dx \\
& -\int_0^l k_v[\dot{y}_r(x,t)-\dot{y}(x,t)]^2dx \\
=& -[\dot{y}_r(x,t)-\dot{y}(x,t)]EI[y_r'''(x,t)-y'''(x,t)]|_0^l \\
& +\int_0^l [\dot{y}_r'(x,t)-\dot{y}'(x,t)]EI[y_r'''(x,t)-y'''(x,t)]dx \\
& -\int_0^l k_v[\dot{y}_r(x,t)-\dot{y}(x,t)]^2dx \\
=& -[\dot{y}_r(x,t)-\dot{y}(x,t)]EI[y_r'''(x,t)-y'''(x,t)]|_0^l \\
& +[\dot{y}_r'(x,t)-\dot{y}'(x,t)]EI[y_r''(x,t)-y''(x,t)]|_0^l \\
& -\int_0^l [\dot{y}_r''(x,t)-\dot{y}''(x,t)]EI[y_r''(x,t)-y''(x,t)]dx \\
& -\int_0^l k_v[\dot{y}_r(x,t)-\dot{y}(x,t)]^2dx
\end{aligned} \tag{5.158}$$

holds. Next, (5.158) and the time derivative of (5.157) into the time derivative of (5.155) gives

$$\begin{aligned}
\dot{v} =& -\int_0^l k_v[\dot{y}_r(x,t)-\dot{y}(x,t)]^2dx \\
& +p_{\mathbf{B}}-p_{\mathbf{T}},
\end{aligned} \tag{5.159}$$

where

$$\begin{aligned}
p_{\mathbf{B}} =& [\dot{y}_r(0,t)-\dot{y}(0,t)]EI[y_r'''(0,t)-y'''(0,t)] \\
& -[\dot{y}_r'(0,t)-\dot{y}'(0,t)]EI[y_r''(0,t)-y''(0,t)] \\
=& [\dot{y}_r(0,t)-\dot{y}(0,t)](f_{\mathbf{B}r}-f_{\mathbf{B}}) \\
& +[\dot{y}_r'(0,t)-\dot{y}'(0,t)](m_{\mathbf{B}r}-m_{\mathbf{B}})
\end{aligned} \tag{5.160}$$

$$\begin{aligned}
p_{\mathbf{T}} =& [\dot{y}_r(l,t)-\dot{y}(l,t)]EI[y_r'''(l,t)-y'''(l,t)] \\
& -[\dot{y}_r'(l,t)-\dot{y}'(l,t)]EI[y_r''(l,t)-y''(l,t)] \\
=& [\dot{y}_r(l,t)-\dot{y}(l,t)](f_{\mathbf{T}r}-f_{\mathbf{T}}) \\
& +[\dot{y}_r'(l,t)-\dot{y}'(l,t)](m_{\mathbf{T}r}-m_{\mathbf{T}})
\end{aligned} \tag{5.161}$$

denote the *virtual power flows* at the ends of the beam, in view of (5.4)-(5.7) and (5.9)-(5.12). Finally, consider the fact that the *flexible link* has one *driving cutting point* associated with point **T** and one *driven cutting point* associated with point **B**. Using (5.155)-(5.157), (5.159) and Definition 3.7 completes the general proof. [16, pp. 341-343]

Furthermore, in view of [17, pp. 3-4], in case the force and moment at point **T** are measurable and their respective counterparts at point **B** are controllable, the following design is convenient to apply:

$$f_{\mathbf{T}r} = f_{\mathbf{T}} + k_{fT}[\dot{y}_r(l,t) - \dot{y}(l,t)] \tag{5.162}$$

$$m_{\mathbf{T}r} = m_{\mathbf{T}} + k_{mT}[\dot{y}'_r(l,t) - \dot{y}'(l,t)] \tag{5.163}$$

$$f_{\mathbf{B}} = f_{\mathbf{B}r} + k_{fB}[\dot{y}_r(0,t) - \dot{y}(0,t)] \tag{5.164}$$

$$m_{\mathbf{B}} = f_{\mathbf{B}r} + k_{mB}[\dot{y}'_r(0,t) - \dot{y}'(0,t)], \tag{5.165}$$

which gives

$$\begin{aligned} \dot{\nu} = &- \int_0^l k_\nu[\dot{y}_r(x,t) - \dot{y}(x,t)]^2 dx \\ &- k_{fB}[\dot{y}_r(0,t) - \dot{y}(0,t)]^2 \\ &- k_{mB}[\dot{y}'_r(0,t) - \dot{y}'(0,t)]^2 \\ &- k_{fT}[\dot{y}_r(l,t) - \dot{y}(l,t)]^2 \\ &- k_{mT}[\dot{y}'_r(l,t) - \dot{y}'(l,t)]^2. \end{aligned} \tag{5.166}$$

From $\nu \geq 0$ it follows that

$$\begin{aligned} \dot{y}_r(0,t) - \dot{y}(0,t) &\in L_2 \\ \dot{y}'_r(0,t) - \dot{y}('0,t) &\in L_2 \\ \dot{y}_r(l,t) - \dot{y}(l,t) &\in L_2 \\ \dot{y}'_r(l,t) - \dot{y}'(l,t) &\in L_2. \end{aligned} \tag{5.167}$$

Reference signals and their respective derivatives being bounded, the continuity of the

states is ensured by the flexibility of the link. This leads to the asymptotic stability

$$\begin{aligned} \dot{y}_r(0,t) - \dot{y}(0,t) &\to 0 \\ \dot{y}'_r(0,t) - \dot{y}('0,t) &\to 0 \\ \dot{y}_r(l,t) - \dot{y}(l,t) &\to 0 \\ \dot{y}'_r(l,t) - \dot{y}'(l,t) &\to 0. \end{aligned} \tag{5.168}$$

Adding the integral terms to the control equations (5.25) and (5.26) does not affect the stability result [17, p. 5].

5.7.2 Zero-mass object 2

Theorem 5.2. *The zero-mass object 2 described by (5.46) and (5.53)-(5.55), combined with its control equations (5.90), (5.108), and (5.109), is virtually stable in the sense of Definition 3.7.*

Proof: It follows from (5.53) and the summation of (5.108) and (5.109) that

$${}^{\mathbf{T}_{cc}}F_r - {}^{\mathbf{T}_{cc}}F = ({}^{\mathbf{T}_1}F_r - {}^{\mathbf{T}_1}F) + ({}^{\mathbf{T}_2}F_r - {}^{\mathbf{T}_2}F) \tag{5.169}$$

holds. Let the non-negative accompanying function be zero. Premultiplying (5.169) by $({}^{\mathbf{T}_{cc}}V_r - {}^{\mathbf{T}_{cc}}V)^T$ and using (5.46), (3.16) and (5.90) yields

$$0 = p_{\mathbf{T}_1} + p_{\mathbf{T}_2} - p_{\mathbf{T}_{cc}}. \tag{5.170}$$

Noting that the zero-mass *object* 2 has one *driving cutting point* associated with frame $\{\mathbf{T}_{cc}\}$ and two *driven cutting points* associated with frames $\{\mathbf{T}_1\}$ and $\{\mathbf{T}_2\}$, the theorem is proven in view of Definition 3.7. [16, p. 177]

5.7.3 Open chain 1

Theorem 5.3. *The open chain 1 described by (5.41), (5.42), (5.49), (5.50), (5.56), (5.57), and (5.64), combined with its respective control equations (5.85), (5.86), (5.104), (5.105), (5.110), (5.111), and (5.117) is virtually stable with its affiliated vectors ${}^{\boldsymbol{B}_1}V_r - {}^{\boldsymbol{B}_1}V$ and ${}^{\boldsymbol{B}_{11}}V_r - {}^{\boldsymbol{B}_{11}}V$ being virtual function in both L_2 and L_∞ in the sense of Definition 3.7.*

Proof: Select the non-negative accompanying function of the *open chain* 1 as

$$\nu = \nu_{\mathbf{B}_1} + \nu_{\mathbf{B}_{11}}, \tag{5.171}$$

where

$$\nu_{\mathbf{B}_1} = \frac{1}{2}({}^{\mathbf{B}_1}V_r - {}^{\mathbf{B}_1}V)^T \mathbf{M}_{\mathbf{B}_1}({}^{\mathbf{B}_1}V_r - {}^{\mathbf{B}_1}V) \tag{5.172}$$

$$\nu_{\mathbf{B}_{11}} = \frac{1}{2}({}^{\mathbf{B}_{11}}V_r - {}^{\mathbf{B}_{11}}V)^T \mathbf{M}_{\mathbf{B}_{11}}({}^{\mathbf{B}_{11}}V_r - {}^{\mathbf{B}_{11}}V) \tag{5.173}$$

are the non-negative accompanying functions assigned to the two rigid links affiliated with the *open chain* 1. In view of [16, pp. 76-77] and with appropriate frame substitution, it follows from (5.49), (5.50), (5.104) and (5.105) that

$$\begin{aligned} \dot{\nu}_{\mathbf{B}_1} \leq & -({}^{\mathbf{B}_1}V_r - {}^{\mathbf{B}_1}V)^T \mathbf{K}_{\mathbf{B}_1}({}^{\mathbf{B}_1}V_r - {}^{\mathbf{B}_1}V) \\ & + ({}^{\mathbf{B}_1}V_r - {}^{\mathbf{B}_1}V)({}^{\mathbf{B}_1}F_r^* - {}^{\mathbf{B}_1}F^*) \end{aligned} \tag{5.174}$$

$$\begin{aligned} \dot{\nu}_{\mathbf{B}_{11}} \leq & -({}^{\mathbf{B}_{11}}V_r - {}^{\mathbf{B}_{11}}V)^T \mathbf{K}_{\mathbf{B}_{11}}({}^{\mathbf{B}_{11}}V_r - {}^{\mathbf{B}_{11}}V) \\ & + ({}^{\mathbf{B}_{11}}V_r - {}^{\mathbf{B}_{11}}V)({}^{\mathbf{B}_{11}}F_r^* - {}^{\mathbf{B}_{11}}F^*) \end{aligned} \tag{5.175}$$

In view of (3.16), (5.41), (5.42), (5.56), (5.57), (5.64), (5.85), (5.86), (5.110), (5.111), and (5.117), it results in

$$({}^{\mathbf{B}_1}V_r - {}^{\mathbf{B}_1}V)({}^{\mathbf{B}_1}F_r^* - {}^{\mathbf{B}_1}F^*) = p_{\mathbf{B}_1} - p_{\mathbf{B}_{11}} \tag{5.176}$$

$$({}^{\mathbf{B}_{11}}V_r - {}^{\mathbf{B}_{11}}V)({}^{\mathbf{B}_{11}}F_r^* - {}^{\mathbf{B}_{11}}F^*) = p_{\mathbf{B}_{11}} - p_{\mathbf{T}_1}. \tag{5.177}$$

Substituting (5.176) and (5.177) into (5.174) and (5.175) yields

$$\begin{aligned} \dot{\nu} &= \dot{\nu}_{\mathbf{B}_1} + \dot{\nu}_{\mathbf{B}_{11}} \\ &\leq -({}^{\mathbf{B}_1}V_r - {}^{\mathbf{B}_1}V)^T \mathbf{K}_{\mathbf{B}_1}({}^{\mathbf{B}_1}V_r - {}^{\mathbf{B}_1}V) \\ &\quad -({}^{\mathbf{B}_{11}}V_r - {}^{\mathbf{B}_{11}}V)^T \mathbf{K}_{\mathbf{B}_{11}}({}^{\mathbf{B}_{11}}V_r - {}^{\mathbf{B}_{11}}V) \\ &\quad + p_{\mathbf{B}_1} - p_{\mathbf{T}_1}. \end{aligned} \tag{5.178}$$

Consider the fact that the *open chain* 1 has one *driving cutting point* associated with frame $\{\mathbf{T}_1\}$ and one *driven cutting point* associated with frame $\{\mathbf{B}_1\}$. The proof is complete using (5.171)-(5.173), (5.178) and Definition 3.7. [16, pp. 177-179]

5.7.4 Open chain 2

Lemma 5.1. *The open chain 2 described by (5.43)-(5.45), (5.51), (5.52), (5.58), (5.59), (5.62), (5.63) and (5.65), combined with its respective control equations (5.87)-(5.89), (5.106), (5.107), (5.112), (5.113), (5.115), (5.116) and (5.118). Let*

$$v_2 = v_{\boldsymbol{B}_{21}} + v_{\boldsymbol{B}_{22}}, \tag{5.179}$$

be the non-negative accompanying functions assigned to the open chain 2, where

$$v_{\boldsymbol{B}_{21}} = \frac{1}{2}({}^{\boldsymbol{B}_{21}}V_r - {}^{\boldsymbol{B}_{21}}V)^T \boldsymbol{M}_{\boldsymbol{B}_{21}}({}^{\boldsymbol{B}_{21}}V_r - {}^{\boldsymbol{B}_{21}}V) \tag{5.180}$$

$$v_{\boldsymbol{B}_{22}} = \frac{1}{2}({}^{\boldsymbol{B}_{22}}V_r - {}^{\boldsymbol{B}_{22}}V)^T \boldsymbol{M}_{\boldsymbol{B}_{22}}({}^{\boldsymbol{B}_{22}}V_r - {}^{\boldsymbol{B}_{22}}V) \tag{5.181}$$

are the non-negative accompanying functions assigned to the two rigid bodies, piston and cylinder, affiliated with the open chain 2. The time derivative of (5.179) is written as

$$\begin{aligned}\dot{v}_2 &= \dot{v}_{\boldsymbol{B}_{21}} + \dot{v}_{\boldsymbol{B}_{22}} \\ &\leq -({}^{\boldsymbol{B}_{21}}V_r - {}^{\boldsymbol{B}_{21}}V)^T \boldsymbol{K}_{\boldsymbol{B}_{21}}({}^{\boldsymbol{B}_{21}}V_r - {}^{\boldsymbol{B}_{21}}V) \\ &\quad -({}^{\boldsymbol{B}_{2}}V_r - {}^{\boldsymbol{B}_{22}}V)^T \boldsymbol{K}_{\boldsymbol{B}_{22}}({}^{\boldsymbol{B}_{22}}V_r - {}^{\boldsymbol{B}_{22}}V) \\ &\quad + p_{\boldsymbol{B}_2} - p_{\boldsymbol{T}_2} \\ &\quad + (\dot{x}_r - \dot{x})(f_{cr} - f_c),\end{aligned} \tag{5.182}$$

where $p_{\boldsymbol{B}_2}$ and $p_{\boldsymbol{T}_2}$ denote the two virtual power flows by Definition 3.6 at the two cutting points of the open chain 2.

Proof: In view of [16, pp. 76-77] and from (5.51), (5.52), (5.106), (5.107), (5.116), (5.118), (5.49), (5.49), and (5.105), it follows that

$$\begin{aligned}\dot{v}_{\mathbf{B}_{21}} &\leq -({}^{\mathbf{B}_{21}}V_r - {}^{\mathbf{B}_{21}}V)^T \mathbf{K}_{\mathbf{B}_{21}}({}^{\mathbf{B}_{21}}V_r - {}^{\mathbf{B}_{21}}V) \\ &\quad + ({}^{\mathbf{B}_{21}}V_r - {}^{\mathbf{B}_{21}}V)({}^{\mathbf{B}_{21}}F_r^* - {}^{\mathbf{B}_{21}}F^*)\end{aligned} \tag{5.183}$$

$$\begin{aligned}\dot{v}_{\mathbf{B}_{22}} &\leq -({}^{\mathbf{B}_{22}}V_r - {}^{\mathbf{B}_{22}}V)^T \mathbf{K}_{\mathbf{B}_{22}}({}^{\mathbf{B}_{22}}V_r - {}^{\mathbf{B}_{22}}V) \\ &\quad + ({}^{\mathbf{B}_{22}}V_r - {}^{\mathbf{B}_{22}}V)({}^{\mathbf{B}_{22}}F_r^* - {}^{\mathbf{B}_{22}}F^*)\end{aligned} \tag{5.184}$$

hold. In view of (3.16), (5.43), (5.45), (5.58), (5.59), (5.62), (5.63), (5.65), (5.87)-(5.89),

(5.112), (5.113), (5.115), (5.116) and (5.118), it results in

$$({}^{\mathbf{B}_{21}}V_r - {}^{\mathbf{B}_{21}}V)({}^{\mathbf{B}_{21}}F_r^* - {}^{\mathbf{B}_{21}}F^*) \tag{5.185}$$

$$= p_{\mathbf{B}_2} - p_{\mathbf{B}_{22}} + (\dot{x}_r - \dot{x})(f_{cr} - f_c) \tag{5.186}$$

$$({}^{\mathbf{B}_{22}}V_r - {}^{\mathbf{B}_{22}}V)({}^{\mathbf{B}_{22}}F_r^* - {}^{\mathbf{B}_{22}}F^*) \tag{5.187}$$

$$= p_{\mathbf{B}_{22}} - p_{\mathbf{T}_2}. \tag{5.188}$$

Substituting (5.185) and (5.187) into (5.183) and (5.184) yields (5.182). The term $(\dot{x}_r - \dot{x})(f_{cr} - f_c)$ in (5.182) prevents the *virtual stability* of the *open chain* 2 from being held. Next, the *virtual stability* of the hydraulic actuator assembly is examined, which will complete the *virtual stability* proof of the *open chain* 2. [16, pp. 179-180]

5.7.5 Hydraulic actuator assembly

A non-negative accompanying function for the fluid dynamics is given by the following lemma:

Lemma 5.2. *Consider the hydraulic cylinder dynamics described by (5.128), (5.129), (5.141), and (5.142) and combined with the control equations (5.149) and (5.151)-(5.153). The time derivative of*

$$v_c = \frac{1}{2\beta}(f_{pr} - f_p)^2 \tag{5.189}$$

is

$$\dot{v}_c \leq -K_{fp}(f_{pr} - f_p)^2 - K_x(f_{cr} - f_c)(\dot{x}_r - \dot{x}). \tag{5.190}$$

Theorem 5.4. *The open chain 2 described by (5.43)-(5.45), (5.51), (5.52), (5.58), (5.59), (5.62), (5.63), (5.65), (5.128), (5.129), (5.141), and (5.142), combined with the control equations (5.87)-(5.89), (5.106), (5.107), (5.112), (5.113), (5.115), (5.116), (5.118), (5.149) and (5.151)-(5.153), is virtually stable with its affiliated vectors and variables ${}^{\boldsymbol{B}_{21}}V_r - {}^{\boldsymbol{B}_{21}}V$, ${}^{\boldsymbol{B}_{22}}V_r - {}^{\boldsymbol{B}_{22}}V$, and $f_{pr} - f_p$ being virtual functions in both L_2 and L_∞, in the sense of Definition 3.7.*

Proof: The proof follows from Lemmas 5.1 and 5.4. Define the non-negative accompanying function of the *open chain* 2 as follows:

$$v = v_2 + \frac{v_c}{K_x}, \tag{5.191}$$

in which ν_2 is defined by (5.179) and ν_c is defined by (5.189), respectively. From (5.182) and (5.190) if follows that

$$\begin{aligned}\dot{\nu} &= \dot{\nu}_2 + \frac{\dot{\nu}_c}{K_x} \\ &\leq -({}^{\mathbf{B}_{21}}V_r - {}^{\mathbf{B}_{21}}V)^T \mathbf{K}_{\mathbf{B}_{21}} ({}^{\mathbf{B}_{21}}V_r - {}^{\mathbf{B}_{21}}V) \\ &\quad -({}^{\mathbf{B}_{22}}V_r - {}^{\mathbf{B}_{22}}V)^T \mathbf{K}_{\mathbf{B}_{22}} ({}^{\mathbf{B}_{22}}V_r - {}^{\mathbf{B}_{22}}V) \\ &\quad -\frac{K_{fp}}{K_x}(f_{pr} - f_p)^2 + p_{\mathbf{B}_2} - p_{\mathbf{T}_2}\end{aligned} \tag{5.192}$$

holds. Finally, consider the fact that the *open chain* 2 has one *driving cutting point* associated with frame $\{\mathbf{T}_2\}$ and one *driven cutting point* associated with frame $\{\mathbf{B}_2\}$. Using (5.179), (5.189), (5.191), (5.192), and Definition 3.7 completes the proof. [16, pp. 185-187]

5.7.6 Zero-mass object 1

Theorem 5.5. *The zero-mass object 1 described by (5.40) and (5.61), combined with its control equations (5.84) and (5.114), is virtually stable in the sense of Definition 3.7.*

Proof: It follows from (5.61) and (5.114) that

$${}^{\mathbf{B}_{cc}}F_r - {}^{\mathbf{B}_{cc}}F = ({}^{\mathbf{B}_1}F_r - {}^{\mathbf{B}_1}F) + ({}^{\mathbf{B}_2}F_r - {}^{\mathbf{B}_2}F) \tag{5.193}$$

holds. Let the non-negative accompanying function be zero. Premultiplying (5.193) by $({}^{\mathbf{B}_{cc}}V_r - {}^{\mathbf{B}_{cc}}V)^T$ and using (5.40), (3.16) and (5.84) yields

$$0 = p_{\mathbf{B}_1} + p_{\mathbf{B}_2} - p_{\mathbf{B}_{cc}}. \tag{5.194}$$

Noting that the zero-mass *object* 1 has two *driving cutting point* associated with frames $\{\mathbf{B}_1\}$ and $\{\mathbf{B}_2\}$ and one *driven cutting point* associated with frame $\{\mathbf{B}_{cc}\}$, the theorem is proven in view of Definition 3.7. [16, pp. 180-181]

6. EXPERIMENTAL IMPLEMENTATION

The designed controller was tested out in simulation with the FE model. As the controller was seemingly functioning, it was implemented into the real-time environment using dSPACE CP1103 PPC Controller Board with ControlDesk 3.7.1 software as the user interface. The sensors and filters used in the real-time setup are collectively presented in Appendix A.

6.1 Sensors

The boom angle is measured from the rotating axis of the joint with an incremental encoder. The encoder used is Sick Stegmann DGS60, which is designed for rough environmental conditions. The encoder can send 10000 pulses per 90°, which gives a measuring step of

$$enc_{res} = \frac{360^\circ}{4 \times 10000} = 0.009^\circ. \tag{6.1}$$

Three pressures are measured: the supply pressure and both cylinder chamber pressures. The supply pressure is measured with a Trafag 8891.74 pressure sensor, with a measuring range of $0-250$ bar. For the chamber pressures A and B, Unik 5000 pressure sensors are used, with the same measuring ranges.

The boom also has three MEMS (microelectromechanical system) sensors containing IMUs (inertial measurement units), which measure linear accelerations and angular velocities with respect to three different axis. The sensors are mounted so that their placement correspond to the nodal points in the created FE model of the boom.

The tip displacement is required for (5.22) and the tip angle for (5.24). These are hard to measure directly, especially the tip displacement. In this thesis, the two variables are obtained as estimates, from a dynamic observer. The observer is detailed in Appendix B.

6.2 Signal conditioning

It is necessary to calculate derivatives using the signal values of previous time steps. Traditional backward differentiation is problematic due to the method causing noisy signals. Therefore a real-time estimation of the derivatives of motion, presented in [3], is used to obtain most of the derivatives required as follows:

$$\dot{x}(kh) = \frac{5x(kh) + 3x(kh-h) + x(kh-2h) - x(kh-3h) - 3x(kh-4h) - 5x(5h)}{35h}. \quad (6.2)$$

Here x is the original signal, $\dot{x}$ being its derivative and h being the sampling time.

In addition, GMA (Geometric Moving Average) filtering is applied to the pressure measurements, calculated piston forces and piston velocities. The equation for the filter is presented [7, p. 13] as

$$y(k) = (1 - \alpha_{gma})y(k-1) + \alpha_{gma}u(k), \quad (6.3)$$

where α_{gma} is a filter constant, for which a value of 0.04 was used. The signal to be filtered is u.

6.3 Applied parameters and control gains

The parameters of the four rigid bodies associated with the *closed chain* were obtained from a 3D CAD (Computer Aided Design) model and are presented in Table 6.1.

Table 6.1 *Rigid body parameters.*

Body frame	m_A [kg]	r_x [m]	r_y [m]	I_{Azz} [kgm^2]
$\{\mathbf{B}_1\}$	58.22	0.10	0.14	5.88
$\{\mathbf{B}_{11}\}$	5.01	0.17	0.03	0.21
$\{\mathbf{B}_{21}\}$	2.32	0	0	0.22
$\{\mathbf{B}_{22}\}$	2.30	0	0	0.21

The mass of a rigid body, expressed in body frame $\{\mathbf{A}\}$, is denoted by m_A. The distance from body frame $\{\mathbf{A}\}$ to the center of mass along x-axis, expressed in frame $\{\mathbf{A}\}$, is denoted by r_x. Respectively, the distance along y-axis is denoted by r_y. The moment of inertia, expressed in frame $\{\mathbf{A}\}$, around the center of mass about z-axis is denoted by I_{Azz}.

The four valve flow coefficients were determined from the valve specification sheet and are presented in Table 6.2.

Table 6.2 *Valve flow coefficients.*

c_{p1}	$2.1e^{-8}$	c_{n1}	$2.1e^{-8}$
c_{p2}	$2.1e^{-8}$	c_{n2}	$2.1e^{-8}$

The friction parameters associated with the cylinder friction model are presented in Table 6.3.

Table 6.3 *Friction parameters.*

k_{cp}	600	k_{fp}	800
k_{cn}	600	k_{fn}	800
k_{vp}	-1800	z_{ss}	0.0001
k_{vn}	-1800	δ	1
Φ	-1	δ_1	500

The control gains for both the *closed chain* and *flexible link* are given in Table 6.4.

Table 6.4 *Control gains.*

Closed chain		Flexible link	
K_{Fp}	$5e^{-8}$	k_{fv}	19.3
K_x	0.025	k_{mv}	5
λ_x	6	k_{fi}	0.6
K_{B1}	0	k_{mi}	5
K_{B11}	0	k_{fb}	204
K_{B21}	0	k_{mb}	2022
K_{B22}	0	λ_f	180
		λ_m	180

Other parameters include Young's modulus of 210 GPa, bulk modulus of 1200 GPa and the amount of discrete sections the flexible link is divided in was $N = 5$. Finally, a sampling period of 2 ms was used.

6.4 Path planning

A cubic function presented in [5, pp. 729-730] is used to generate a predefined trajectory for the boom. A rest-to-rest path can be written as

$$q(t) = a_0 + a_1 t + a_2 t^2 + a_3 t^3, \tag{6.4}$$

where

$$a_0 = -\frac{q_1 t_0^2 (t_0 - 3t_f) + q_0 t_f^2 (3t_0 - t_f)}{(t_f - t_0)^3} - t_0 t_f \frac{q_0' t_f + q_1' t_0}{(t_f - t_0)^2} \tag{6.5}$$

$$a_1 = 6 t_0 t_f \frac{q_0 - q_1}{(t_f - t_0)^3} + \frac{q_0' t_f (t_f^2 + t_0 t_f - 2t_0^2) + q_1' t_0 (2t_f^2 - t_0^2 - t_0 t_f)}{(t_f - t_0)^3} \tag{6.6}$$

$$a_2 = -\frac{q_0 (3t_0 + 3t_f) + q_1 (-3t_0 - 3t_f)}{(t_f - t_0)^3} - \frac{q_1' (t_0 t_f - 2t_0^2 + t_f^2) + q_0' (2t_f^2 - t_0^2 - t_0 t_f)}{(t_f - t_0)^3} \tag{6.7}$$

$$a_3 = \frac{2q_0 - 2q_1 + q_0' (t_f - t_0) + q_1' (t_f - t_0)}{(t_f - t_0)^3} \tag{6.8}$$

with

$$q(t_0) = q_0 \tag{6.9}$$

$$q(t_f) = q_f \tag{6.10}$$

$$\dot{q}(t_0) = q_0' \tag{6.11}$$

$$\dot{q}(t_f) = q_f'. \tag{6.12}$$

Here q_0 is the starting point and q_f the final point. Respectively, t_0 denotes the initial time and t_f the final time. Fig. 6.1 shows example trajectories for the boom angle and boom velocity, designed using the cubic path algorithm. The rest-to-rest path starts from 22.68 degrees rising to 50 degrees, the transition time being 3 seconds.

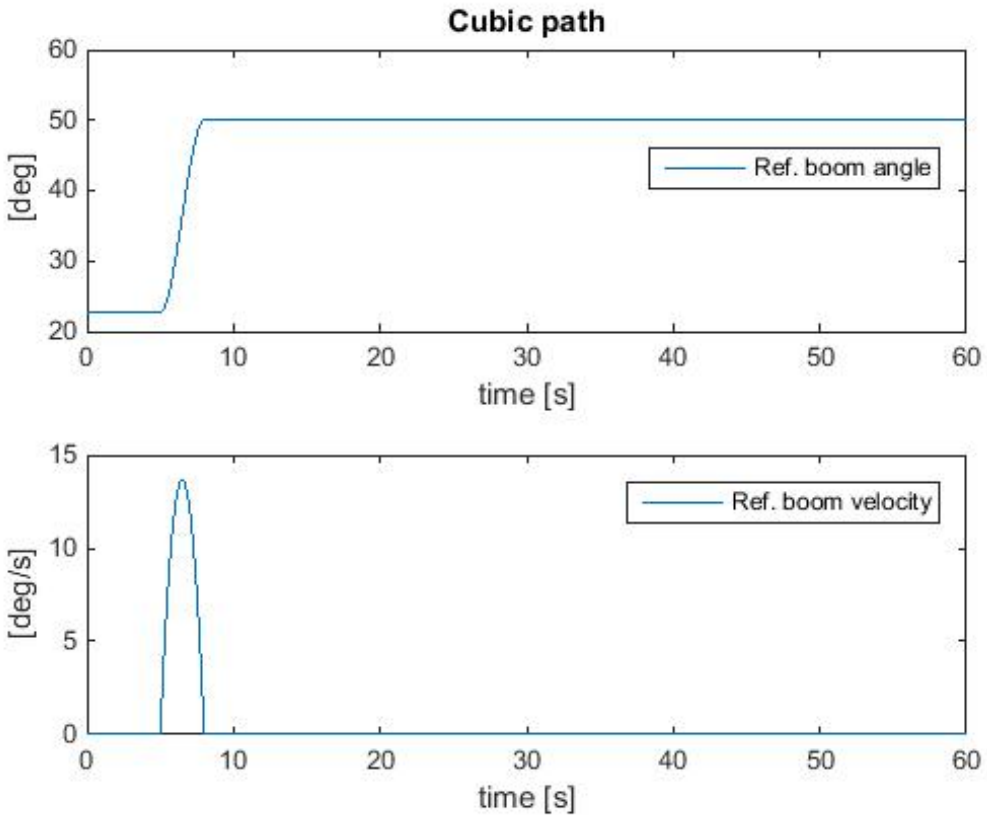

Figure 6.1 *The designed path used in measurement 1.*

The path presented was used in measurement 1, while for other measurements the transition time was increased to 10 seconds.

7. RESULTS AND DISCUSSION

In this chapter measurement results using the designed VDC controller are presented. The parameters and control gains used in the measurements are presented in section 6.3.

In measurement 1, the controller's ability to dampen vibration was studied. For this purpose a cubic path was generated using a fast transition time of 5 seconds. For comparison, the same path was driven using a P-controller. Measurement 1 results are presented in Figs. 7.1- 7.3. The results are presented so that first the reference and measured boom angles are given, along with the tracking error between the two. Respective figures are given for the tip position, piston velocity, piston position and piston force. As a reminder, the tip position refers to the tip arc approximation (5.22) that uses the estimated tip displacement obtained from the dynamic observer. The valve control signal is also given. The comparison results for measurement 1, using P-control, are presented in Fig. 7.4.

In both control cases, the reference appears to be too fast, since both controllers struggle to keep up with the reference. This was intended however, so that the differences between the two control methods would be visible. As it is evident, with P-control the boom tip starts vibrating around the desired steady state value. With the VDC, the tip vibration is dampened relatively swiftly. The tracking error is also much smaller during the rise time and steady state with the VDC.

In measurements 2-4, a longer transition time was applied to achieve better performance during the transition. A sine wave was also added to the reference signal, starting from around 30 seconds of running time. An amplitude of 2 degrees was used with each measurement, while the frequency was varied. With measurement 2 a frequency of 1 Hz was used, with measurement 3 a frequency of 3 Hz and with measurement 4 a frequency of 10 Hz was used. The results for measurement 2 are presented in Figs. 7.5- 7.7, while measurement 3 is presented in Appendix C and measurement 4 in Appendix D.

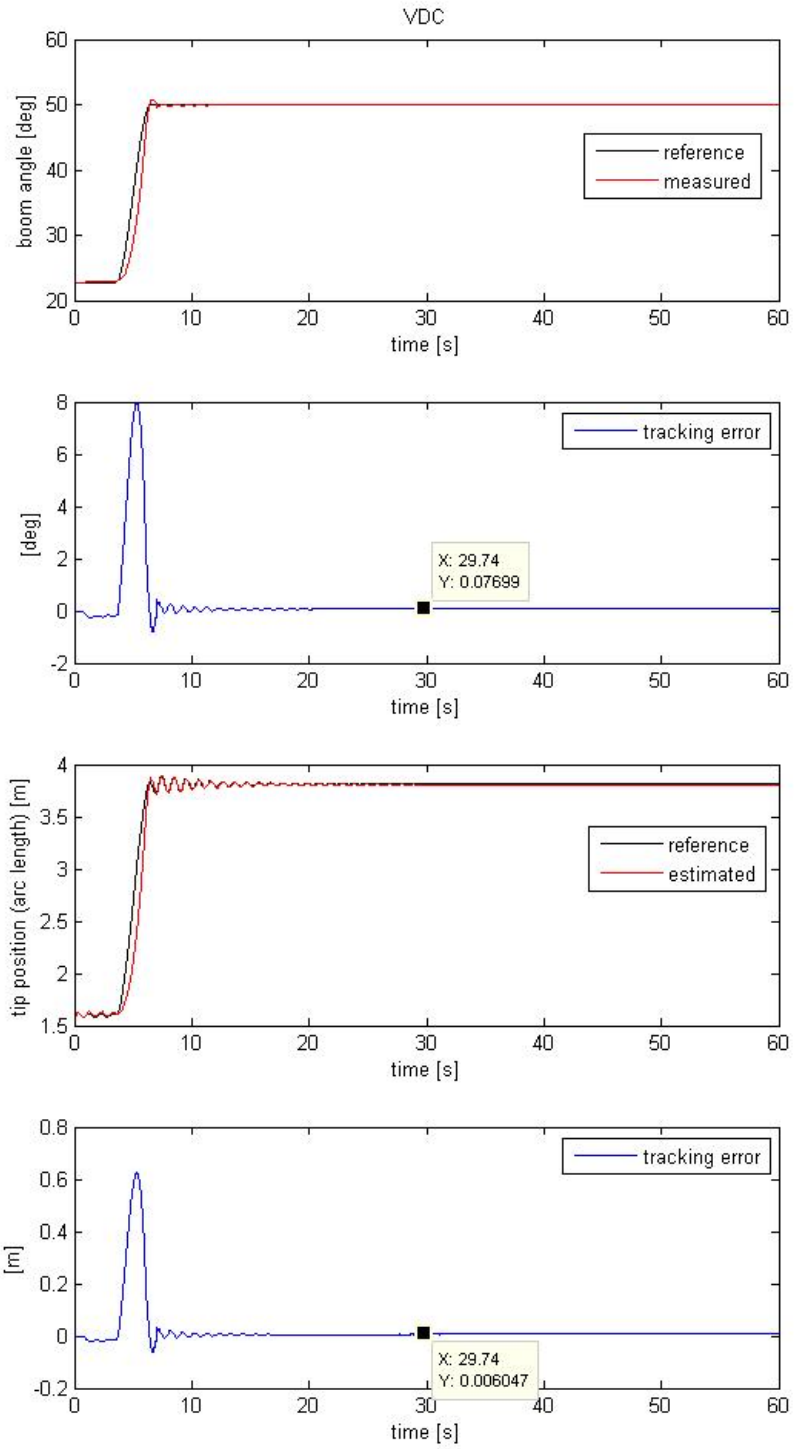

Figure 7.1 *Measurement 1 results (1/3).*

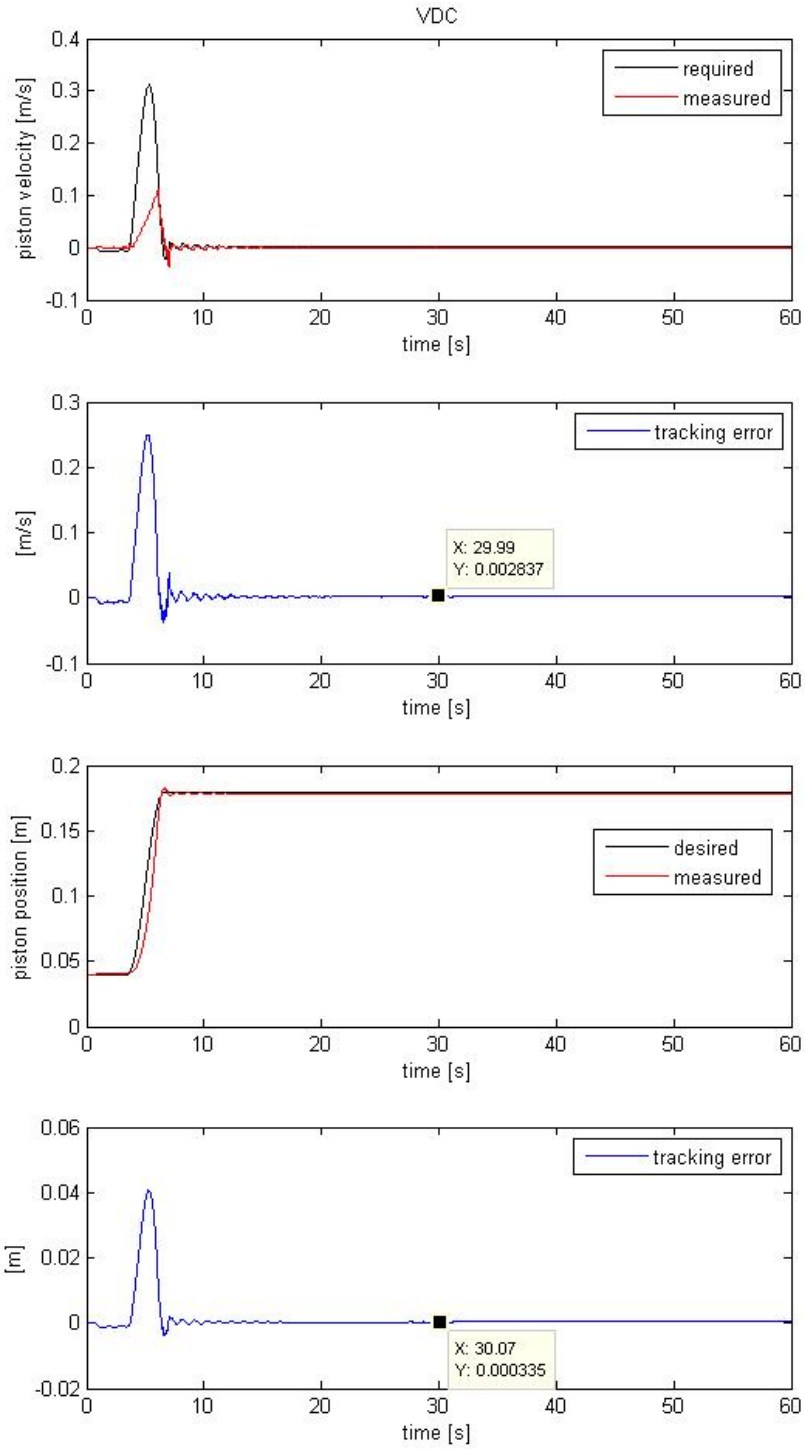

Figure 7.2 *Measurement 1 results (2/3).*

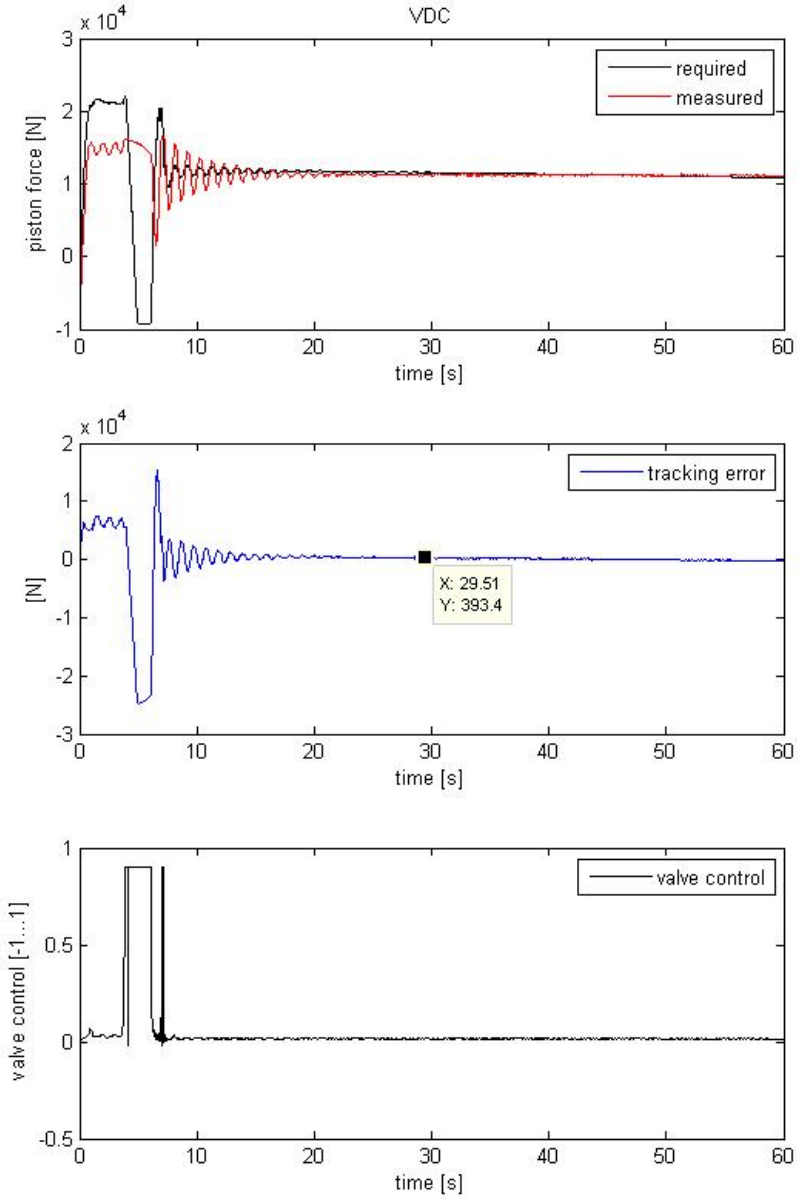

Figure 7.3 *Measurement 1 results (3/3).*

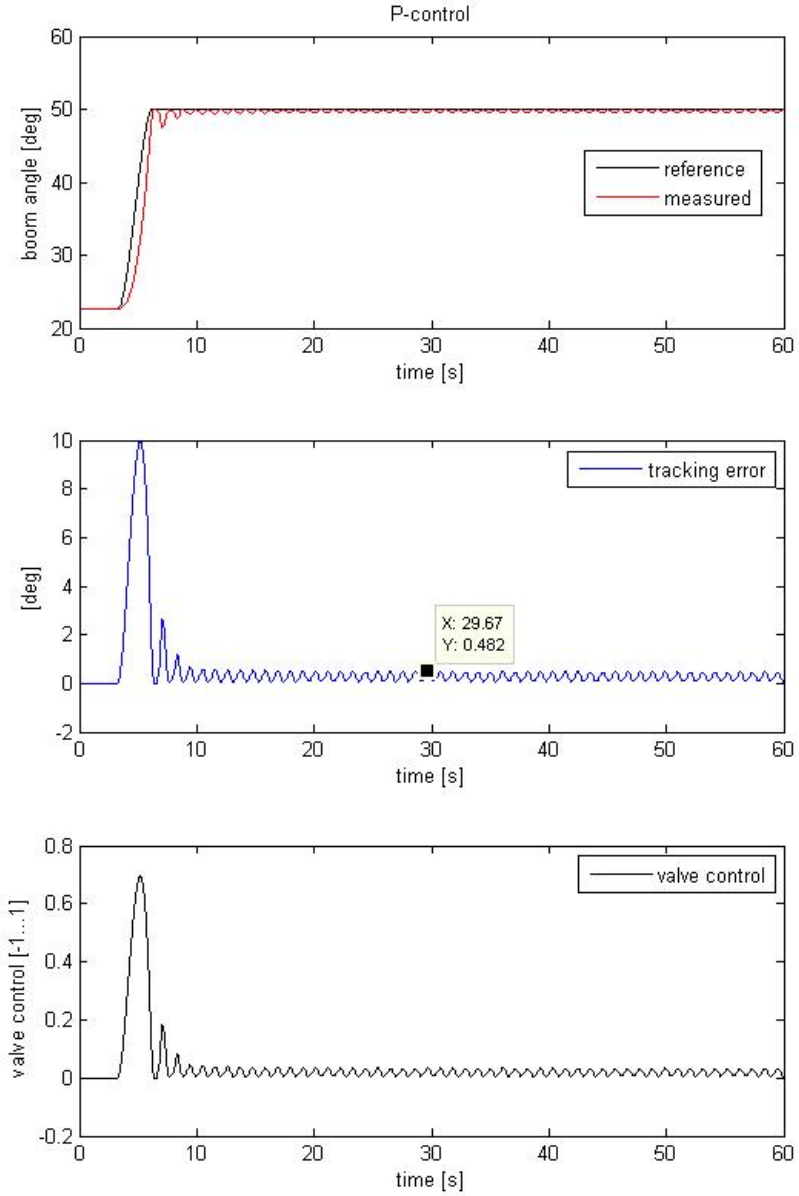

Figure 7.4 *P-control comparison for measurement 1.*

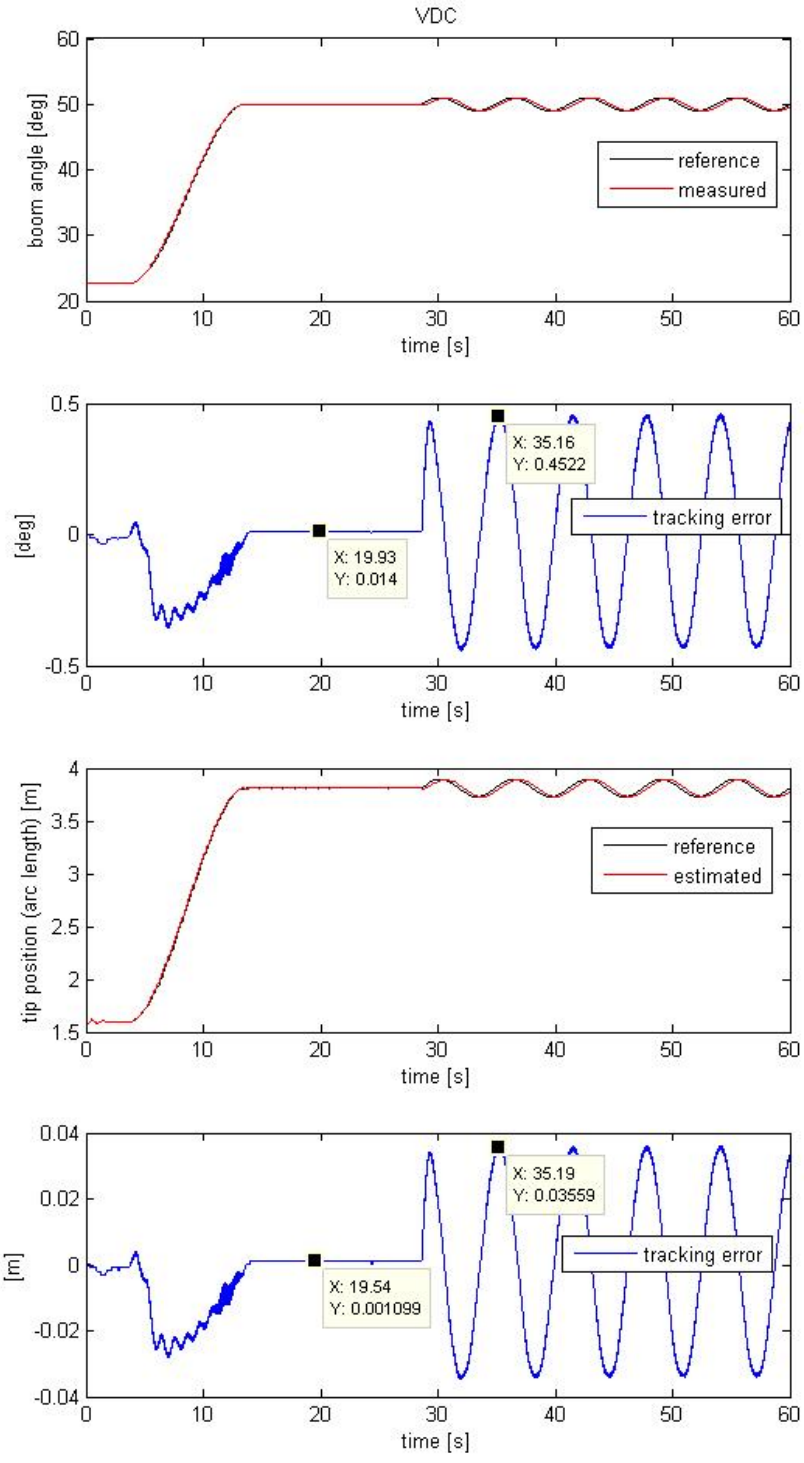

Figure 7.5 *Measurement 2 results (1/3).*

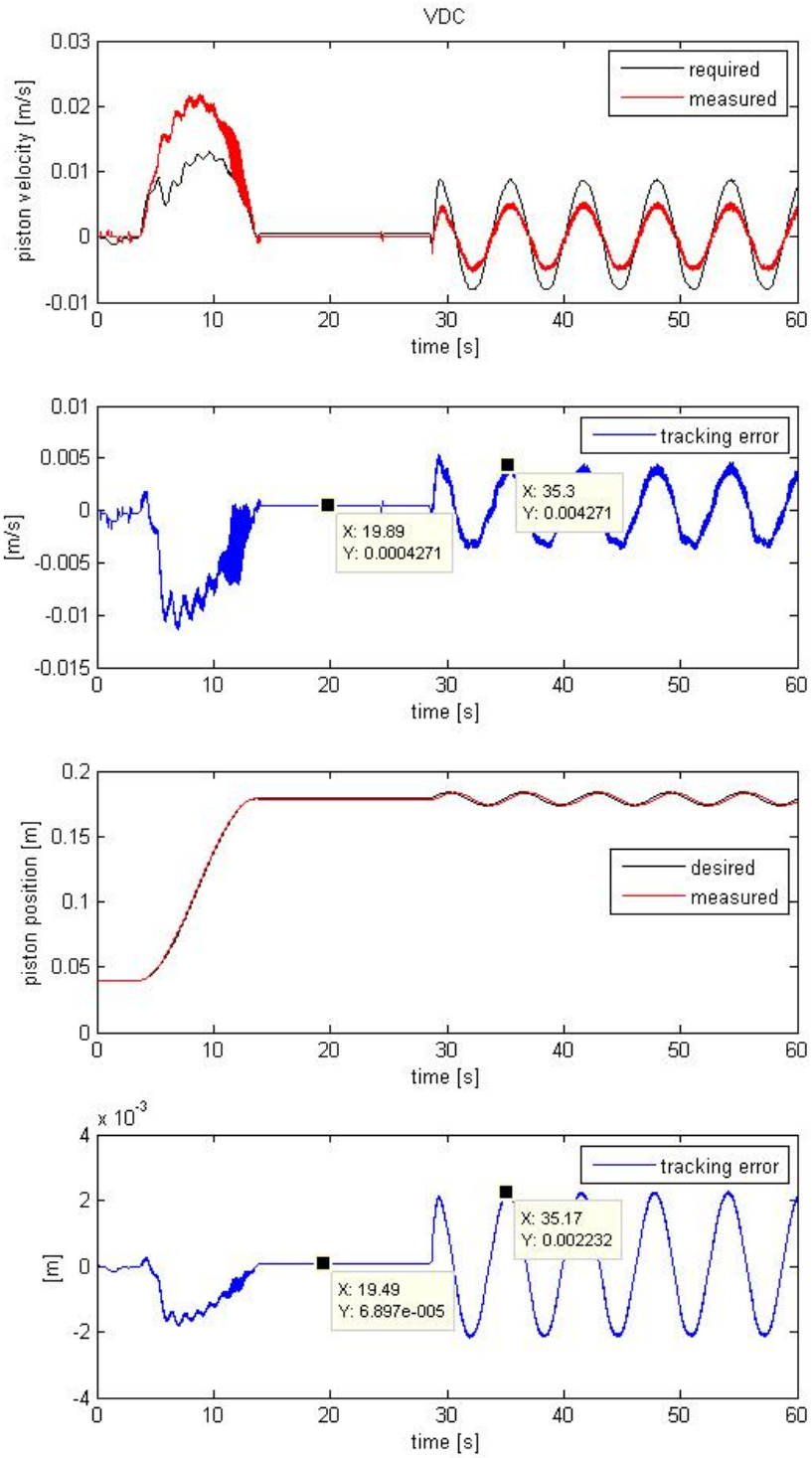

Figure 7.6 *Measurement 2 results (2/3).*

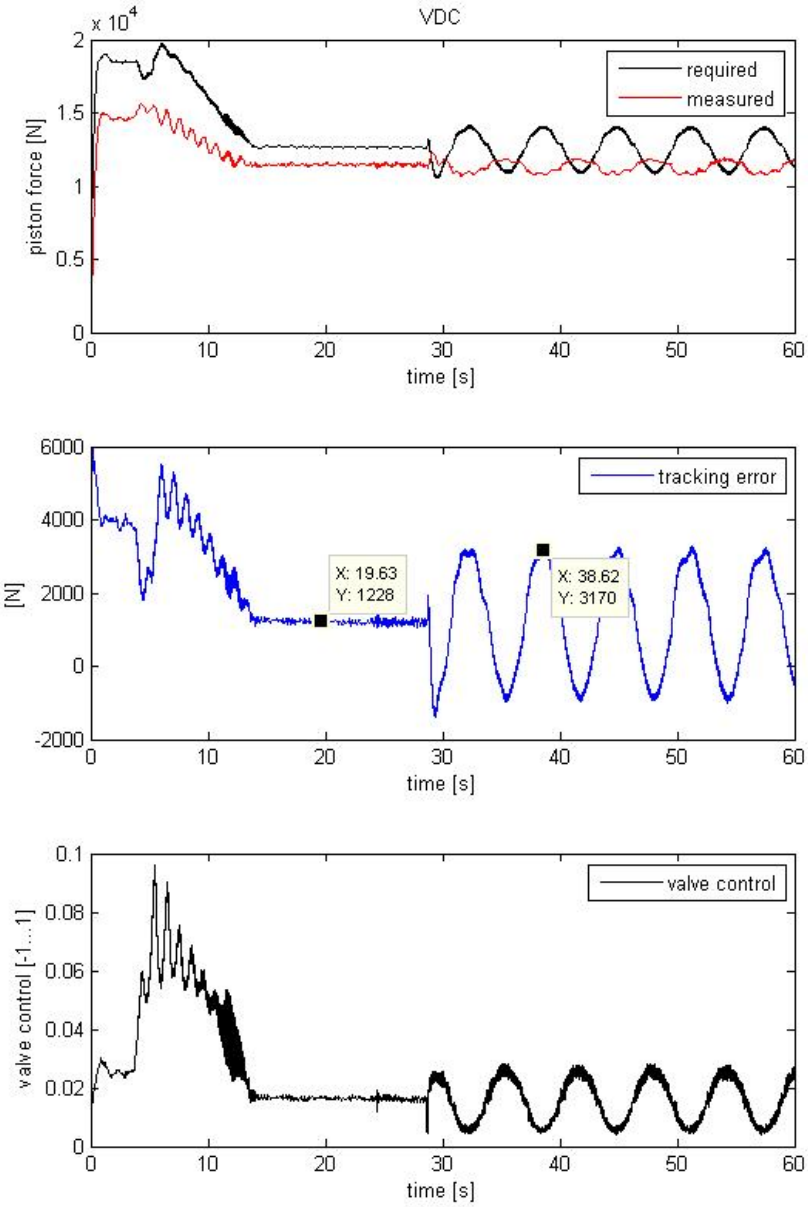

Figure 7.7 *Measurement 2 results (3/3).*

During the sine reference the tracking errors increase considerably, which appears to be caused mainly by a phase shift between the reference and measured variables. It can also be seen from the piston forces and piston velocities that there is room for improvement, as the respective reference and measured variables differ from each other. It is possible to improve the equivalency of these signals by tuning the parameters and control gains. The stability of the boom and the effectiveness of vibration dampening are lost relatively easily, however. Because of this, the controller's ability to track the boom angle and tip position were prioritized, when tuning the controller. The operational range of the target system can be defined as the cylinder stroke, which is between $0-0.3$ m. Stability of the system is able to be maintained in the whole operational range, with appropriate parametrization. The accuracy of control results seem to depend on the operational point. To address the controller's inability to track a sine reference well, it was experimented with in simulation also, with similar results. This may indicate an issue in the feedforward design of the controller.

A lot of filtering was also required to obtain acceptable signals that would keep the system stable. By no means can it be stated that the filtration is optimal, thus it also may have an effect on the results. The derivate approximation given in (6.2) was used to avoid the need of filtering backward differentiated signals. The value of the constant α_{gma}, used in the GMA-filter in (6.3), was also a compromise between disturbance attenuation and low phase lag [7, p. 13].

Due to the strong, inherent nonlinearities of the dynamics of hydraulics and flexible structure, controlling the target system proved to be a challenging task. Especially the parametrization process was very iterative and required compromises. Getting accurate results on the whole operational range, using the same control gains and other parameters did not seem plausible. That being said, an important aspect of the VDC approach was disregarded in the scope of this thesis. This aspect is parameter adaption, which could potentially improve the control behavior across the board, including during a sine reference. The implementation of parameter adaption would add approximately 40 lower and upper bounds for parameters, along with the same amount of control gains. This increases the difficulty of the parametrization process, which already is a tedious task. However, to achieve more accurate results in other points of the operational range, implementing the parameter adaption can be treated as a necessity and should be the next step in future research. Using non-constant friction parameters and effective bulk modulus, for example, naturally makes sense due to the nonlinear nature of friction and hydraulics.

8. CONCLUSIONS

This thesis was a part of an experimental research project at the department of Intelligent Hydraulics and Automation (IHA) in Tampere University of Technology (TUT). The installation under review was a single-link flexible manipulator attached to a rigid base structure and actuated using a hydraulic cylinder. The flexible link was made out of a strong steel hollow section, dimensioned $60 \times 60 \times 3$ mm and 4.5 m in total length. A load mass of 60 kg was attached near the tip to achieve static bending and a low natural frequency. The objective of this thesis was to first build a simulation model for the rotating flexible beam using the finite element method (FEM) in Matlab and Simulink environment. Then a controller for the system was to be built using the virtual decomposition control (VDC) approach. The designed controller was also to be implemented into the real-time environment using dSPACE and ControlDesk software. The ultimate goal was to study the VDC's performance in the target system.

A predefined trajectory was planned for the system by using a cubic polynomial. First, the VDC's ability to dampen vibration was tested. A fast rest-to-rest path was generated for this purpose. The same path was then driven by using a simple P-controller. This was mainly to verify that the boom tip would start vibrating. The VDC succesfully dampened any vibration and outperformed, not surprisingly, the P-control. The VDC's dynamic capabilities were then tested by adding a sine reference, which was delayed by 30 seconds with respect to the running time of the control system. It was noticed that the VDC has difficulties to follow a sine reference accurately, which was mainly caused by a phase shift between the reference and measured variables. This likely indicates an inaccuracy in the feedforward portion of the controller.

An important aspect of the VDC approach, namely parameter adaption, was not implemented in the scope of this thesis. Considering the highly nonlinear dynamics of the target system, adding adaptive capabilities to the designed VDC could potentially improve its performance considerably. The greatest challenge in implementing the parameter adaption is parametrization, due to a large number of additional control gains along with lower

and upper bounds for each parameter to be adapted.

Another future challenge is the validation of the tip position. In this thesis an arc approximation was used as the tip position. Furthermore, this approximation was formed by using an estimate of the tip displacement, obtained from a dynamic observer. The controller tracks a given tip position reference, but there is no knowledge of the validity. This is a fundamental problem, when it comes to the tip position control of flexible arms.

Despite the challenges, the results of this thesis demonstrate the effectiveness and potential of the VDC approach in controlling flexible arms with hydraulic actuation. At the core, the most problematic side of the VDC approach is the parametrization. Future work should include the implementation and tuning of parameter adaption into the control structure. Improving the tip position approximation, along with its validation, should also be areas of future consideration.

BIBLIOGRAPHY

[1] T. R. Chandrupatla and A. D. Belegundu, *Introduction to Finite Elements in Engineering*, 2nd ed. Prentice-Hall, Inc., 1997, 459 p.

[2] S. K. Dwivedy and P. Eberhard, "Dynamic analysis of flexible manipulators, a literature review," *Mechanism and Machine Theory 41*, pp. 749–777, 2006, 29 p.

[3] A. Harrison and D. Stoten, "Generalized finite difference methods for optimal estimation of derivatives in real-time control problems," *Proceedings of the Institution of Mechanical Engineers, Part I: Journal of Systems and Control Engineering 209: 67*, 1995, 13 p.

[4] J.-W. Huang and J.-S. Lin, "Backstepping control design of a single-link flexible robotic manipulator," *Proceedings of the 17th World Congress, The International Federation of Automatic Control, Seoul, Korea*, pp. 11 775–11 780, July 6-11, 2008, 6 p.

[5] R. N. Jazar, *Theory of Applied Robotics - Kinematics, Dynamics and Control*, 2nd ed. Springer, 2010, 893 p.

[6] J. Koivumaki, "Virtual decomposition control of a hydraulic manipulator," Master of Science thesis, 2012, Tampere University of Technology, 133 p. Available: https://dspace.cc.tut.fi/dpub/bitstream/handle/123456789/21370/Koivumaki.pdf?sequence=3 (visited 13.7.2016).

[7] J. Koivumaki and J. Mattila, "High performance nonlinear motion/force controller design for redundant hydraulic construction crane automation," *Automation in Construction 51*, pp. 59–77, 2015, 19 p.

[8] Y. W. Kwon and H. Bang, *The Finite Element Method using MATLAB*, 1st ed. CRC Press LLC, 1997, 527 p. Available: https://www.scribd.com/doc/49217904/The-Finite-Element-Method-Using-MATLAB (visited 14.7.2016).

[9] H. Lee, "Effect of gravity on the stability of a rotating cantilever beam in a vertical plane," *Computers & Structures, Vol. 53, No. 2*, pp. 351–355, 1994, 5 p.

[10] M. Linjama, "The modeling and actuator space control of flexible hydraulic cranes," *Acta Polytechnica Scandinavica, Mechanical Engineering Series No. 129, Espoo 1998, 110 p. Published by the Finnish Academy of Technology*.

[11] A. Lynch and D. Wang, "Flatness-based control of a flexible beam in a gravitational field," *Proceedings of the 2004 American Control Conference, Boston, Massachusetts*, pp. 5449–5454, June 30-July 2, 2004, 6 p.

[12] H. Rahimi and M. Nazemizadef, "Dynamic analysis and intelligent control techniques for flexible manipulators: a review," *Advanced Robotics, 28:2*, pp. 63–76, 2013, 15 p.

[13] M. Thabet, "Finite element modelling and simulation of the iha experimental flexible beam," *Department of Intelligent Hydraulics and Automation, Tampere University of Technology*, 2016, 8 p.

[14] Z. Tiemin, L. Youwu, Y. Shaoze, Z. Qing, and Z. Haigen, "Comparative study on the acceleration feedback and the strain feedback of a flexible manipulator," *Mechanical Engineering Department, Tianjin University, Tianjin, 300072, China*, 1996, 5 p.

[15] G. Zhu, T. Lee, and S. Ge, "Tip tracking control of a single-link flexible robot: A backstepping approach," *Dynamics and Control, 7*, pp. 341–360, 1997, 20 p.

[16] W.-H. Zhu, *Virtual Decomposition Control - Towards Hyper Degrees of Freedom Robots*, 1st ed. Springer-Verlag Berlin Heidelberg, 2010, 459 p.

[17] W.-H. Zhu, C. Lange, and M. Callot, "Virtual decomposition control of a planar flexible-link robot," *Proceedings of the 17th World Congress, The International Federation of Automatic Conrol, Seoul, Korea, July 6-11*, pp. 1697–1702, 2008, 6 p.

[18] W.-H. Zhu and J.-C. Piedboeuf, "Adaptive output force tracking control of hydraulic cylinders with applications to robot manipulators," *Transactions of the ASME, Vol. 127, June 2005*, pp. 206–217, 12 p.

APPENDIX A. SENSORS AND FILTERS USED

This appendix details the measurements and respective sensors, along with the filters used. Table 1 presents the sensors.

Table 1 *Sensors used.*

Measured parameter	**Sensor**
Supply pressure	Trafag 8891.74
Chamber A pressure	Unik 5000
Chamber B pressure	Unik 5000
Boom angle	Sick Stegmann DGS60
Ang. velocity and lin. acceleration	3× MEMS

Table 2 presents the filtered signals. The filter assoaciated with the optimal estimation of derivative refers to (6.2), while GMA-filter refers to (6.3).

Table 2 *Filters used.*

Description	**Signal**	**Filter**
Ref. tip arc velocity	$\dot{y}_d(l,t)$	Optimal estimation of derivative
Tip arc velocity	$\dot{y}(l,t)$	Optimal estimation of derivative
Ref. tip angular velocity	$\dot{y}'_d(l,t)$	Optimal estimation of derivative
Tip angular velocity	$\dot{y}'(l,t)$	Optimal estimation of derivative
Boom angular velocity	$\dot{\theta}$	Optimal estimation of derivative
Change in the req. piston force	$\dot{f}_{pr}$	Optimal estimation of derivative
Supply pressure	p_s	GMA
Chamber A pressure	p_a	GMA
Chamber B pressure	p_b	GMA
Required piston force	f_{pr}	GMA
Piston force	f_c	GMA
Measured piston force	f_p	GMA
Required piston velocity	$\dot{x}_r$	GMA
Piston velocity	$\dot{x}$	GMA

APPENDIX B. DYNAMIC OBSERVER

A dynamic observer is a well known mathematical algorithm in modern control theory that is used for state estimation. In practice, the observer is a mathematical model of a given system. In this case the model is a FE presentation of the beam, similar with the one given in chapter 4. Measured angular velocity of the boom tip, obtained from an IMU sensor, is used as the first input to the observer. The observer then gives estimates of all the nodal variables. The accuracy of the observer was evaluated by comparing measured angular velocities from the IMU sensors to their respective estimates, obtained from the observer. The load force at the tip was the second input to the observer. The force was implemented as a function of the tip angle using a simple lookup table. Design of the observer can be found in [8, pp. 485-490]. Constructing the dynamic observer was not part of this thesis. More details on the implementation can be found in [13], although the mathematical formulation is also given in this appendix.

A dynamic system can be presented using the state-space formulation:

$$\{\dot{x}\} = [A]\{x\} + [B]\{u\} \tag{1}$$
$$\{y\} = [C]\{x\} + [D]\{u\}. \tag{2}$$

Considering (4.33), the equation of motion corresponding to the FE model of the boom can be written as:

$$[\mathbf{M}]\{\ddot{q}\} + [\mathbf{C}]\{\dot{q}\} + [\mathbf{K}]\{q\} = F\{u\} \tag{3}$$

The second order system is transformed into a first order system using the state-space presentation. The presentation can be written as [8, p. 441]

$$\{\dot{x}\} = \frac{d}{dt}\begin{Bmatrix} q \\ \dot{q} \end{Bmatrix} = \begin{Bmatrix} \dot{q} \\ -[\mathbf{M}]^{-1}[\mathbf{C}]\dot{q} - [\mathbf{M}]^{-1}[\mathbf{K}]q + [\mathbf{M}]^{-1}[F]u \end{Bmatrix} \tag{4}$$
$$= \begin{bmatrix} 0 & I \\ -[\mathbf{M}]^{-1}[\mathbf{K}] & -[\mathbf{M}]^{-1}[\mathbf{C}] \end{bmatrix}\begin{Bmatrix} q \\ \dot{q} \end{Bmatrix} + \begin{bmatrix} 0 \\ [\mathbf{M}]^{-1}F \end{bmatrix} u \tag{5}$$
$$\equiv [A]\{x\} + [B]\{u\} \tag{6}$$

A dynamic observer can then be expressed as

$$\{\dot{\hat{x}}\} = [A]\{\hat{x}\} + [B]\{u\} + [L](\{y\} - \{\hat{y}\}) \tag{7}$$

$$\{\hat{y}\} = [C]\{\hat{x}\} + [D]\{u\}, \tag{8}$$

where $[L]$ contains observer gains and $\{y\}$ denotes the sensor output that is provided into the observer dynamics. The variables with $\hat{()}$ denote the estimated variables.

LQR (Linear Quadratic Regulator) algorithm is used for deriving the observer gains. This is made possible by treating $([A]^T, [C]^T)$ as if they were $([A], [B])$ in the control law design. This is due to the fact that the eigenvalues of a transpose matrix are equal to those of the respective original matrix, written as follows:

$$\lambda_i([A] - [L][C]) \equiv \lambda_i([A]^T - [C]^T[L]^T), \tag{9}$$

where λ_i contains the eigenvalues. The observer gains are obtained by solving the ARE (Algebraic Riccati Equation):

$$[A][S] + [A]^T[S] - [S][B][R]^{-1}[B]^T[S] + [Q] = 0, \tag{10}$$

where R and Q denote positive definite or semidefinite weighting matrices, which are given design variables. The Riccati matrix, denoted by S, is solved using the ARE. Then the feedback gain matrix can be solved from

$$[G] = [R]^{-1}[B]^T[S]. \tag{11}$$

To obtain the observer gain matrix $[L]$ from (11) instead of the LQR gain matrix $[G]$, $([A], [B])$ are replaced with $([A]^T, [C]^T)$ in the ARE (10). [8, pp. 472-477]

APPENDIX C. MEASUREMENT 3 RESULTS

This appendix presents the results of measurement 3.

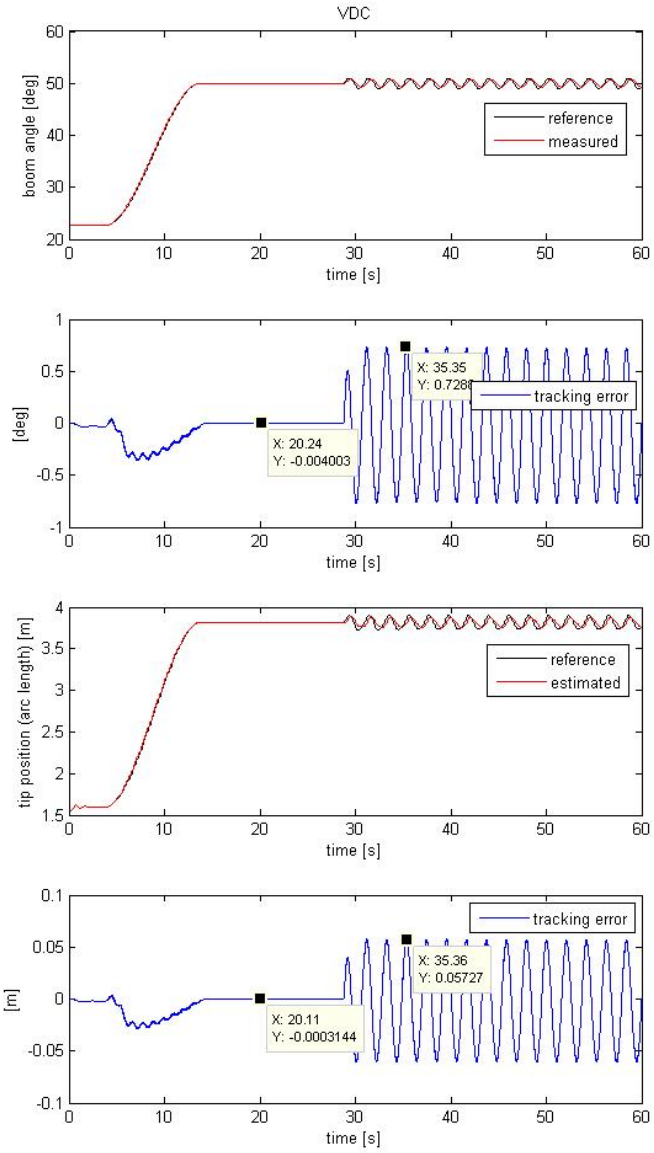

Figure 1 *Measurement 3 results (1/3).*

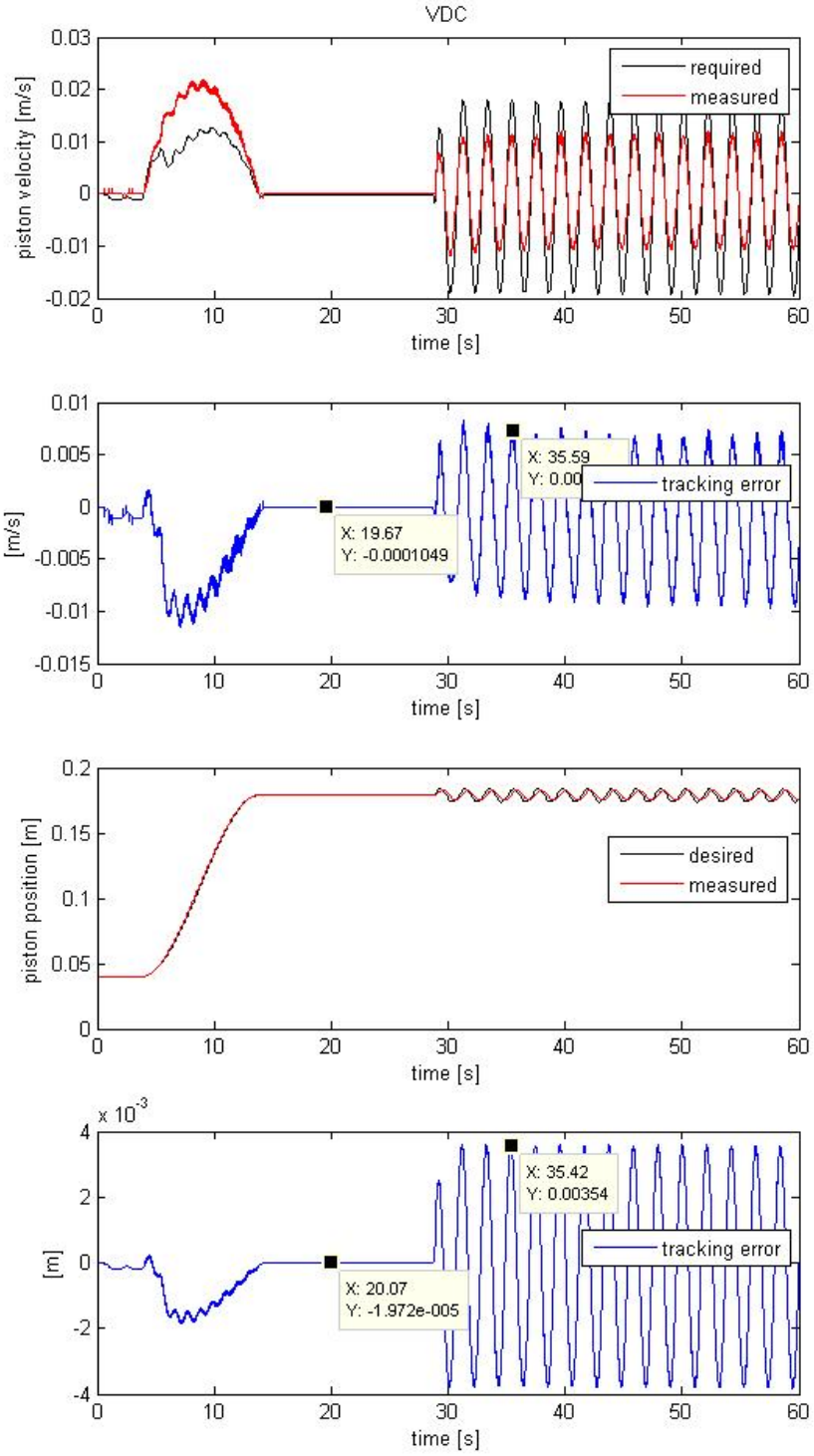

Figure 2 *Measurement 3 results (2/3).*

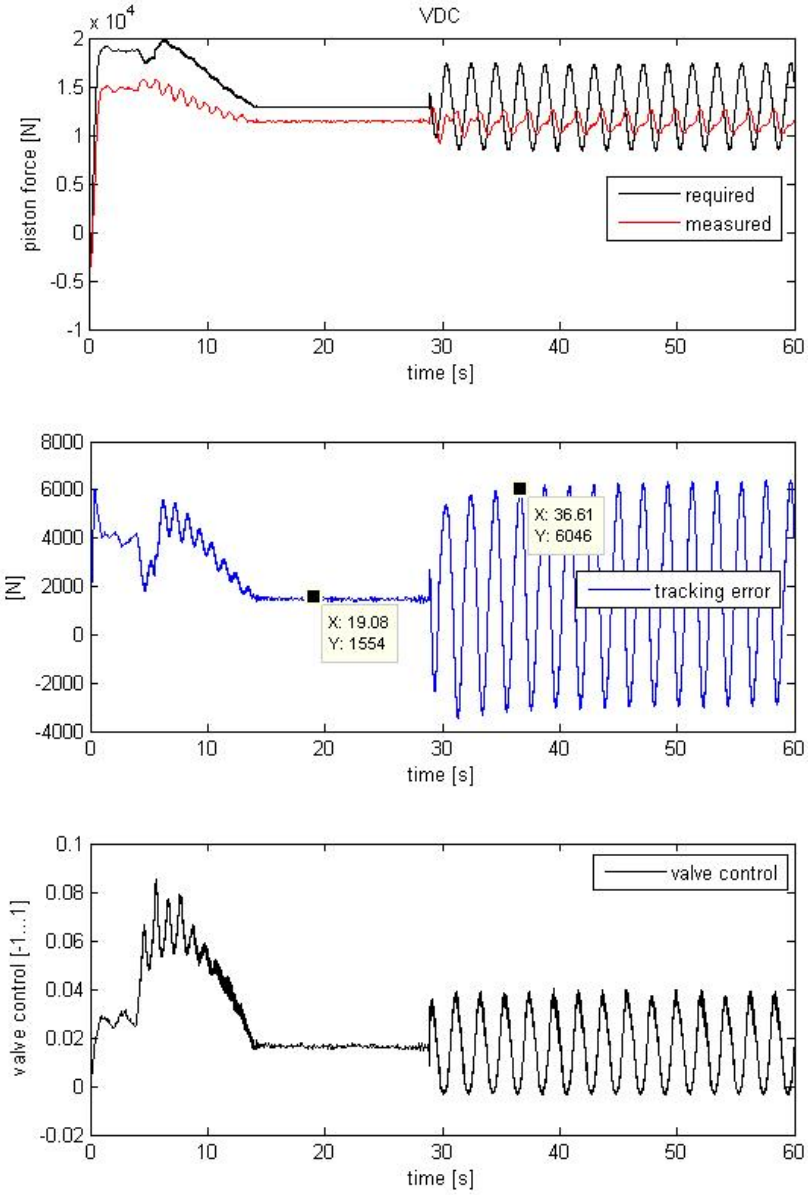

Figure 3 *Measurement 3 results (3/3).*

APPENDIX D. MEASUREMENT 4 RESULTS

This appendix presents the results of measurement 4.

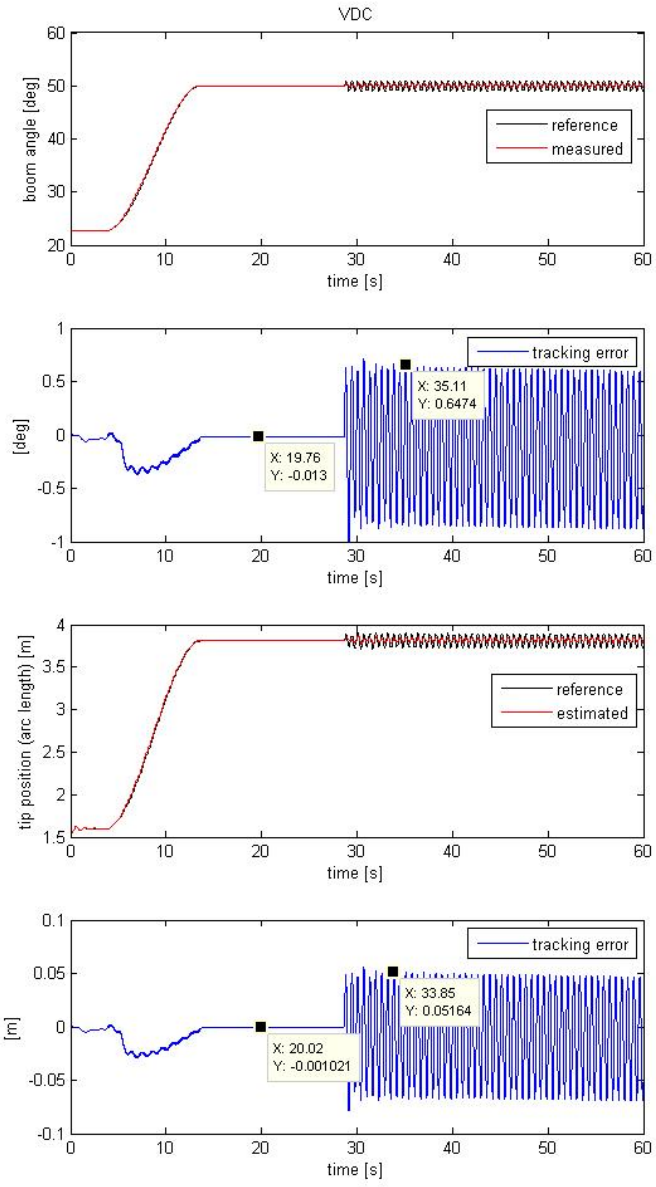

Figure 4 *Measurement 4 results (1/3).*

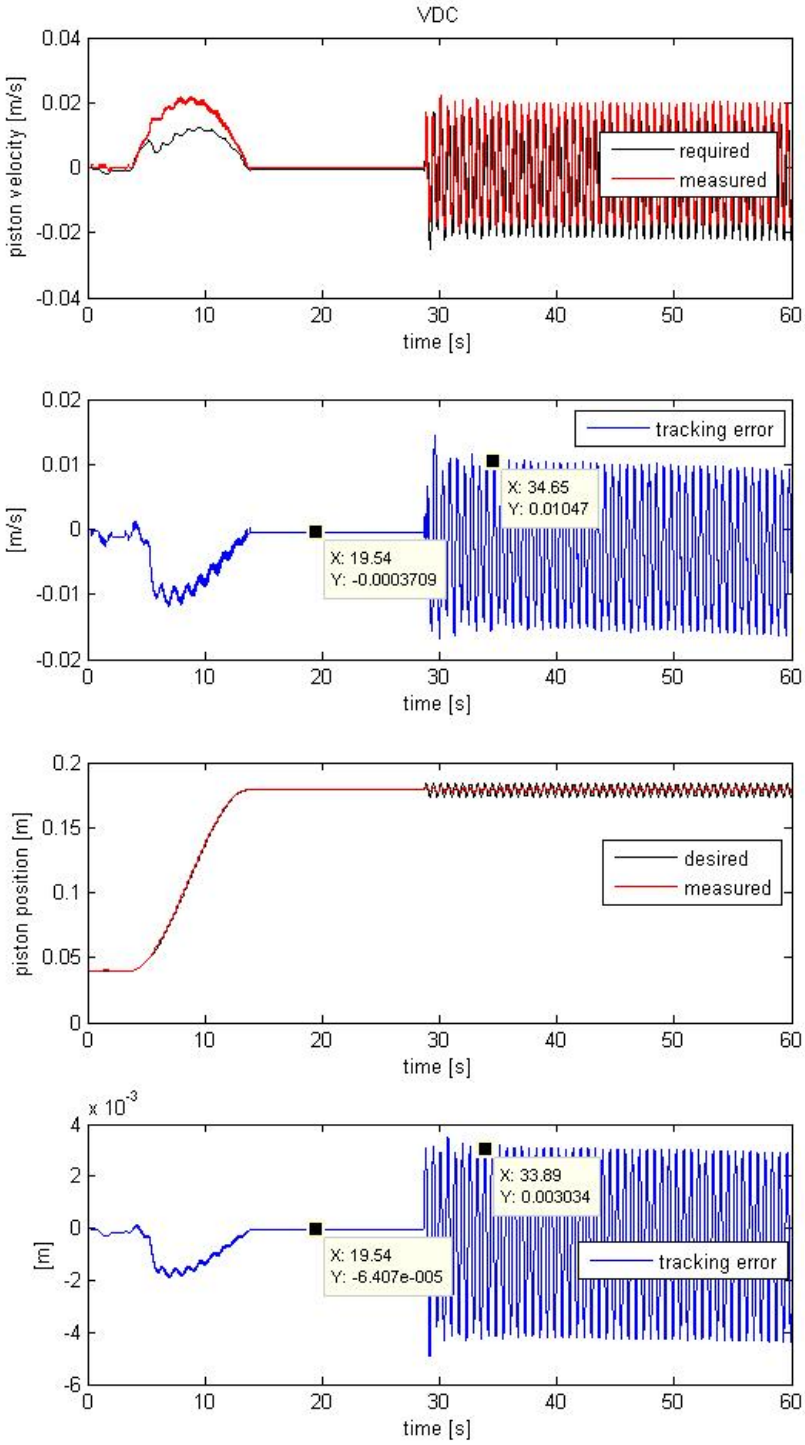

Figure 5 *Measurement 4 results (2/3).*

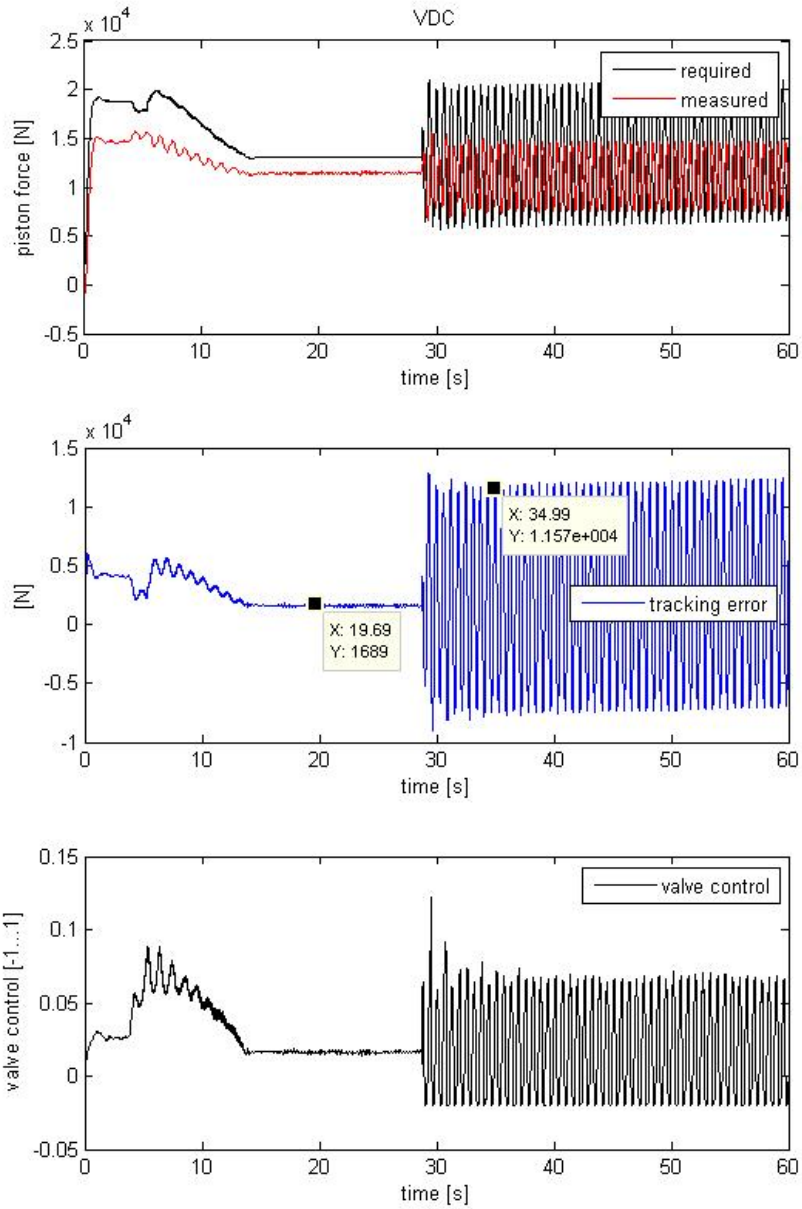

Figure 6 *Measurement 4 results (3/3).*